

**REGENERATION OF THE ANTERIOR CRUCIATE LIGAMENT
USING RESORBABLE METALLIC
AND EXTRACELLULAR MATRIX BIOSCAFFOLDS**

by

Kathryn Frances Farraro

Bachelor of Science, University of California, Davis, 2008

Master of Science, University of California, Davis, 2010

Submitted to the Graduate Faculty of
Swanson School of Engineering in partial fulfillment
of the requirements for the degree of
Doctor of Philosophy

University of Pittsburgh

2015

UNIVERSITY OF PITTSBURGH
SWANSON SCHOOL OF ENGINEERING

This dissertation was presented

by

Kathryn Frances Farraro

It was defended on

June 29, 2015

and approved by

Alejandro J. Almarza, Ph.D., Associate Professor, Department of Oral Biology

Stephen F. Badylak, D.V.M., Ph.D., M.D., Professor, Department of Surgery

Patrick J. McMahon, M.D., Adjunct Associate Professor, Department of Bioengineering

Vesselin Shanov, Ph.D., Professor, Department of Chemical and Materials Engineering,

University of Cincinnati

Dissertation Director: Savio L-Y. Woo, Distinguished University Professor,
Department of Bioengineering

Copyright © by Kathryn Frances Farraro

2015

REGENERATION OF THE ANTERIOR CRUCIATE LIGAMENT USING RESORBABLE METALLIC AND EXTRACELLULAR MATRIX BIOSCAFFOLDS

Kathryn Frances Farraro, PhD

University of Pittsburgh, 2015

The anterior cruciate ligament (ACL) is the most frequently injured knee ligament. Because of its low healing capacity, the current standard of treatment is surgical ACL reconstruction. However, follow-up studies 10 years or more after surgery have shown that patients frequently experience long-term complications, including the early development of osteoarthritis. For this reason, scientists and clinicians have explored alternative treatment methods. With the advent of functional tissue engineering, there has been renewed interest in regenerating an injured ACL using biological augmentation. Still, due to the slow process of ACL healing, mechanical augmentation is also needed to restore stability to the knee immediately after surgery, as well as to load the ACL throughout the healing process.

The purpose of this dissertation was to develop and test a bioresorbable magnesium (Mg) device for mechanical augmentation of a transected ACL in a goat model. First, a ring-shaped device was designed based on the geometry of the goat ACL, and evaluated using a parametric finite element analysis. Then, a robotic/universal force-moment sensor testing system was used to measure the joint stability and in-situ forces in the ACL after repair of the ACL in cadaveric goat stifle joints using the Mg ring ("Mg ring repair"). Under externally applied loads simulating those used in clinical examinations, Mg ring repair could restore joint stability and in-situ forces in the ACL close to normal levels. With these positive findings, *in vitro* cytocompatibility testing was performed by culturing goat ACL fibroblasts with Mg degradation products. Results

on cell proliferation and collagen production suggested that the presence of Mg neither impeded nor enhanced the healing process. Finally, the Mg ring was used to repair a surgically transected ACL in skeletally mature goats alongside biological augmentation using an extracellular matrix (ECM) sheet and hydrogel. In this *in vivo* study, by 6 weeks post-operatively, neo-tissue had begun to fill in the gap between the transected ends of the ACL. By 12 weeks, the ACL was found to have healed and the continuous neo-tissue was composed of aligned collagen fibers, but without hypertrophy. Biomechanically, the structural properties of the healing femur-ACL-tibia complex were improved compared to ECM treatment alone.

With the results from this dissertation, the advantages of using combined biological and mechanical augmentation to improve healing of a transected ACL have been demonstrated. Building off these findings, future studies can be performed to further enhance ACL healing, as well as extend the application to the healing of other injured ligaments and tendons. It is our hope that in the future, such an approach could be used clinically to improve short and long-term patient outcomes after orthopaedic surgery.

TABLE OF CONTENTS

PREFACE.....	XVI
1.0 BACKGROUND	1
1.1 ACL ANATOMY AND FUNCTION.....	1
1.2 ACL INJURIES	4
1.2.1 Incidence and consequence of ACL injuries.....	4
1.2.2 Clinical treatments	5
1.2.2.1 Conservative treatments	5
1.2.2.2 Surgical repair	6
1.2.2.3 ACL reconstruction	7
1.2.2.4 Rationale for a new treatment option	8
1.3 LIGAMENT HEALING	10
1.3.1 MCL healing.....	10
1.3.2 Functional tissue engineering approaches	11
1.3.2.1 Growth factors	12
1.3.2.2 Stem cells	13
1.3.2.3 Extracellular matrix scaffolds	13
1.3.3 Challenges for ACL healing.....	16
1.3.4 Current and new approaches to ACL healing.....	17

1.3.4.1	Biological augmentation	18
1.3.4.2	Mechanical augmentation	19
1.3.4.3	Combined biological and mechanical augmentation.....	20
1.4	MAGNESIUM AS A BIOMATERIAL FOR ORTHOPAEDIC APPLICATIONS	20
1.4.1	Background on orthopaedic biomaterials.....	20
1.4.2	Biocompatibility	23
1.4.3	Historical use of Mg for orthopaedic implants.....	24
1.4.4	Recent advances in Mg materials	24
1.4.4.1	Alloying and mechanical properties.....	25
1.4.4.2	Corrosion behavior	26
1.4.4.3	<i>In vitro</i> and <i>in vivo</i> cytocompatibility and healing potential.....	27
1.4.5	Rationale for use of Mg for ACL healing.....	30
2.0	OBJECTIVES	32
2.1	OVERALL GOALS	32
2.2	SPECIFIC AIMS	32
3.0	DESIGN AND FINITE ELEMENT ANALYSIS	37
3.1	GEOMETRY	37
3.2	DEVICE DESIGN AND SUTURE TECHNIQUE.....	38
3.3	FINITE ELEMENT ANALYSIS	43
3.3.1	Background.....	43
3.3.2	Model development	44
3.3.3	Finite element analysis results.....	51
4.0	<i>IN VITRO</i> ROBOTIC/UFS EVALUATION OF MG RING REPAIR OF THE ACL	57

4.1	EXPERIMENTAL DESIGN	57
4.2	ROBOTIC TESTING PROCEDURE	58
4.3	RESULTS.....	61
5.0	COMBINED BIOLOGICAL AND MECHANICAL AUGMENTATION FOR ACL HEALING.....	67
5.1	<i>IN VITRO</i> CELL CULTURE STUDIES	67
5.1.1	Background.....	67
5.1.2	Experimental Methods	70
5.1.2.1	Preparation of extracts from Mg materials.....	70
5.1.2.2	Cell culture methods.....	71
5.1.2.3	Cell proliferation assay.....	71
5.1.2.4	Collagen production assay	73
5.1.3	Results	74
5.2	<i>IN VIVO</i> ACL HEALING STUDY	80
5.2.1	Experimental Methods	80
5.2.1.1	Animal model	80
5.2.1.2	Preparation of Mg ring devices	80
5.2.1.3	Preparation of ECM bioscaffolds.....	82
5.2.1.4	Surgical procedure.....	83
5.2.1.5	Post-operative care	84
5.2.1.6	Gross morphology.....	85
5.2.1.7	Histological evaluation	86
5.2.1.8	<i>In vivo</i> degradation of the Mg ring.....	86
5.2.1.9	Analysis of synovial fluid.....	88

5.2.1.10	Biomechanical testing	89
5.2.1.11	Data analysis.....	92
5.2.2	Results	93
5.2.2.1	Gross morphology of the healing ACL	93
5.2.2.2	Histological evaluation	96
5.2.2.3	Degradation of the Mg ring	100
5.2.2.4	Cytology and total protein content of synovial fluid	102
5.2.2.5	Joint stability and in-situ forces	103
5.2.2.6	Tensile properties.....	108
5.2.2.7	Comparison to ECM treatment alone.....	109
6.0	DISCUSSION AND FUTURE DIRECTIONS.....	114
6.1	DISCUSSION OF THE MG RING DESIGN	115
6.2	<i>IN VITRO</i> ROBOTIC TESTING.....	117
6.3	IMPACT OF THE <i>IN VITRO</i> AND <i>IN VIVO</i> EVALUATION OF THE MG RING FOR ACL HEALING	118
6.4	IMPACT AND IMPLICATION FOR TISSUE ENGINEERING AND REGENERATIVE MEDICINE.....	123
6.5	LIMITATIONS.....	124
6.6	FUTURE DIRECTIONS	127
	BIBLIOGRAPHY	132

LIST OF TABLES

Table 1: Dimensional parameters estimated from geometry of a goat ACL	38
Table 2: Designs of the Mg ring used in the parametric finite element analysis.....	45
Table 3: Mechanical properties of Mg alloys for finite element model	45
Table 4: Resulting Von Mises stress from the parametric finite element analysis of the Mg ring (* indicates a value that has exceeded the yield stress; # indicates a value that has exceeded the failure stress)	53
Table 5: Experimental protocol and data obtained using the robotic/UFS testing system under a 67-N anterior tibial load without (I-III.A) and with (I-III.B) 100 N axial compression...	59
Table 6: Anterior tibial translation (mean \pm SD) of the goat stifle joints tested at 30°, 60°, and 90° of flexion in response to: (A) a 67-N anterior tibial load and (B) a 67-N anterior tibial load + 100 N axial compression.....	63
Table 7: In-situ forces in N (mean \pm SD) in the: (I) ACL and (II) medial meniscus of the goat stifle joints at 30°, 60°, and 90° of flexion in response to (A) a 67-N anterior tibial load and (B) a 67-N anterior tibial load with 100 N axial compression.....	63
Table 8: Initial (left) and final (right) pH values of Mg extracts	74
Table 9: Lameness scoring scale.....	84
Table 10: Qualitative scale describing degradation of the Mg ring.....	86
Table 11: Scores representing the degradation of the Mg ring at 12 weeks of healing.....	96
Table 12: Anterior-posterior tibial translation (A) and in-situ forces in the ACL (B) of the sham- operated and Mg ring-repaired goat stifle joints at 30°, 60°, and 90° of joint flexion (*indicates a statistically significant different compared to sham-operated controls; $P \leq$ 0.05)	105

Table 13: Structural properties of the healing and sham-operated FATCs (*indicates a statistically significant different compared to sham-operated controls; $P \leq 0.05$)	108
--	-----

LIST OF FIGURES

Figure 1: A schematic diagram of the human knee joint, illustrating the ACL as well as surrounding structures.....	2
Figure 2: A representative load-elongation curve of a goat femur-ACL-tibia complex.....	3
Figure 3: Histogram showing the number of publications each year on research of Mg and its alloys and stainless steel as biomaterials	22
Figure 4: Gradual shift in the contribution to ACL function over time of a Mg device versus the healing tissue.....	31
Figure 5: (A) Geometry and working length of the goat ACL, (B) Cross-sectional shape as measured by a laser micrometer system	38
Figure 6: Prototypes of the Mg ring.....	39
Figure 7: Procedural details for Mg ring repair, depicting attachment of repair and fixation sutures to the ACL (A), followed by attachment and fixation of the ring (B).....	42
Figure 8: Illustration of 3 predicted types of in-situ loading of the Mg ring	46
Figure 9: Initial rendering (A) and final 3-D model (B) of the goat stifle joint	47
Figure 10: Schematic diagram illustrating that the Mg ring could not be driven into the femoral intercondylar notch by axial compression	48
Figure 11: The Mg ring in Ansys software modeled with a cone of the same inner diameter to constrain the device from rigid body motion under loading.....	49
Figure 12: Directions of loading in the finite element model simulating tension from fixation sutures with a 40 N tensile load (left) and 20 N load normal to the surface of the Mg ring (right)	50
Figure 13: Medial and lateral loads applied to the Mg ring (A= anterior, P= posterior).....	51

Figure 14: Results on the Von Mises stress distributions for the parametric finite element analysis of the Mg ring	54
Figure 15: Photograph of the testing set-up for Specific Aim 2, depicting the cadaveric goat stifle joint (A), universal force-moment sensor (B), and robotic manipulator (C)	60
Figure 16: Normalized anterior tibial translation of the Mg ring-repaired and suture-repaired goat stifle joints at 30°, 60°, and 90° of flexion under (A) a 67-N anterior tibial load and (B) a 67-N anterior tibial load with 100 N axial compression.....	65
Figure 17: Normalized in-situ forces in (I) the ACL and (II) the medial meniscus in the Mg ring-repaired and suture-repaired goat stifle joints at 30°, 60°, and 90° of flexion under (A) a 67-N anterior tibial load and (B) a 67-N anterior tibial load with 100 N axial compression	66
Figure 18: Mg materials selected for in vitro testing in Specific Aim 3.1.....	68
Figure 19: Osmolality (mOsm/kg) of Mg extract dilutions	75
Figure 20: Resulting proliferation (% of control) of goat ACL fibroblasts after 3 days of culture with extracts prepared from single crystal Mg (mean ± SD).....	76
Figure 21: Resulting proliferation (% of control) of goat ACL fibroblasts after 3 days of culture with extracts prepared from Mg materials (mean ± SD)	77
Figure 22: Soluble collagen produced (% of controls) by goat ACL fibroblasts after 3 days of culture with extracts prepared from single crystal Mg (mean ± SD) (* indicates a statistically significant difference).....	78
Figure 23: Soluble collagen produced (% of control) by goat ACL fibroblasts after 3 days of culture with extracts prepared from Mg materials (mean ± SD) (* indicates a statistically significant difference, # indicates statistical difference from all other materials).....	79
Figure 24: A single crystal of Mg produced using the Bridgman technique (courtesy of Dr. V. Shanov)	81
Figure 25: Single crystal Mg rings before (left) and after coating via micro-arc oxidation (right)	82
Figure 26: Cross-sectional slice of the degrading Mg ring from micro-CT scan (A), with manually-selected region of interest surrounding the Mg ring depicted in black and intact Mg depicted in white (B)	88
Figure 27: A schematic illustrating a joint being tested on the robotic/UFS testing system at preselected angles of joint flexion, providing 5-DOF joint kinematics (AP – anterior-	

posterior, FE – flexion-extension, IE – internal-external, ML – medial-lateral, PD – proximal-distal, VV – varus-valgus).....	90
Figure 28: The FATC mounted on the materials testing machine for uniaxial tensile testing	92
Figure 29: Gross morphology of the healing ACL at 6 weeks	94
Figure 30: Gross morphology of the sham-operated ACL (A) and Mg ring-repaired ACL (B) ..	95
Figure 31: Cross-sectional area and shape of the sham-operated and healing ACL	95
Figure 32: Histology of the sham-operated ACL, depicting longitudinally-aligned collagen bundles (A) and normal synovium (B) (L – ligament)	97
Figure 33: Histological section of the healing FATC at 6 weeks of healing using H&E staining (T= tibia, A= ACL, P= PCL, F= femur)	98
Figure 34: Histological image of the Mg ring–repaired ACL (A), pitting corrosion lined with hyalinized collagen (B), small degrading fragments of the Mg ring (C), and lack of normal synovium around ACL tissue adhered to inner surface of the Mg ring (D) (G= granulation tissue, M= Mg ring, C= collagen).....	99
Figure 35: Histological section of the healing FATC at 12 weeks of healing using H&E staining (T= tibia, A= ACL, F= femur; arrow indicates Mg fragment)	100
Figure 36: 3D rendering of the degrading Mg ring at 6 weeks of healing in the goat stifle joint with femoral and tibial bone blocks.....	101
Figure 37: Total protein content in synovial fluid from sham-operated and healing goat stifle joints at 12 weeks of healing ($P < 0.05$)	103
Figure 38: Average curves for the APTT in the sham-operated and Mg ring-repaired joints at 60° of stifle joint flexion under a 67-N anterior-posterior tibial load (mean ± standard error)	104
Figure 39: In-situ forces in the MCL, soft tissue, medial meniscus, lateral meniscus, bony contact, and ACL in the sham-operated and Mg ring-repaired goat stifle joints at 30° (A), 60° (B), and 90° (C) of joint flexion.....	107
Figure 40: Gross morphology of the healing ACL with ECM treatment + Mg ring repair (A) and ECM treatment alone (B).....	109
Figure 41: Cross-sectional area (% of control) of the ECM-treated ACL and ECM + Mg ring-repaired ACL	110

Figure 42: Normalized APTT (A) and in-situ forces in the ACL (B) in the healing goat stifle joints with ECM-treated or ECM + Mg ring-repaired ACLs	111
Figure 43: Normalized stiffness (A) and ultimate load (B) of the femur-ACL-tibia complex with the ECM-treated and ECM + Mg ring-repaired ACL.....	113
Figure 44: Photographs illustrating sliding of the femoral fixation sutures at 12 weeks of healing in 2 specimen, showing the gap between the Endobutton and femur before (left) and after applying tension (right).....	123
Figure 45: Schematic diagram for further development of a combined biological and mechanical augmentation strategy to heal an injured ACL	129

PREFACE

When I moved across the country and entered the Bioengineering Ph.D. program at Pitt in 2010, nothing could have prepared me for the challenges, obstacles, and eventual growth that lay ahead. However, although this process has been a transformative one for me, it would never have been possible without the collaboration, help, and support of many others. I would like to acknowledge these individuals for their contributions to this work.

I would first like to thank my mentor, Dr. Savio L-Y. Woo, for shaping me as a scientist, researcher, and person. You have helped me to become a confident and capable researcher, and I am forever grateful for that. You taught me to respect and learn from the past, to always ask questions, and to strive to always be different and better. It is because of you that I now “think like a contrarian.”

Of course, this work would not have been possible without the help and support of the rest of the MSRC. Thank you to Diann DeCenzo for keeping the MSRC in order and for also being a friend and the best lunch companion I could ask for. To Dr. Kwang Kim, thank you for being my “big brother” in lab and guiding me until I could stand on my own two feet. To Jonquil Flowers, thank you for your help in completing this work, as well as for being my teammate. Thank you to our orthopaedic surgeon residents, Matteo Tei, Andrea Speziali, Norihiro Sasaki, and Antonio Pastrone, for your tireless and enthusiastic work to make the vision

of the “Mg ring” a reality. Finally, thank you to the numerous undergraduate students who have dedicated their time and effort into the MSRC and made the lab a livelier place.

I would also like to thank the numerous collaborators who contributed significantly to this thesis. Throughout my time in the Ph.D. program, I have had the excellent opportunity to work with top-notch researchers and clinicians from all over the world, and they have greatly impacted and shaped this work. To Drs. Vesselin Shanov, Yeoheung Yun, Prashant Kumta, Stephen Badylak, Kostas Verdelis, and Steven Abramowitch, Alejandro Almarza, as well as many of your students, I am indebted to you for your help and collaboration on this work. To Dr. Patrick McMahon, thank you for your feedback and guidance on the clinical side of this project.

Lastly, I thank my friends and family. I am so happy to now have networks of friends on the east and west coasts, both of which have supported me along this journey. To my brothers, Eric and Ryan, thank you for making my life more colorful and inspiring me with your own success (and encouraging my competitive nature to try to one-up you!). To my parents, Raymond and Charlene, I am truly grateful for your endless support and love. From helping me with elementary school science projects to aiding me with my algebra and calculus homework to encouraging me to take a physiology class, you fostered in me a love of math and science that has led me to where I am today. Thank you.

1.0 BACKGROUND

1.1 ACL ANATOMY AND FUNCTION

The anterior cruciate ligament, or ACL, is the most important stabilizer in the knee (Figure 1) ³⁹. Its function to restrain excessive anterior tibial translation ^{136, 179}, and it also plays a role in controlling internal-external ¹¹² and varus-valgus rotations ^{76, 111}. Originating at the posterolateral intercondylar notch of the femur, it becomes larger in cross-section as it approaches the anterior intercondylar eminentia of the tibia ⁵⁵. The cross-sectional shape of the ACL is irregular and varies with knee flexion, muscular activity, and external loads. Based on the tensioning patterns of the ACL during passive flexion-extension, it has been considered that the ACL has two distinct fiber bundles: the anteromedial (AM) bundle and posterolateral (PL) bundle ⁸³. The AM bundle is important for the restraint of anterior tibial translation ^{136, 199}, and the PL bundle is important for restraint of rotatory motion ¹⁷⁹.

The ACL is 65-70% water by weight, with 70-80% of the dry weight composed of Type I collagen organized into longitudinally-aligned fibrils with a crimped pattern ¹⁸⁹. The unique crimp pattern serves a protective function, as it permits for some tissue deformation in tension without damage as the crimped fibrils straighten and are recruited gradually. As these fibrils are aligned along the axis of loading, the ACL is also well-equipped to withstand larger tensile loads. This allows the ACL to guide joint motion under low loads during normal activities, as

well as to limit excessive motion and prevent injury under greater loading. Under uniaxial tensile testing of the femur-ACL-tibia complex (FATC), a nonlinear load-elongation curve is produced, whereby there is first a toe region of low stiffness as the collagen fibrils of the ACL straighten, followed by a linear region of higher stiffness as the fibers are stretched. Finally, the ultimate load is reached, after which failure of the FATC occurs (Figure 2) ²²⁶.

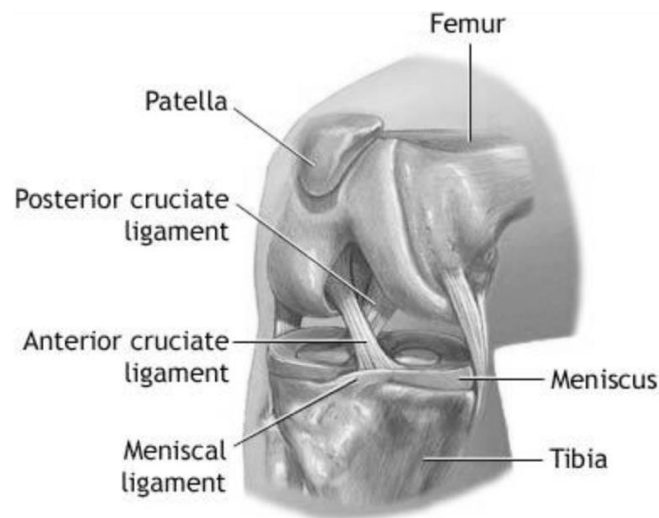


Figure 1: A schematic diagram of the human knee joint, illustrating the ACL as well as surrounding structures

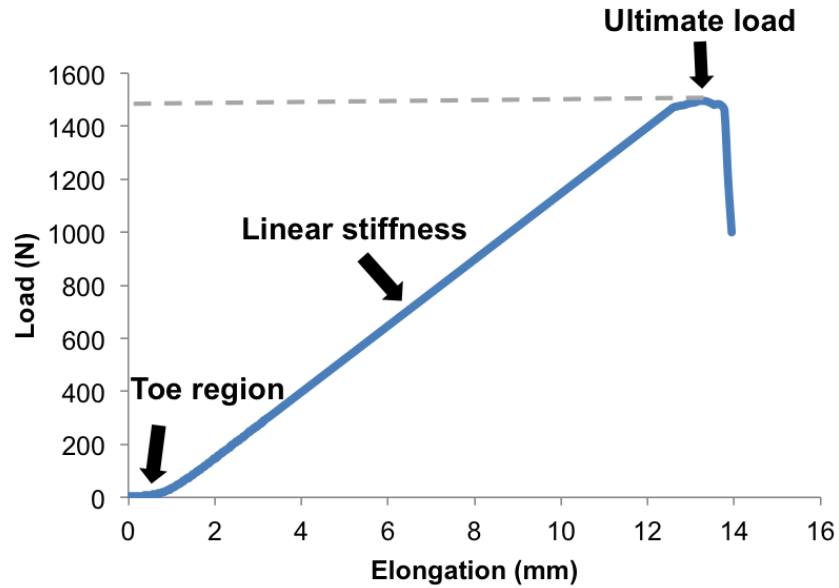


Figure 2: A representative load-elongation curve of a goat femur-ACL-tibia complex

Biochemically, the ACL also contains glycosaminoglycans, proteoglycans, elastin, and cells. Nutrition is mostly provided by the middle genicular artery, with branches extending along the length of the ACL beneath its protective synovial layer, as well as some endoligamentous vessels⁵⁵. Innervation of the ACL is by branches of the tibial nerve and consists of nerve fibers with vasomotor functions as well as mechanoreceptors, including Ruffini and Pacini receptors¹⁹. These provide a proprioceptive ability that serves to protect and prevent injury to the ACL^{28,90}.

1.2 ACL INJURIES

1.2.1 Incidence and consequence of ACL injuries

The ACL is the most frequently-injured ligament in the knee, with an estimated 200,000 injuries per year in the United States^{29, 84}. Most occur during sports-related activities through noncontact mechanisms that involve cutting, pivoting, or landing occurs with the knee near full extension⁸⁴. However, unlike extra-articular ligaments such as the medial collateral ligament (MCL), which heals spontaneously after injury¹⁰⁰, the intra-articular ACL has been shown to typically exhibit a poor healing response following injury, even in the case of a partial tear³⁶. The reasons for this limited healing capacity will be discussed in Section 1.3.3.

The loss of this key stabilizer can lead to many serious consequences. ACL deficiency results in immediate knee instability, primarily due to an increase in anterior tibial translation and internal rotation of the tibia that could result in persistent pain or buckling of the knee. With such a change in the knee kinematics, other supporting structures in the knee, including the medial meniscus, MCL, and the posterolateral structures would be subjected to large amounts of compensatory loading, increasing their risk of injury^{12, 110, 180}. These complications can have a significant effect on a patient's knee-related quality of life, particularly in the case of active patients. Many patients are forced to modify their activity level, and many athletes are not able to return to their previous sport⁵⁰.

In addition to the biomechanical changes that occur with ACL injury, biochemical changes related to cartilage degeneration have also been observed, even just one year after injury^{40, 156, 175}. As a result, long-term consequences of ACL injury can be catastrophic, as these degenerative changes in the knee can lead to the early onset of osteoarthritis¹¹. A recent meta-

analysis based on a number of long-term follow-up studies of ACL reconstruction has shown a significant risk for developing radiographic osteoarthritis. Compared to contralateral knees, this risk quadrupled at 10 years after surgery, regardless of whether the patient received surgical ACL reconstruction or underwent conservative treatment ⁸. The numbers are even more staggering for athletes, with one study reporting radiographic osteoarthritis in 78% of young male soccer players 14 years after ACL injury ²⁰⁷. Particularly in the case of younger patients with many years of knee function ahead, these degenerative effects could eventually lead to the need for extreme measures such as a total joint replacement.

1.2.2 Clinical treatments

The major aims of clinical treatments for ACL injury are to restore ACL function and knee stability to manage short-term symptoms, with the hope of precluding the development of osteoarthritis. These treatments have consisted of conservative management using rehabilitation programs, as well as surgical techniques.

1.2.2.1 Conservative treatments

Approximately one-third of patients today elect to undergo non-operative, conservative treatment for their ACL injury. Typically, conservative treatment consists of rehabilitation programs designed to strengthen the hamstrings and quadriceps muscles, restore balance and knee range of motion, in addition to recommended bracing ⁸².

The use of conservative treatment following ACL injury has been controversial. Although some have reported that the modification of physical activity and rehabilitation to

restore neuromuscular function led to good long-term knee function ^{46, 125}, many others have found less favorable results. Anterior and rotatory instability have been reported in a large number of patients, as well as subsequent injury to other structures in the knee ^{114, 119, 145}. Additionally, many conservatively-treated patients eventually sought surgical treatment to manage complications. In a follow-up study of 40 conservatively-treated patients (average age: 22 years, range: 15 – 43 years), 30% eventually elected to undergo surgical treatment within 4 years ⁹¹. Similarly, in a study of 18 conservatively-treated pediatric patients, one-third had elected to undergo surgery within 3 years post-injury ¹⁴⁷. Thus, due to the long-term consequences and risks associated with ACL deficiency, as well as the higher activity levels of younger patients, this treatment is now usually limited to older and less active patients with no concomitant knee injuries ^{31, 37, 75}.

1.2.2.2 Surgical repair

Surgical techniques were first developed in the 1960s to repair an injured ACL by reapproximating the torn ends using sutures ^{163 18, 162, 182}. However, due to the ACL's poor healing response, these studies generally achieved limited success. In 1976, a study by Feagin, et al. of West Point cadets who underwent primary repair after ACL injury demonstrated that by 5 years post-surgery, the majority of patients experienced poor functional outcomes, including reinjury, chronic instability, and impairment of daily activities ⁶¹. In 1983, a randomized control trial by Sandberg and colleagues demonstrated no difference between suture repair and conservative treatment of the ACL ¹⁸², while Engebretson and associates showed that replacing the injured ACL with a soft tissue graft (ACL reconstruction) provided significantly improved functional outcomes ⁵⁶. These findings led to a shift in the late 1970s and 1980s towards ACL reconstruction, which was successful in immediately restoring stability to the joint.

1.2.2.3 ACL reconstruction

ACL reconstruction has become the gold standard of treatment to restore knee stability following ACL injury to allow patients to return to sport or work, with the hope of also preventing the early development of osteoarthritis. Today, it is performed on approximately two-thirds of patients and is the sixth most common orthopaedic procedure ⁸⁴.

During an arthroscopic ACL reconstruction, the damaged ACL is removed and replaced with a soft tissue autograft or allograft, which is fixed into place within tunnels drilled in the femur and tibia. The most popular graft choice is the hamstrings tendon (semitendinosus and gracilis) ^{47, 143, 238}, although the bone-patellar tendon-bone (BPTB) graft has also been used ^{108, 184, 203, 230, 244}, as well as the quadriceps tendon ^{9, 42, 51, 201}.

Although human cadaveric studies ^{138, 235, 236} as well as short-term clinical studies ^{238, 239 4} have shown that ACL reconstruction could restore stability to the knee immediately after surgery, post-operative complications are common and can have a significant effect on a patient's knee-related quality of life. Graft failure and the need for a subsequent revision surgery occur in 10-15% of patients ^{79, 172}, and a significant number also experience include graft donor site morbidity ^{117, 197}, extension deficits ^{101, 116}, and persistent knee pain or numbness ^{48, 178}. Furthermore, the long-term benefits of ACL reconstruction are unclear, as data on its ability to reduce the development of knee osteoarthritis is lacking. In fact, results from many long-term follow-up studies have indicated a high prevalence of osteoarthritis following ACL reconstruction that was similar to that following conservative treatment ^{7, 50, 72, 105, 107, 119, 207}. For example, a recent study found that 10-15 years after ACL reconstruction, 71% of patients showed radiographic signs of osteoarthritis, and 24% were classified as moderate to severe (Kellgren and Lawrence grade 3 or 4) ¹⁶⁵. In another 14-year follow-up study, a three-fold

increase in the prevalence of osteoarthritis was found in ACL-reconstructed knees compared to contralateral uninjured controls²⁷.

There are multiple factors that may explain the mechanism behind these long-term complications following ACL reconstruction, some of which may actually be attributed to the injury rather than the surgery itself. For instance, degradative biochemical changes may have already begun to occur in the knee joint as a result of the ACL injury^{40, 156, 175}. Furthermore, concomitant injuries to other structures in the knee, such as the MCL or medial meniscus^{30, 50, 139}, may be problematic regardless of treatment of the ACL.

Other factors may be attributed directly to the ACL reconstruction surgery. An example of this would be iatrogenic problems including damage to the articular cartilage²⁴⁶ or nerves⁸⁹, as well as improper tunnel placement, widening, or over-drilling^{30, 126}. A lack of proper rehabilitation could also impede the recovery process post-surgery. However, perhaps the most significant problem with ACL reconstruction is the inability of the ACL replacement graft to replicate the biomechanical function of the native ACL. Clearly, with its irregular geometry and double-bundle structure^{55, 179}, it is not possible to duplicate the complex anatomy and function of the native ACL with a soft tissue graft. Secondly, the preferred autografts for ACL reconstruction (hamstrings tendon or BPTB grafts) have been chosen for their strength and do not match the stiffness of the ACL^{161, 228}. Together, these lead to altered knee kinematics and over time, they could result in degenerative effects including degradation of the articular cartilage.

1.2.2.4 Rationale for a new treatment option

With the prevalence of complications following ACL reconstruction, it is logical that either improvement in surgical technique would be warranted, or else replacement by a new treatment

option. Indeed, a plethora of modifications to ACL reconstruction have been described in scientific and medical literature throughout the past 30 years. A literature search in PubMed on “anterior cruciate ligament reconstruction” or “ACL reconstruction” as the search criteria yields over 6,000 scientific papers, many of these describing new surgical techniques, graft types, and fixation methods. This abundance of publications on new methods suggests that there is no reconstruction method capable of yielding good long-term results, and the quest to improve treatment for ACL injury is ongoing.

Rather than continuing to strive to improve reconstruction, an alternative treatment option could be considered to reduce or eliminate the associated complications. To this end, healing the ACL would be an attractive alternative to ACL reconstruction for many reasons. Similar to reconstruction, an effective ACL healing technique could be designed to restore knee stability immediately after surgery. But unlike reconstruction, healing the ACL would preserve its complex anatomy, biomechanical properties, and proprioceptive function. It would also eliminate the need for a soft tissue graft or large bone tunnels (up to 9 mm) drilled through the femur and tibia. With a less aggressive surgical procedure, patients would be able to heal faster and return to activities of daily living as well as sports-related activities. Finally, by preserving the ACL’s structure and biomechanical function, healing the ACL could succeed where reconstruction has not by preventing the early development of osteoarthritis.

Although the ACL’s low healing capacity is well known, new functional tissue engineering approaches have recently been developed that show promise in healing a variety of “hard-to-heal” tissues, including the ACL. These studies give hope to the idea that given the appropriate biological and mechanical environment, ACL healing could successfully occur.

However, to develop such an approach, understanding and overcoming the complex factors limiting its healing intrinsically would be required.

1.3 LIGAMENT HEALING

Different ligaments and tendons have been shown to exhibit unique healing responses following injury. For example, despite the low healing capability of the ACL and posterior cruciate ligament (PCL), the medial collateral ligament (MCL) exhibits a good healing response, even without surgical treatment^{71, 100, 227, 229}. It is likely that the healing response is multi-factorial, with mechanical forces, vascularity and nutrition, location in the body (intra-articular versus extra-articular), and cellularity modulating the healing process. Due to these differing healing capabilities, it is not possible to characterize a “typical” healing process for ligaments and tendons. However, in order to understand how to heal the ACL, it is useful to first understand the healing process of ligaments and tendons that exhibit a better natural healing response. The MCL has been extensively studied due to its relatively consistent healing, and is an excellent model to provide insight to understand the healing process and to help guide functional tissue engineering strategies that could be applied to the healing of other injured ligaments and tendons.

1.3.1 MCL healing

Studies of MCL injury have demonstrated spontaneous regeneration of a torn MCL^{71, 215}. Such studies have allowed for characterization of 3 distinct, overlapping phases of ligament healing: the inflammatory, reparative, and remodeling phases⁷¹. The inflammatory phase begins

immediately after injury and consists of formation of a hematoma, proliferation of cells from the surrounding tissue, and conversion of the clot into granulation tissue and collagenous tissue ⁷⁰. After about two weeks, in the subsequent reparative phase, the inflammation diminishes and newly formed collagen fibers continue to grow and strengthen. Finally, two to four weeks later, in the remodeling phase, the collagen fibers realign and mature into tissue that is similar to normal. However, unlike the inflammatory and reparative phases, which each last about two weeks, the remodeling phase lasts substantially longer, and sometimes months or years are required for the healing tissue to reach a pre-injury state ^{100, 215}.

In the case of the MCL, it has been found to heal better with non-operative treatment than surgical repair ²²⁴, even in the case of a concomitant ACL injury ^{17, 57}. However, animal studies have demonstrated that the gross morphology, biochemical composition, and biomechanical properties of the healing ligament remained abnormal even after a year ^{160, 164, 215}. With the hope of improving the quality of the healing MCL as well as other injured ligaments and tendons, new augmentation approaches for are being explored, collectively coined as “functional tissue engineering.”

1.3.2 Functional tissue engineering approaches

With the advent of tissue engineering around the 1980s, biological approaches were developed to improve the healing of injured or pathological tissues and organs. Branching from this, the term “functional tissue engineering” was coined in 1998 by the United States National Biomechanics Committee (USNBC) to describe the repair or replacement of an injured tissue with cells, scaffolds, growth factors, or proteins, with the goal of restoring its biomechanical function ³⁸. Among the factors of importance for the creation of such an approach are the understanding of

the native *in vivo* environment and tissue, including the time-varying stress and strain, fluid pressure and flow, and biomechanical properties. Clearly, with their important biomechanical functions, preserving or restoring these would be key for successful healing of injured ligaments and tendons. Thus, many researchers have applied principles of functional tissue engineering to improve the healing of these tissues, using a variety of methodologies.

1.3.2.1 Growth factors

Many growth factors have been identified that play important roles in the process of ligament and tendon healing, including fibroblast growth factor (FGF), transforming growth factor beta (TGF- β), vascular endothelial growth factor (VEGF), and platelet-derived growth factor (PDGF)^{148, 183}. As such, researchers have applied individual growth factors as therapeutic agents for functional tissue engineering, with promising results. For example, after surgical transection of the rabbit MCL, the administration of TGF- β 2 led to improvement in the structural properties of the healing femur-MCL-tibia complex (FMTC)¹⁹⁵. However, reported results have been mixed, particularly when a combination of growth factors has been employed. PDGF or a combination of PDGF and FGF also led to improvements in the structural properties of a healing bone-ligament-bone complex, although a combination of PDGF and insulin-like growth factor Type 1 did not¹²⁸. Similarly, the application of PDGF-BB led to improvements in the structural properties of the FMTC, while the addition of TGF β -1 did not result in additional improvements⁹² and TGF β -1 alone did not improve healing.

More recently, as an autologous source of multiple growth factors including PDGF-2 and VEGF, many have investigated the use of platelet-rich plasma (PRP) for soft tissue healing⁵⁸. PRP has also been applied clinically in a variety of musculoskeletal procedures, including

treatment of patellar ¹²⁴ and Achilles tendinopathy ⁷⁷, rotator cuff repair ¹⁷⁶, treatment of cartilage lesions ¹⁶⁶, and ACL reconstruction ¹⁶⁶. However, despite the clinical interest and widespread media coverage, the efficacy of PRP for treatment of musculoskeletal injuries remains unknown, as there have not been randomized controlled clinical studies demonstrating the efficacy of PRP treatment for ligament and tendon healing ^{168, 185, 200}.

1.3.2.2 Stem cells

In addition to the application of growth factors, stem cells have also been used for the healing of ligaments and tendons ^{44, 88, 127}. In a rabbit study, autologous, marrow-derived mesenchymal stem cells (MSCs) suspended in a collagen gel were found to improve the structural properties, cross-sectional area, and collagen fiber alignment following an Achilles tendon gap injury ²⁴¹. Similarly, MSCs were also found to improve the incorporation of a hamstrings tendon autograft following ACL reconstruction in a rabbit model, with a near-normal insertion site and increased stiffness and ultimate load compared to control groups ¹³⁴. However, as a therapeutic agent, the delivery mechanism and biological and mechanical environments would be important to ensure appropriate differentiation for the intended healing application ^{43, 249}.

1.3.2.3 Extracellular matrix scaffolds

Extracellular matrix (ECM) bioscaffolds are composed of naturally-occurring ECM derived from animal or human tissue that has been decellularized and lyophilized ²². Common sources include the porcine small intestine submucosa (SIS) ^{20, 24, 122, 174} and urinary bladder matrix (UBM) ^{21, 23}. These scaffolds have been used since the 1990s for the healing of various injured tissues and organs, and can be prepared as single or multi-laminate sheets ⁷³ as well as powders ^{81, 205, 231}. By retaining the natural composition of the tissue (collagen, elastin, glycosaminoglycans,

glycoproteins, and growth factors)^{22, 93, 209}, as well as retaining their natural architecture, the scaffolds and their degradation products could assist in biological and mechanical augmentation of an injured tissue to promote site-specific, constructive remodeling⁵³. With an additional pepsin digest, an ECM hydrogel can also be prepared to be used for injectable applications^{74, 221, 222}. Many ECM-derived products have been approved by the Food and Drug Administration and used clinically for therapeutic applications²¹, including those in orthopaedic applications^{53, 206}. In the past 15 years, millions of allogeneic and xenogeneic ECM scaffolds have been implanted in patients worldwide¹¹⁸.

The host response to ECM bioscaffolds involves the source tissue, processing methods, and other device-specific factors¹¹⁸. Ultimately, the goal of ECM scaffolds is to manipulate the healing response away from scar tissue deposition and towards the site-specific regeneration of functional tissue. The mechanism behind which these scaffolds promote constructive remodeling is not yet completely understood, but is heavily influenced by the recruitment of stem and progenitor cells to the injury site⁵, as well as modulation of the immune response⁶⁷. In particular, a relationship between T helper (Th) cell response and constructive remodeling has been found, whereby ECM scaffolds promoted the Th2 phenotype (wound-healing, anti-inflammatory¹⁴⁶) as opposed to the Th1 phenotype (pro-inflammatory, implant rejection)²¹. Similarly, macrophage polarization has been found to be a strong indicator of the healing response, and ECM bioscaffolds have been found to promote the M2 phenotype (anti-inflammatory, constructive remodeling¹⁶) in favor of the M1 phenotype (pro-inflammatory, pathogen killing)^{26, 188}.

ECM bioscaffolds have yielded promising results when used for the healing of ligaments and tendons^{25, 80, 152}. For example, when used for repair of a 1.5 cm Achilles tendon defect in

dogs, a multi-laminate scaffold derived from the porcine SIS had fully degraded by 60 days after surgery, and by 90 days had been replaced with organized, aligned collagen tissue that was histologically similar to that of the native tendon⁸⁰. In addition, when a 10-ply multi-laminate SIS sheet was applied to repair a completely resected infraspinatus tendon in dogs, the defect was completely filled in by 3 months of healing⁵². The gross and histologic appearance of the healing tendon was similar to the native tendon, with a well-organized, aligned collagen matrix.

With these promising results using ECM scaffolds for tissue regeneration, our research center has studied the application of these scaffolds for the healing of an MCL gap injury^{133, 152, 225} as well as a patellar tendon defect¹¹⁵. When an SIS sheet was applied to a 6 mm gap injury of the rabbit MCL, the SIS-treated MCL had improved collagen fibril alignment with larger collagen fibril diameters compared to a control group with a non-treated defect, as well as a collagen V/I ratio that was closer to that of the native MCL²²⁵. Results of uniaxial tensile testing also showed that the SIS-treated FMTC had a tangent modulus that was 88% higher than that of the control group. When this study was extended to 26 weeks of healing, the mechanical properties of the healing MCL were again improved significantly over the control group, with a 33% increase in Young's modulus and a 50% increase in tensile strength¹³³.

In addition to the MCL, our research center also explored the application of SIS for the healing of a patellar tendon defect, applying SIS strips to the anterior and posterior sides of a central-third defect in rabbits¹¹⁵. By 12 weeks of healing, the defect had been filled in completely with healing tissue, whereas the neo-patellar tendon in a non-treated control group could not fill the space. The SIS-treated patellar tendons were also composed of collagen fibers with better organization and alignment than those of the control, with more spindle-shaped cells. Biomechanically, the stiffness of the SIS-treated bone-patellar-tendon-bone complex was 98%

higher than that of the non-treated group, and the ultimate load was 113% higher. Thus, the results of these studies demonstrated the potential of ECM bioscaffolds to successfully heal ligaments and tendons.

1.3.3 Challenges for ACL healing

With the advances in functional tissue engineering and promising results demonstrating the healing of other tissues, healing the ACL has become an encouraging possibility in spite of its low intrinsic healing capability. However, the limitations to ACL healing are complex and multi-factorial, and pose a unique challenge for functional tissue engineering. In humans as well as in animal models, it has been observed that the ACL rapidly degenerates after injury in as little as 6 weeks^{14, 213}. Although the mechanism behind this rapid degeneration is only partially understood, it is clear that biological and mechanical factors both play a significant role.

Biologically, differences observed between the MCL and ACL *in vitro* and *in vivo* have shed light on the mechanisms behind the ACL's poor healing response. In a side-by-side comparison of primary cell lines derived from the ACL and MCL, ACL fibroblasts were found to exhibit significantly reduced proliferation and migration^{15, 153}, as well as a differential expression of matrix metalloproteases (MMPs) and tissue inhibitors of metalloproteases (TIMPs)²⁴⁸. This suggests that even at the cellular level, the ACL is at a disadvantage for healing. The ACL has also been found to have reduced cellularity and vascular supply compared to the MCL, which could also limit its healing response^{34, 55}. In a rabbit study of partial transection of the ACL or MCL, the MCL was found to have increased blood flow and an angiogenic response, while the ACL had a minimal vascular response and showed signs of atrophy^{33, 35}. Finally, the

loss of the synovium is likely one of the ACL's most significant biologic barriers to healing, as this outer sheath protects it from the harsh synovial environment of the knee joint. Indeed, it was found that removal of the synovial layer led to an increase in collagenase production and degradation of the ACL remnants¹³. The exposure of the injured ACL to synovial fluid following the loss of the synovium could in turn prevent the formation of a hematoma, which would be a crucial step in the healing process as a bridging scaffold between the two torn ends.

In addition to these biological factors, mechanical factors also limit the ACL's ability to heal. Due to its primary role in knee stability, a gap would form between the two torn ends following injury, with its width changing based on the loading of the knee. Thus, even if a bridging scaffold were able to form, the slowly-forming neo-tissue would likely be pulled apart before it could fully regenerate.

With these multi-factorial barriers to healing, a functional tissue engineering strategy to successfully heal the ACL would face particular obstacles to overcome them.

1.3.4 Current and new approaches to ACL healing

Much as the barriers to ACL healing can be divided into biological and mechanical factors, the strategies employed to engineer the healing of the ACL can be divided similarly. Since the 1990s, the majority of work on ACL healing has focused on biological augmentation of the injured ACL to help to stimulate and accelerate tissue growth and remodeling. However, within the past 10 years, mechanical augmentation methodologies have also been explored, and most recently, these techniques have been combined for a combined approach for ACL healing.

1.3.4.1 Biological augmentation

Early work on biological augmentation of an injured ACL included the application of hyaluronic acid ²¹⁶, individual growth factors ¹²⁰, and mesenchymal stem cells ^{6, 113}. These studies reported increased neo-tissue formation and organization of the healing ACL compared to an untreated control group, but the morphological appearance and biomechanical function of the healing ACL were abnormal and inferior to that of the native ACL.

For the past 10 years, Murray and associates have studied ACL healing using a collagen-PRP hydrogel, which was injected into the defect of a transected ACL to act as a bridging scaffold between its two torn ends ¹⁵¹. By 15 weeks of healing in a porcine model, the addition of PRP led to significant improvements in neo-tissue formation and remodeling, structural properties of the FATC, and cellularity compared to a second group treated with a collagen hydrogel alone. However, significant hypertrophy of the PRP-treated ACL was observed, with the average cross-sectional area more than twice that of the normal ACL. The structural properties of the healing FATC were also found to be significantly lower than those of the normal FATC, reaching only 26% and 18% of its stiffness and ultimate load, respectively. Thus, treatment of the ACL with the collagen-PRP hydrogel led to abundant scar tissue formation that did not restore its biomechanical function. The authors speculated that this may be due to the inability of the suture repair technique to restore stability to the joint immediately after surgery, which could affect the loading and remodeling of the healing ACL ¹⁵⁰.

Given the encouraging results in our research center using scaffolds derived from the porcine ECM for the healing of a patellar tendon defect ¹¹⁵ and a 6 mm wide MCL gap injury ^{133, 152}, these scaffolds were next applied in sheet and hydrogel form to successfully heal a fully transected ACL in a goat model ⁶⁶. At 12 weeks post-surgery, the healing ACL had an organized

collagen matrix with spindle-shaped cells, but without hypertrophy. Biomechanical testing revealed that the stiffness of the healing femur-ACL-tibia complex (FATC) was 2.5 times greater than suture repair alone, and the ultimate load was 90% higher. These results on the gross morphology and tensile properties were close to those obtained in another study that utilized ECM bioscaffolds with a locking suture repair technique for healing of a transected ACL in goats ¹⁵⁸.

However, when our laboratory performed a second study at a subsequent longer time point; i.e., 26 weeks, the mode of failure was found to have moved from the midsubstance (at 12 weeks) to its femoral insertion. This was a result of continuing improvement of the healing ACL while its insertion sites became weakened due to the lack of adequate stress in the FATC ²²⁷. These results also suggested that biological augmentation alone was not able to adequately load the ACL, and mechanical augmentation would be needed to limit the disuse atrophy of its insertion sites.

1.3.4.2 Mechanical augmentation

Published *in vitro* ^{65, 68} and *in vivo* ¹⁵⁰ studies have shown that mechanical augmentation of an injured ACL could help to stabilize the knee, leading to improvement in its healing. For example, when sutures were applied to provide bone-to-bone fixation between the femur and tibia, joint stability could be restored, as well as the functions of the ACL and medial meniscus when the knee was subjected to externally applied loads ⁶⁵. The same technique used in an *in vivo* study also led to an improved healing response of a transected ACL when compared with a suture repair technique alone ¹⁵⁰. However, due to the slow process of ACL healing and aforementioned limiting factors, mechanical augmentation alone would also not be able to successfully regenerate an injured ACL.

1.3.4.3 Combined biological and mechanical augmentation

While biological and mechanical augmentation have separately shown promise in healing a transected ACL, it is likely that a combined form of biological and mechanical augmentation would be required for its full regeneration. While mechanical augmentation would restore stability to the knee immediately after surgery and help to load the healing ACL to prevent disuse atrophy of its insertion sites, biological augmentation would stimulate and accelerate the healing response. Combined, these approaches would work together to restore both the form and biomechanical function of the native ACL.

Murray and colleagues studied ACL healing using combined biological and mechanical augmentation in a porcine model ¹⁵⁰. Using bone-to-bone fixation between the femur and tibia to complement their collagen-PRP hydrogel, they found improvements in the structural properties of the FATC compared to a second group with collagen-PRP hydrogel alone. However, no differences could be observed in the anterior-posterior joint laxity, which was significantly higher than that in the normal joint. Furthermore, the structural properties of the healing FATC in both treatment groups remained well below those of the normal FATC. Thus, further work on ACL healing using combined biological and mechanical augmentation is warranted.

1.4 MAGNESIUM AS A BIOMATERIAL FOR ORTHOPAEDIC APPLICATIONS

1.4.1 Background on orthopaedic biomaterials

Biomaterials are often used in orthopaedic surgery for bone substitutes, fixation, and stabilization of fractured bones, ligament and tendon reconstruction procedures, total joint arthroplasties, and

so on. Historically, non-degradable metals, namely stainless steel, cobalt-chromium, and titanium alloys, have been commonly used because they possess good mechanical strength, biocompatibility, and corrosion resistance. However, because they do not degrade and remain present in the body indefinitely, their removal requires secondary surgeries. In addition, due to wear processes, they sometimes release toxic metallic particles into the body that could lead to a cytotoxic response^{103, 104, 194, 212}.

However, with the advent of functional tissue engineering, the potential for regenerating tissues as well as their biomechanical function has been realized. Thus, bioresorbable materials have gained much attention and their usage has increased, as they could be replaced by the patient's own tissue over time, as well as be used for delivery of bioactive molecules to improve healing of various hard and soft tissues¹⁵⁵. These biomaterials are chosen based on the needed properties for the desired application, including specific mechanical properties, porosity, degradation profiles, biocompatibility, and adherence and incorporation into adjacent tissue.

Depending on the specific structure, properties, and function of the tissue to regenerate, there are now many options for biomaterials in orthopaedic surgery¹⁵⁵. For the repair or replacement of ligaments and tendons, fibrous collagen, extracellular matrix, silk, and synthetic polymer scaffolds have been explored^{78, 206, 245}. In addition, hydrogels have become an attractive option to fill irregularly-shape voids and aid in the delivery of cells, growth factors, and other bioactive molecules⁵⁴. For regeneration of the soft tissue-to-bone interface (e.g. ACL insertion to the femur), polymers have become a popular choice as they can be engineered to possess multi-phasic properties¹⁴⁰.

However, polymeric materials may not be an ideal choice for some orthopaedic applications. With poly-L-lactic acid (PLLA) interference screws were used for graft fixation

during ACL reconstruction, the devices often fractured during implantation due to their brittleness ¹⁹⁰. Further, their rate of degradation varied greatly between patients and in most cases was very slow, with the screw remaining intact even after 2 years ¹⁰⁶. Also, after degradation, the void left was not filled with regenerating bone. A 10-year follow-up study showed that an osseous cyst had formed after complete degradation of an interference screw ²¹⁰. Thus, an alternative resorbable biomaterial that eliminates these complications would be advantageous.

To this end, one of the most promising classes of orthopaedic bioresorbable materials is magnesium (Mg) and its alloys. Due to the advantageous and desirable properties of these materials, there has recently been increased interest in these materials for biomedical applications. In fact, a search of Web of Science using “magnesium” and “stainless steel” as search queries under the category “biomaterials” revealed that the number of publications on Mg has exponentially increased in the past ten years, compared to those on stainless steel, which only saw a modest increase (Figure 3).

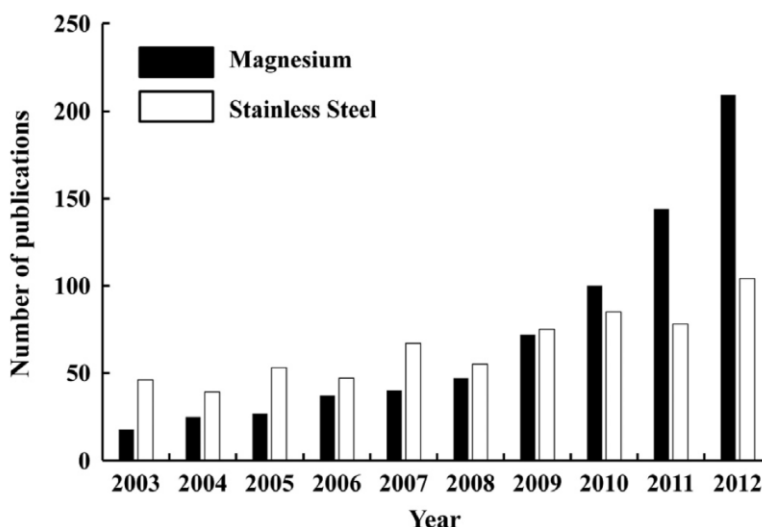


Figure 3: Histogram showing the number of publications each year on research of Mg and its alloys and stainless steel as biomaterials

Mg-based materials have significantly lower moduli than titanium-based materials (41-45 GPa vs. 110-117 GPa)⁹⁷. As a result, their mechanical properties are closer to those of cortical bone and could reduce the level of stress-shielding when used as bony implants. In terms of tensile strength, Mg-based materials are 3-16 times stronger than polymers (160-250 MPa vs. 16-69 MPa). They are also more ductile and have a higher ultimate strain that reaches up to 16%, which could reduce the risk of device fracture during implantation. These alloys have the mechanical properties required to meet loading requirements during and after implantation, but would not interfere with common imaging modalities for post-operative care, such as MRI and CT.

1.4.2 Biocompatibility

The biocompatibility of Mg in humans has been well established, as it is naturally present in the human body and is responsible for numerous physiological processes, including protein synthesis, control of blood glucose, nerve and muscle function, development of bone, maintenance of normal heart rhythm, and regulation of blood pressure^{198, 208}. The adult human body contains about 1 mol (24 g) of Mg, which is found primarily in the bone (60-65%) and muscles (27%). Mg in the body can be acquired through diet, medication, or commercially-available oral supplements, with a recommended maximum intake of 250-350 mg per day. Uptake of Mg in the human body is mostly through the ileum and jejunum, with excess excreted through the kidneys. Due to the body's ability to eliminate excess Mg, high doses in a healthy individual are generally not problematic; however, Mg toxicity has been noted with extreme intakes (> 5,000 mg/day).

1.4.3 Historical use of Mg for orthopaedic implants

The initial use of bioresorbable Mg implants in orthopaedic surgery was during the early twentieth century, with Mg implants used for regaining or preservation of joint motion, fracture fixation, and bony separation ²¹⁷. In both human and animal studies, a number of investigators reported that Mg implants stimulated soft tissue production and promoted new bone growth, while being completely resorbed over time ^{144, 252}.

However, the most common complication was rapid degradation, coupled with pockets of hydrogen gas formation around the Mg implants ²¹⁷. Although the gas evolution was reported as not harmful to the surrounding tissue and did not cause any adverse clinical effect such as infection, the inability to control the rate of degradation *in vivo* led to the abandonment of the use of Mg. Surgeons had then gone on to use more corrosion-resistant metals, such as stainless and titanium.

1.4.4 Recent advances in Mg materials

To combat the aforementioned challenges involving the use of Mg in orthopaedics, new methods for alloying, coating, surface treatment, and processing have been developed to control mechanical properties, corrosion rate, and biocompatibility. These have resulted in the development of materials with improved properties that have renewed the possibility that Mg could be promising for orthopaedic applications.

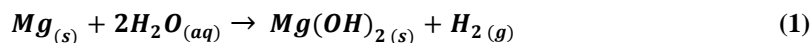
1.4.4.1 Alloying and mechanical properties

With a yield strength of 21 MPa as-cast and 115-140 MPa as-rolled, pure Mg possesses mechanical properties that may be not be strong enough for loading-bearing biomedical applications²⁵¹. However, the alloying of Mg with various elements has led to the development of many materials with greatly enhanced mechanical properties. With these improvements, Mg materials are better-suited for use as biomaterials for orthopaedic applications, where the ability to withstand loading without failure is of key importance. Among the most common Mg alloys are those including aluminum (Al), which increases the corrosion resistance by forming an insoluble layer of Al_2O_3 on its surface when exposed to simulated body fluid (SBF)²¹⁹. Al has commonly been alloyed with zinc (Zn) to produce popular alloys AZ31 (3% Al, 1% Zn), AZ61 (6% Al, 1% Zn), and AZ91 (9% Al, 1% Zn)¹²¹, as Zn increases material strength and is accepted to be biocompatible^{41, 219}. With its similar advantageous properties, calcium (Ca) has also commonly been used as an alloying element in Mg alloys, and is particularly attractive for bone healing applications^{130, 131}. Recently, rare earth metals, including yttrium (Y), zirconium (Zr), and neodymium (Nd) have also been used in Mg alloys due to their improvements on the mechanical properties, creep resistance, and corrosion rate of Mg^{45, 96, 97, 220}.

In addition to altering its composition by alloying, others have used different strategies to modify the microstructure of the Mg material to change its properties. For example, a Mg calcium phosphate scaffold was designed to be porous in order to have its mechanical properties similar to those of cancellous bone, thus making it ideal to be used as a bone substitute²¹⁴. Others have investigated the growth of monocrystalline forms of Mg (single crystal Mg), which eliminates grain boundaries and has improved ductility, exhibiting superplastic behavior^{109, 135, 186, 187, 193}.

1.4.4.2 Corrosion behavior

Pure Mg degrades in an aqueous environment via an electrochemical reaction to produce magnesium hydroxide and hydrogen gas (Equation 1).



Although these corrosion products are not cytotoxic, the rapid degradation of pure Mg is of concern for medical applications, particularly when corrosion-enhancing impurities are present, such as iron, copper, or nickel²⁵¹. The accompanying generation of excess amounts of hydrogen gas would be undesirable for clinical applications, as it could impede healing and lead to complications. As noted in Section 1.4.3, this has historically been the most significant limiting factor in the use of Mg in orthopaedic applications²¹⁷.

Fortunately, with advances in alloying and processing capabilities, the corrosion rate of Mg materials has been greatly improved. Elements that have been shown to improve the corrosion resistance of Mg include Al¹⁹², Y²¹⁹, Ca²³², Mn²³⁴, Zn¹⁹¹, and Zr¹⁹¹. Modifications of the material surface using treatments and coatings have also been developed to slow the corrosion of Mg^{102, 251}. One of the most well-established surface coating to reduce the corrosion rate of Mg alloys is the generation of a surface oxide layer using anodization. Techniques including anodic oxidation and micro-arc oxidation (also called plasma electrolytic oxidation, or PEO) have been commonly used for their corrosion-resistant properties^{32, 85, 243}. A calcium-phosphate (Ca-P) coating can also be achieved through relatively simple chemical treatment and has been shown to slow down degradation of AZ31 by 2 orders of magnitude¹⁰². Further, polymers such as PLGA have been used to control degradation of Mg-based alloys¹⁶⁷, although

challenges of durability still remain. Other coating methods that have been shown to be effective are physical vapor deposition of high-purity Mg¹⁸¹, fluoride treatment^{218, 237}, and alkaline-heat treatment⁸⁶.

1.4.4.3 *In vitro* and *in vivo* cytocompatibility and healing potential

However, despite the promise of new Mg materials with enhanced mechanical and corrosion properties, their cytocompatibility must be demonstrated to determine their potential to be used in biomedical applications. To this end, a number of experiments have been performed to screen for cytocompatibility of these materials using *in vitro* and *in vivo* experiments.

By culturing U2OS (osteoblast) cells with or without a Mg (99.95% purity) sample, it was found that there were no differences in cell viability or proliferation, not mineralization²⁴². Similarly, when fibroblasts, osteoblasts, or blood vessel-related cells were cultured on 9 different Mg alloys, no significant reduction in cell viability was observed⁸⁷. But in addition to being cytocompatible, many studies have indicated that Mg may elicit a therapeutic effect on cellular activity. When mouse fibrosarcoma cells (L-929) cells were cultured with extracts prepared from Mg alloys, increased viability was found compared to control groups¹³¹. Further, a Mg-based alloy (AZ21; Al 2% wt and Zn 1% weight) could support stromal cells and promote their differentiation toward osteoblast-like phenotypes *in vitro*¹⁷¹. Using a scaffold with a biomimetic, porous microstructure also proved to be positive for cellular activity, as MG63 cells seeded on a microporous/macroporous Mg-Ca-P scaffold showed significantly better cell proliferation and attachment as well as osteoblast differentiation than those seeded on a Ca-P cement scaffold²¹⁴. Incorporating coatings to these alloys has also been shown to elicit a

beneficial effect on cells. For example, when L-929 cells were cultured on a Ca-P-coated Mg-Mn-Zn alloy, significant improvements in cell proliferation were found ²³³. Thus, these *in vitro* experiments demonstrated that Mg and its alloys are cytocompatible.

In contrast to these positive results, it should be noted that some *in vitro* studies using static cell culture have reported significant reduction in cell viability when cultured with high concentrations of extracts prepared from Mg materials ^{45, 96}. This is believed to be due to osmotic shock caused by the increased osmolality of the extract solution, as well as the increased pH of the extract solution as the Mg alloy degrades. However, these high concentrations are believed to be outside of the physiological range expected *in vivo*, and ten-fold extract dilutions have thus been recommended to study the cytotoxicity of Mg materials ^{62, 211}.

Following *in vitro* experiments, live animal studies have also been conducted to evaluate the *in vivo* biocompatibility and degradation of Mg and its alloys for orthopaedic applications. To date, a majority of these experiments have focused on the use of Mg for bone healing applications. These studies have demonstrated that Mg-based materials are biocompatible with potential osteoinductive effects as well.

In a comparative study, 4 alloys, including AZ31 (Al 3% wt, Zn 1% wt), AZ91 (Al 9% wt, Zn 1% wt), WE43 (Y 4% wt, other rare earth metals 3% wt, and Zr 0.4% wt), and LAE442 (Li 4% wt, Al 4% wt, and rare earth metals 2% wt) were implanted in the femora of guinea pigs for 6 and 18 weeks ²²⁰. The degradable polymer, poly-96L/4D-lactide was used as a control. In the Mg alloy groups, there were statistically significant increases in bone mass and mineral apposition rate at both 6 and 18 weeks, as well as more trabecular-like structures compared to the control. Furthermore, when Mg-Ca rods were implanted in the femora of rabbits, the implants were found to have degraded within 3 months, with new bone formation and high activity of

osteoblasts and osteocytes at the implant site ¹³¹. Thus, the osteoinductive capacity of Mg-based materials could be demonstrated.

Investigators have also alloyed or coated Mg with elements naturally found in the human body, e.g. Ca, Zn, Mn, F, etc. to test their *in vivo* biocompatibility and osteoinductivity. Zhang, et al. tested a Mg-Zn-Mn alloy in the femora of Sprague-Dawley rats and observed significant degradation (~50%) at 26 weeks together with newly formed bone on the degrading surface without fibrous tissues ²⁴⁷. In another study, a Mg-Zn alloy was coated with magnesium fluoride (MgF₂) and implanted in the femora of New Zealand white rabbits ²⁰². Although the presence of the coating was not found to significantly affect the corrosion resistance of the implants, by 3 and 6 months, there was significant endosteal and periosteal growth on both coated and uncoated implants, with bone trabeculae tightly adhered to the implant surfaces.

Modifying the porosity of the Mg scaffold was also explored *in vivo*. When a microporous/macroporous Mg-Ca-P scaffold was implanted into femoral bone defects in rabbits, new bone tissue had formed into the pores of the scaffold by 2 months of healing, and after 6 months, the majority of the scaffold had degraded. In fact, 81% of the bone defect had been replaced by new bone tissue by 6 months, compared with just 47% in a microporous/macroporous calcium phosphate control. Additionally, numerous osteoblasts were visible in a newly-formed osteoid matrix, and the interface between the scaffold and bone was no longer visible ²¹⁴. Thus, the combination of a Mg alloy with a porous structure may be advantageous as a biomimetic approach to functional tissue engineering of bone.

These *in vivo* studies demonstrated that Mg materials could promote bone formation and appropriate degradation rates for replacement by new bone tissue, without cytotoxic effects.

These positive results encourage the further study and development of Mg devices for orthopaedic applications.

1.4.5 Rationale for use of Mg for ACL healing

With the aforementioned advantages for Mg and its alloys, these biomaterials are promising for mechanical augmentation of an injured ACL. They are lightweight and possess suitable mechanical properties such that they could withstand loading *in vivo* without fracture or loss of form; however, due to their ductility, they could undergo deformation to conform to the geometry of the knee to potentially prevent damage to the cartilage, menisci, and other knee structures. In addition, the known biocompatibility of Mg would be attractive for the clinical translation of an ACL healing device. But most importantly, because Mg alloys possess controllable degradation, with measured mass loss rates for different Mg alloys determined to be from $< 0.1 - 100 \text{ mg cm}^{-1} \text{ day}^{-1}$ ¹²¹, an alloy and corrosion-resistant surface coating could strategically be selected to allow for the gradual transfer of loading from the mechanical augmentation device to the healing ACL throughout the healing process (3 – 6 months). As illustrated in Figure 4, the Mg device would protect the injured ACL immediately after surgery by assuming the normal function of the ACL, allowing neo-tissue to form between its two torn ends. Then, as the ACL healed and the device degraded, the contribution to ACL function would shift to the healing ligament. Eventually, the device would disappear, leaving only a healed, functional ACL.

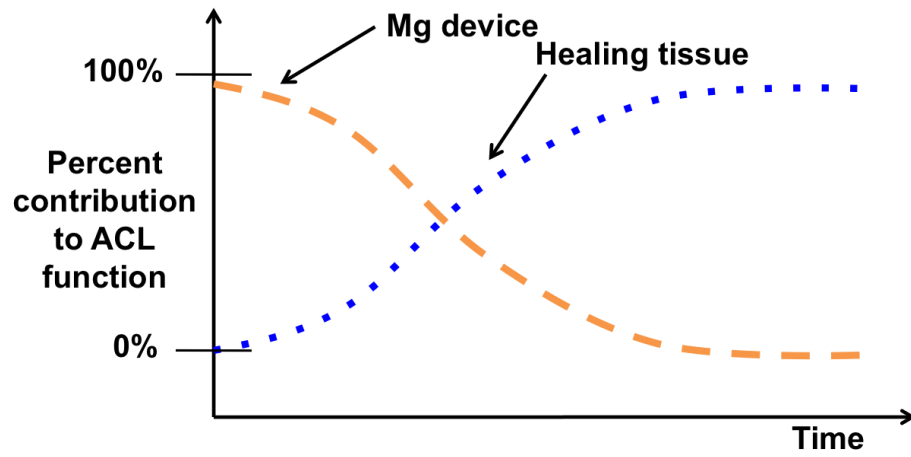


Figure 4: Gradual shift in the contribution to ACL function over time of a Mg device versus the healing tissue

2.0 OBJECTIVES

2.1 OVERALL GOALS

The overall goal of our research center was to develop a novel approach to heal and regenerate a torn ACL by means of combined biological and mechanical augmentation. The specific objectives of this dissertation were to develop a “ring” device made of bioresorbable Mg to reconnect the two ends of a transected ACL, and to quantitatively evaluate its potential for ACL healing *in vivo* when used alongside extracellular matrix bioscaffolds. To accomplish these objectives, the following three Specific Aims were proposed.

2.2 SPECIFIC AIMS

Specific Aim 1: *To design a Mg ring device for mechanical augmentation of a surgically transected ACL in a cadaveric goat model.* Although biological augmentation has shown promise in healing a transected ACL, mechanical augmentation is also needed due to its slow healing process to restore joint stability and load the ACL so that deterioration of its insertion sites due to disuse atrophy in the early stages of healing could be prevented. As a result, a bioresorbable, ring-shaped device made of magnesium (Mg) was designed to reconnect the two ends of a transected ACL. Mg and its alloys were selected as a material for this device because

they possess controllable degradation and suitable mechanical properties, as well as known biocompatibility. For this Aim, we wished to address the following research questions:

- 1) Could a Mg ring device be designed and manufactured to connect the two ends of a surgically transected goat ACL?
- 2) What would be the preferred geometry and Mg material such that the device would be suitable to withstand loading *in vivo*?

Specific Aim 1.1: *To design and fabricate a Mg ring device and develop a corresponding suture technique for repair of a surgically transected ACL in a cadaveric goat stifle joint.*

Success Criteria: The Mg ring design must be successfully manufactured from Mg stock materials, suitable for implantation to repair a surgically transected goat ACL, and able to load the ACL upon implantation by bringing together the transected ends.

Specific Aim 1.2: *To evaluate the Mg ring device design using a parametric finite element analysis to select a suitable design for further in vitro and in vivo testing.* Testing of preliminary prototypes indicated that applying anterior tibial loads to a cadaveric goat stifle joint after implantation of the Mg ring (Mg ring repair) could lead to deformation or fracture of the device. *In vivo*, premature failure of the device may be problematic as it could compromise device function as well as release Mg fragments into the joint space. We thus sought to address the research question of whether modifying the device design or Mg material could reduce the potential for device fracture. The selection of a suitable Mg ring design was made based on results of a finite element analysis after applying loads simulating in-situ forces on the device after Mg ring repair. Parameters of interest were suture hole diameter, notch depth, and Mg alloy, and model outputs were the maximum Von Mises stress and stress distribution.

Success Criteria: The maximum Von Mises stress in the Mg ring device as determined by the finite element analysis must not exceed the failure strength of the selected Mg material. A suitable design will also be selected based on its ability to reduce the maximum stress and stress concentrations on the device.

Specific Aim 2: *To quantitatively evaluate the ability of the Mg ring repaired ACL to restore stifle joint kinematics and in-situ forces in the repaired ACL.* For successful mechanical augmentation of an injured ACL, it would be necessary to restore joint stability and in-situ forces in the ACL to near normal levels such that it would be adequately loaded throughout the healing process. *In vitro* testing using cadaveric goat stifle joints was performed to evaluate the stifle joint kinematics and in-situ forces in the Mg ring-repaired ACL at three preselected angles of joint flexion under externally-applied loads simulating those used in clinical examinations.

Hypothesis: Previous work in our research center on repair of a transected ACL has shown that suture repair could restore anterior tibial translation to within 9 mm of the joint with the intact ACL, and in-situ forces in the ACL to within 12 N of normal^{64, 65}. Due to the additional mechanical augmentation provided by Mg ring repair, we hypothesized that the Mg ring-repaired ACL would be able to restore anterior tibial translation of the Mg ring-repaired ACL to within 6 mm of that of the intact joint, and in-situ force in the repaired ACL to within 10 N of those in the intact ACL.

Specific Aim 3: *To evaluate the biocompatibility and efficacy of the Mg ring for ACL healing.* While Mg and its alloys are generally considered to exhibit suitable biocompatibility, some studies have also reported potential enhancement of the healing response when used in

applications such as bone and blood vessel regeneration. However, the use of Mg for healing of ligaments and tendons has not yet been studied. As the Mg ring was intended to be combined with ECM bioscaffolds, knowledge of therapeutic effects of Mg would be important *in vivo* to help to understand whether ECM alone is modulating the healing response, or if Mg could also enhance healing. Thus, we first wished to assess address the research question: What are the effects of Mg materials on the growth and function of goat ACL fibroblasts? With these results, we proceeded to a live animal model to address the question: Could mechanical augmentation using the Mg ring combined with biological augmentation using an ECM bioscaffold lead to successful healing of a surgically transected goat ACL?

Specific Aim 3.1: *To determine the effects of single crystal Mg and 4 Mg alloys on goat ACL fibroblasts in terms of cell growth and function.* Extracts of single crystal Mg and 4 Mg alloys (Mg-Zn-Sr-Zr alloys ZJ40 and ZJ41, Mg-Ca-Zr, and AZ31) were prepared by incubating Mg stock materials in cell culture media. These extracts were diluted serially and used to culture goat ACL fibroblasts. At 3 days of culture, the resulting cell proliferation and total soluble collagen produced were measured.

Hypothesis: Recent literature from *in vitro* and *in vivo* studies has suggested that Mg may enhance cellular function and tissue healing in orthopaedic applications^{131, 171, 214, 220, 233}. Thus, we hypothesized that lower extract concentrations considered to be physiologically relevant^{62, 211} (< 25% extract) would lead to significantly higher levels of cell proliferation and collagen production compared to non-supplemented cell culture media. However, at higher extract concentrations (\geq 25% extract), the proliferation and collagen production would both decrease due to osmotic shock caused by the increased osmolality of the extract solution.

Specific Aim 3.2: *To assess the positive effects of the Mg ring in combination with an extracellular matrix bioscaffold on healing of a surgically transected goat ACL at 6 and 12 weeks.* For a 6-week pilot study, the gross morphology, histological appearance, and degradation of the Mg ring were assessed. For the 12-week study, the cytology and total protein content of the joint synovial fluid, joint stability, in-situ forces in the ACL, and structural properties of the femur-ACL-tibia complex of treated joints and their respective contralateral sham-operated controls were measured.

Hypothesis: We hypothesized that combining the Mg ring (mechanical augmentation) with the ECM bioscaffold (biological augmentation) would lead to improved ACL healing, as the Mg ring stabilized the stifle joint and loaded the healing ACL, while the ECM bioscaffold stimulated and accelerated the healing response. As a result, the joint stability, biomechanical properties of the femur-ACL-tibia complex, and histomorphology of the healing ACL would be enhanced.

3.0 DESIGN AND FINITE ELEMENT ANALYSIS

3.1 GEOMETRY

The design of the Mg ring device began with the concept of reconnecting the two transected ends of the ACL using a cylindrical sheath. To design such a device, physical dimensions were first calculated based on the geometry of the goat ACL (Table 1, Figure 5A). The “working length” was defined as the area of the ACL that a surgeon would have access during to during a surgical procedure, and was limited by the depth of the femoral intercondylar notch. The diameter and cross-sectional area (CSA) were expressed as a range, as these measurements increased in the superior-inferior direction.

For the purposes of the Mg ring device, the ACL was approximated to be cylindrical in shape, an assumption supported by cross-sectional area measurements derived from a custom laser micrometer system²²³ (Figure 5B). Thus, a cylindrical design of dimensions slightly larger than that of the native ACL was conceived.

Table 1: Dimensional parameters estimated from geometry of a goat ACL

	Working length/ height (mm)	Diameter (mm)	CSA (mm ²)
Normal ACL	5 – 8	5 – 6.5	20 – 33
Proposed dimensions of the Mg ring	5 – 6	6 – 7	28 – 38

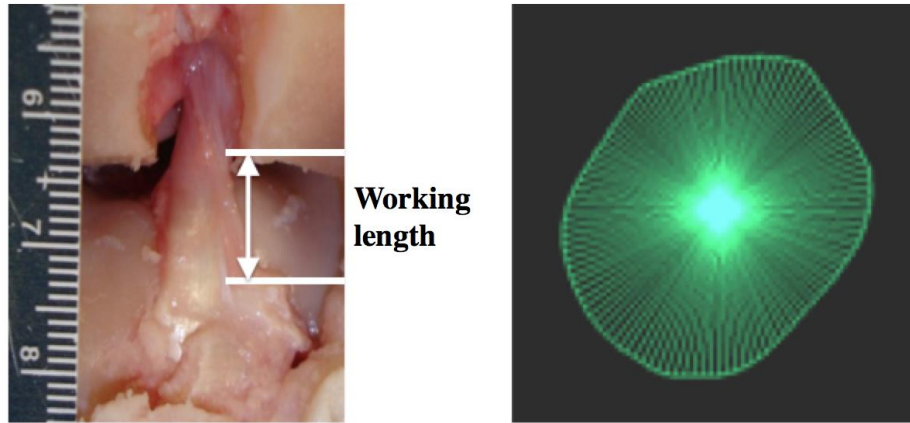


Figure 5: (A) Geometry and working length of the goat ACL, (B) Cross-sectional shape as measured by a custom laser micrometer system

3.2 DEVICE DESIGN AND SUTURE TECHNIQUE

During the iterative design process of the Mg ring, three evaluative criteria were established for to select a design for subsequent testing. In order to be considered successful, each of the following criteria must be met:

1. Manufacturing of the device from pure Mg or Mg alloys must be possible.

2. The device must be feasibly implanted in a goat stifle joint by an orthopaedic surgeon without unreasonable difficulty.
3. Implantation of the Mg ring, henceforth called “Mg ring repair,” must bring the two ends of a transected goat ACL together in tension and load the ACL.

Manufacturing of all device designs was successfully achieved in the University of Pittsburgh’s Bioengineering Machine Shop, in fulfillment of Criterion 1. To produce the devices, the inner and outer diameters were first turned using a lathe, and then surface holes and other features were added using CNC milling with a custom-made mandrill. Mg alloy AZ31 was used for prototype production due to its commercial availability.

The initial design of the Mg ring (Prototype 1) is shown in Figure 6. It was cylindrical in shape, with an inner diameter of 6 mm, height of 6 mm, and wall thickness of 0.25 mm. It also had 8 holes of 1 mm diameter around the top and bottom of the device, such that it could be sutured to the two ends of a surgically transected goat ACL.

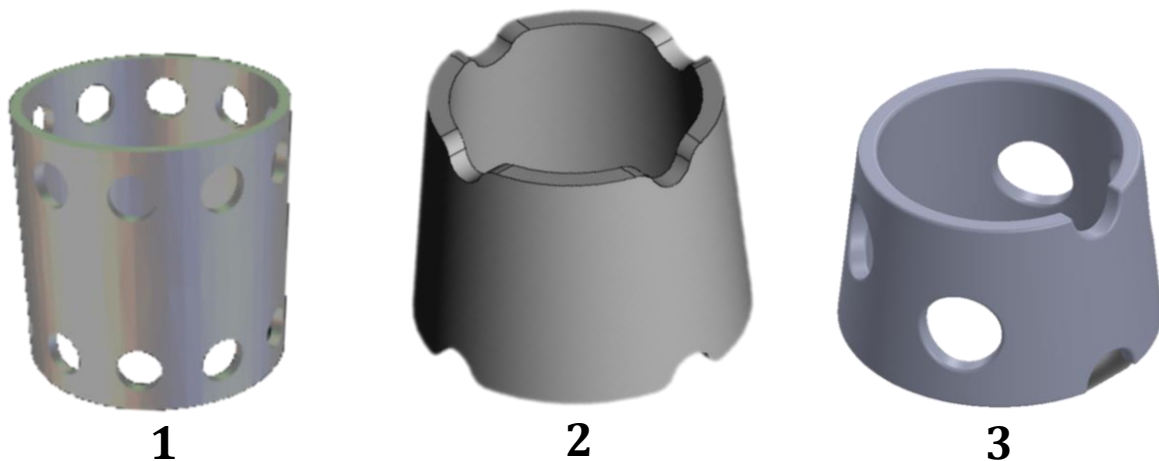


Figure 6: Prototypes of the Mg ring

During preliminary implantations in cadaveric goat stifle joints, it was quickly discerned that Prototype 1 did not satisfy Criteria 2 and 3. It was challenging to pass a ½ circle suture needle through a hole, into the ACL tissue, and out of an opposite hole. Additionally, implantation could only be achieved by removing much of the tissue surrounding the ACL, including the patella, and Mg ring repair using this design did not restore tension to the ACL, as demonstrated by a large gap between the two transected ends.

For Prototype 2, these shortcomings were addressed by replacing the suture holes with 4 sets of equally-spaced notches around the top and bottom of the device, corresponding to the anterior, posterior, medial, and lateral sides of the ACL (Figure 6). To implant this device, 4 sets of sutures were first attached to each of the transected ends of the ACL. The ring was then threaded on by passing the sutures through opposite sides of the ring. Finally, it was tensioned and fixed in place by pulling the sutures and tying them around the ring, with knots held within the notches.

This design was able to meet Criterion 2, as it could be applied to repair the transected ACL with relative ease. However, it failed at Criterion 3, as it was not possible to maintain sufficient suture tension while tying the sutures around the ring to bring the ends of the ACL together and load it in tension.

After the failure of Prototypes 1 and 2, a different strategy was employed to ensure loading of the ACL. Inspired by previous studies of mechanical augmentation of a transected ACL^{64, 65, 68}, bone tunnels in the femur were employed to apply greater tension to sutures used to repair the ACL. The Mg ring design was then modified from Prototype 2 to accommodate these sutures, and the final design, Prototype 3, was developed (Figure 6).

For surgical implantation of Prototype 3, four 1.5 mm bone tunnels were first drilled in the femur and tibia, with two passing anterior to the ACL's femoral insertion site and two passing medial and lateral to its tibial insertion site. Then, two sets each of "repair sutures" and "fixation sutures" were attached to each end of the transected ACL (Figure 7A). The ring was then attached to the ACL, with the repair sutures passing directly through the ring and tied around it with the knots held within the set of notches. The fixation sutures were passed through the suture holes from the inside to the outside, then through the bone tunnels. They were fixed on the outside of the bones using a knot tied over an Endobutton on the femoral side (Smith & Nephew, Andover, MA) and a double-spiked plate and fixation post on the tibial side (Smith & Nephew) (Figure 7B). Originally, an Endobutton was also used for tibial fixation of the Mg ring, but preliminary work in cadaveric goat stifle joints indicated that the use of the double-spiked plate resulted in improved joint stability, as it permitted control of the tension applied to the fixation sutures. This also allowed for a prescribed, repeatable tension to be applied to the fixation sutures during Mg ring repair during each surgical procedure, resulting in greater consistency between tested specimen.

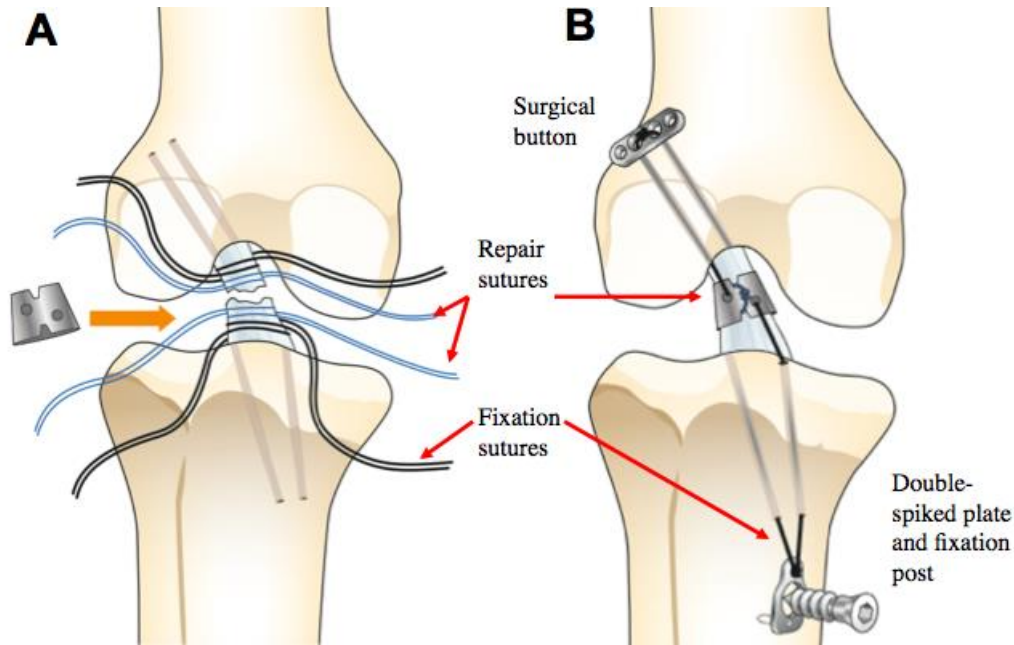


Figure 7: Procedural details for Mg ring repair, depicting attachment of repair and fixation sutures to the ACL (A), followed by attachment and fixation of the ring (B)

Resorbable sutures were selected for the repair sutures. Monofilament poly (p-dioxanone) sutures were used initially (PDS #0, Ethicon, Inc., Bridgewater, NJ), but these were later replaced by braided lactide/glycolide sutures (Vicryl 2-0, Ethicon) due to their improved ease of use for knot tying. Nonresorbable sutures were selected for the load-bearing fixation sutures to prolong the mechanical augmentation of the ACL and to remove the additional variable of suture degradation in *in vivo* applications. Preliminary testing revealed that stronger sutures (Fiberwire #5, Arthrex, Naples, FL) were too large (~1 mm diameter) and led to cutting of the ACL tissue, while weaker sutures (Ethibond Excel #1, Ethicon) occasionally broke during implantation and were not able to restore stability to the stifle joint. Thus, an intermediate suture was selected to successfully overcome these limitations (Ethibond Excel #2, Ethicon). This polyester suture has adequate mechanical properties when quadrupled for Mg ring repair

(stiffness of one suture strand: 13 ± 2 N/mm; ultimate load: 134 ± 9 N) as well as a polybutylate coating to facilitate knot-tying for femoral fixation¹⁵⁴.

With the successful design and fabrication of the Mg ring, as well as demonstration of its ability to be implanted in the cadaveric goat stifle joint to bridge the gap between the two ends of a transected ACL, the criteria for a successful Mg ring design were met. Thus, the goals of Specific Aim 1.1 were achieved.

3.3 FINITE ELEMENT ANALYSIS

3.3.1 Background

To provide mechanical augmentation to the Mg ring-repaired ACL, the purpose of the Mg ring was to sustain forces comparable to those in the normal ACL immediately after implantation in the goat stifle joint. Over time, as the device degraded and the healing ACL strengthened, this loading would be transferred to the ACL. But due to repeated loading of the device and *in vivo* degradation, it would be possible for premature fracture to occur, resulting in fragmentation of the device, compromise of its function, and potentially complications to the animal. Indeed, during preliminary experiments following Mg ring repair of the ACL, it was noted that the ring could experience plastic deformation or even fracture during testing. We thus sought to address the research question of whether modifying the device design or Mg material could reduce the potential for device fracture. In order to select a suitable design for further *in vitro* and *in vivo* testing, a parametric finite element model was developed.

3.3.2 Model development

For the parametric analysis, 18 geometrical models were prepared in Solidworks (Solidworks Corporation, Waltham, MA) corresponding to variations in the Mg ring design. 4 parameters of interest were used, namely the wall thickness, suture hole diameter, and notch depth (Table 2). For these models, the outer diameter of the ring, the notch width, and the midpoint of the suture hole were kept constant. Following fabrication of preliminary prototypes, it was empirically determined that wall thicknesses of 0.25 mm and 1 mm would not be suitable for the Mg ring, as 0.25 mm thick rings were too easily deformable, while 1 mm thick rings were found to be too bulky for the goat stifle joint. Thus, these models were eliminated, and the only the 6 models with a wall thickness of 0.5 mm were used in the finite element analysis.

In addition to consideration of the Mg ring geometry, to study the additional effects of the composition of the ring, mechanical properties of “low,” “medium,” and “high” strength Mg alloys were defined. For each, values for Young’s Modulus, yield strength, and failure strength were defined based on a database in the Engineering Research Center for Revolutionizing Metallic Biomaterials (unpublished; Table 3). The low strength alloy was modeled after a 99.9% purity Mg rod, and the medium and high strength alloys were modeled after two Mg-Ca alloys with enhanced mechanical properties. Thus, a total of 18 models were assessed.

Table 2: Designs of the Mg ring used in the parametric finite element analysis













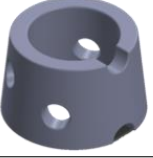





			Suture Hole Diameter (mm)		
			1.5	2	2.5
Wall Thickness (mm)	0.25	Notch Depth			
		Shallow			
	Deep				
	0.5	Shallow			
		Deep			
	1	Shallow			
Deep					

Table 3: Mechanical properties of Mg alloys for finite element models

		Yield Strength (Mpa)	Ultimate Strength (Mpa)	Young's Modulus (GPa)
Alloy Strength	Low	129	222	35
	Medium	293	317	42
	High	335	411	52

To develop the finite element model, the loading of the Mg ring was divided into three categories: compression when the joint was weight-bearing, fixation suture tension, and contact of the Mg ring with the medial and lateral sides of the femoral intercondylar notch.

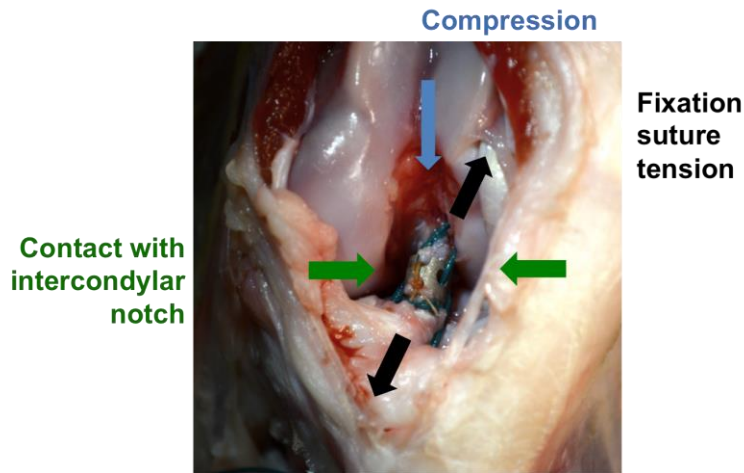


Figure 8: Illustration of 3 predicted types of in-situ loading of the Mg ring

To model these loads, the 3-dimensional (3D) geometry of the goat stifle joint was first prepared. This geometry was reconstructed from a computed tomography (CT) scan of a cadaveric joint (FIDEX, Animage, Pleasanton, CA). Images from the CT scan were converted to an STL format using open-source software (3D Slicer, Boston, MA) and processed to remove surface background noise and surface irregularities (Geomagic, 3D Systems, Rock Hill, SC). The patella was also removed from the model, and the femur and tibia were separated to produce the final bone model (Figure 9).

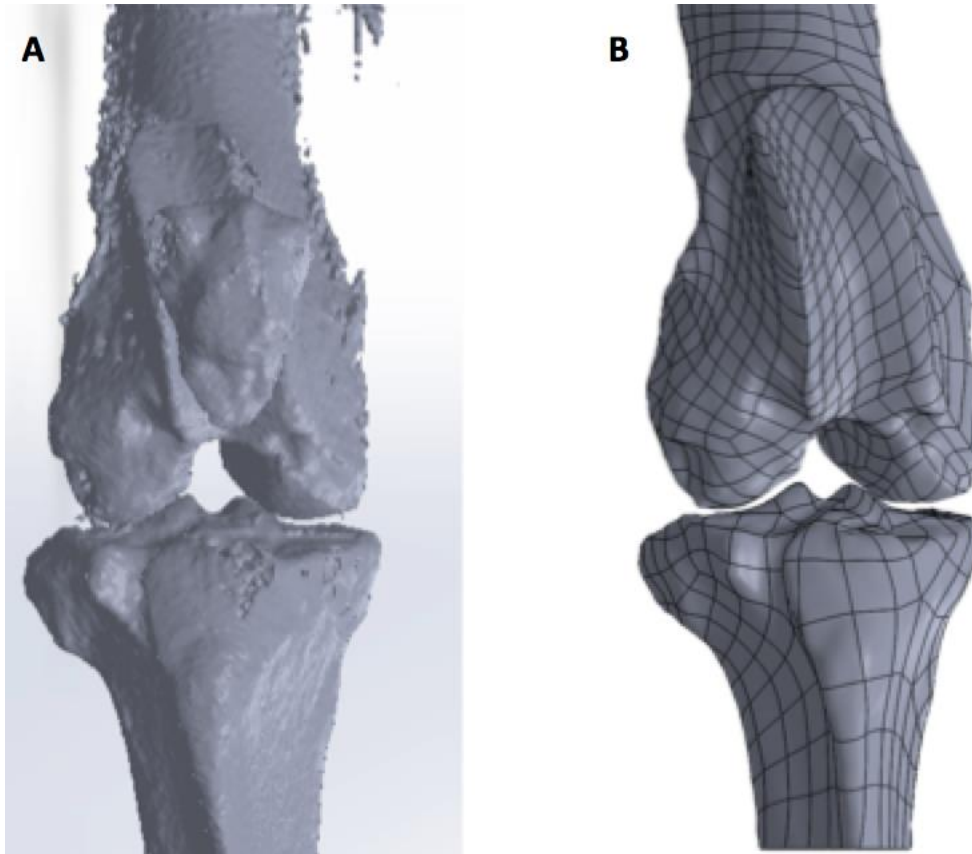


Figure 9: Initial rendering (A) and final 3-D model (B) of the goat stifle joint

Originally, it was intuitively presumed that a major mechanism of loading on the Mg ring was from compression as the ring was pushed into the femoral intercondylar notch when the stifle joint was in a weight-bearing state. However, a preliminary finite element analysis revealed that there was sufficient space in the intercondylar notch such that the ring would not be loaded in compression, even if direct contact were to be made between the femur and tibia (Figure 10). Given these findings and to simplify the model, the geometry of the bones was removed and the ring was subsequently modeled alone.

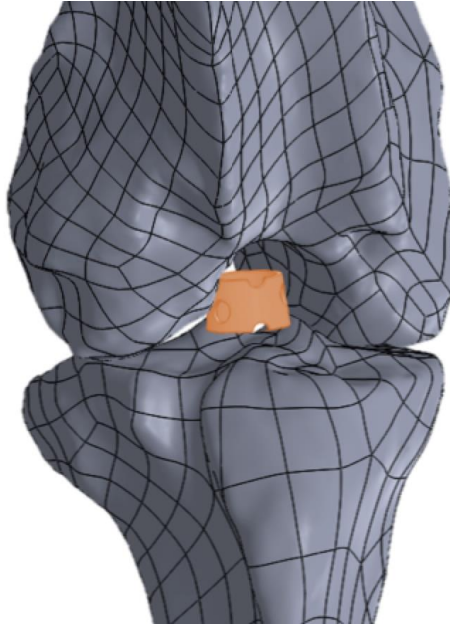


Figure 10: Schematic diagram illustrating that the Mg ring could not be driven into the femoral intercondylar notch by axial compression

The Mg ring geometry was imported into ANSYS Workbench 15.0 (ANSYS, Canonsburg, PA) using a static structural model. In order to perform the analysis, appropriate boundary conditions were required to constrain the device to prevent rigid body motion when it was loaded. To do this, a conical frustum geometry of the same inner diameter as the ring was modeled inside it using ANSYS Design Modeler, with the top and bottom faces fixed rigidly in place. It should be noted that this was not intended to simulate the ACL, but rather to prevent rigid body motion of the ring when loads were applied. The contacting surfaces of the ring and cone were bonded together, and the cone was modeled as an isotropic material (Young's Modulus: 25 MPa, Poisson's ratio: 0.4) with properties such that it would not contribute to the resulting stress on the Mg ring or prevent its deformation under loading. A mesh was then generated over each component, with a total of 40,000-50,000 elements and 140,000-150,000 nodes.

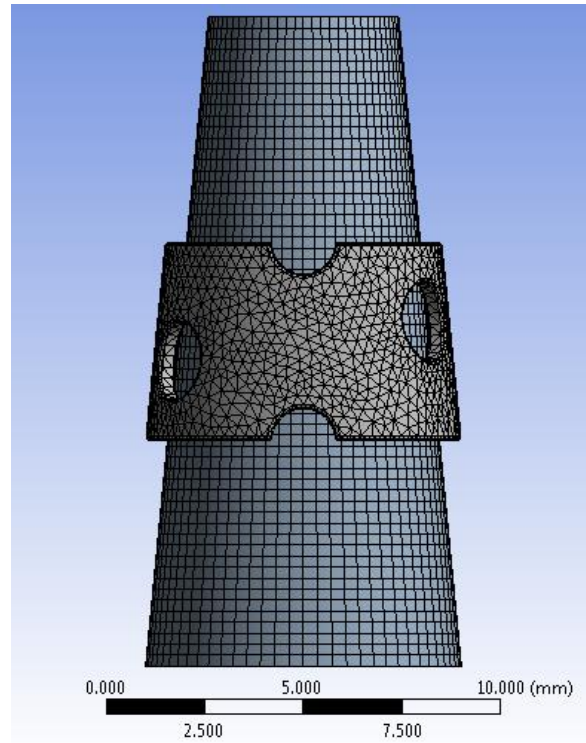


Figure 11: The Mg ring in Ansys software modeled with a cone of the same inner diameter to constrain the device from rigid body motion under loading

After removing the compressive loading, the two remaining types of loading described in Figure 8 were applied to the ring to simulate its in-situ loading. The main mechanism of loading of the Mg ring was tension of the fixation sutures that were attached to the transected ends of the ACL and passed from the inside of the ring to the outside through the suture holes. This was modeled by a combination of (A) a 40-N tensile load and (B) a 20-N load normal to the surface of the Mg ring. The total magnitude of this load was 45 N per suture hole, or 90 N total per side of the ring. This was selected as the highest in-situ load carried by the Mg ring-repaired ACL during testing using a robotic/UFS testing system under a 67-N anterior tibial load with 100 N axial compression. The load was applied as a nodal load to the cluster of nodes on the outer surface of the ring (2 mm wide) that would be in contact with the fixation sutures (Figure 12).

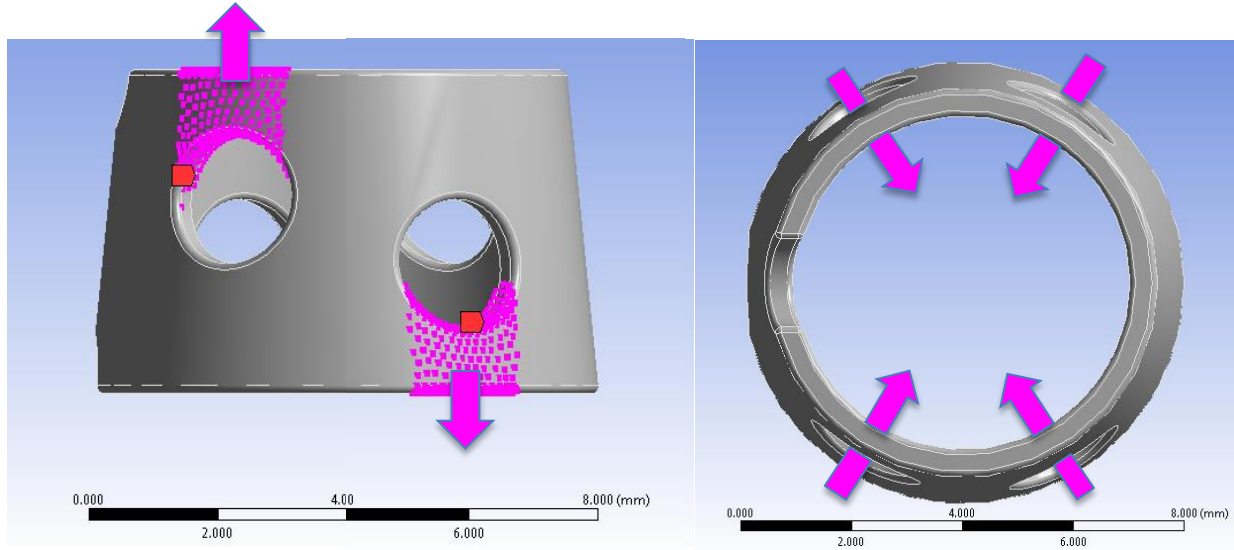


Figure 12: Directions of loading in the finite element model simulating tension from fixation sutures with a 40 N tensile load (left) and 20 N load normal to the surface of the Mg ring (right)

To simulate loads on the Mg ring due to contact with the femoral intercondylar notch, additional nodal forces were applied to the medial and lateral faces of the device. As these loads would be anticipated to be minor relative to the fixation suture loads, they were estimated to be approximately one-tenth of the magnitude (10 N) (Figure 13).

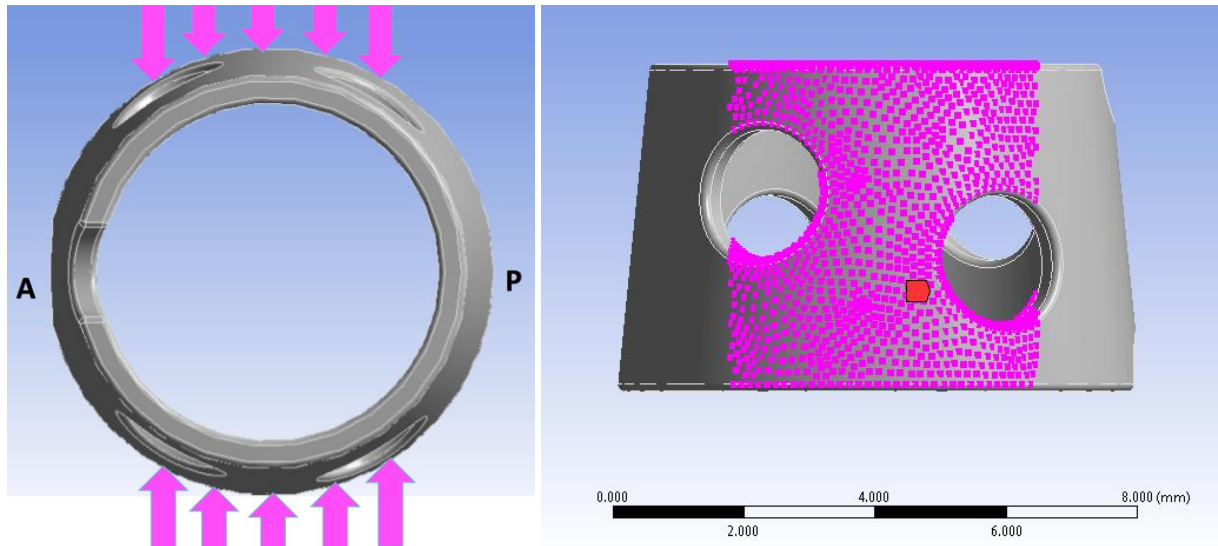


Figure 13: Medial and lateral loads applied to the Mg ring (A= anterior, P= posterior)

The output of interest was the maximum Von Mises stress, which expresses the complex stress state of a body in a single scalar number. This criterion is used often in finite element analyses as a comparison to the yield and failure strength of a material to predict whether it can withstand a loading condition. For each model, the maximum Von Mises stress and its location on the device, as well as the stress distribution were recorded and compared to the yield and failure stress of the material.

3.3.3 Finite element analysis results

Following the simulated loading conditions, the resulting maximum Von Mises stress in each Mg ring design is shown in Table 4. The corresponding stress distributions for each model are depicted in Figure 14. As the stress distributions for each model were similar for all 3 alloy strengths, one representative image of the front and side are presented.

In all cases, the points of maximum stress occurred at the outer edges of the suture holes, which was expected as this would be the point of contact of the ring with the load-bearing fixation sutures. At this point, the maximum Von Mises stress exceeded the yield stress in all 6 designs using the low strength alloy, and exceeded the failure stress in the 2 designs with the 2.5 mm diameter suture holes. Due to the results from preliminary testing that led us to believe that the notches were also a point of weakness in the ring design, the maximum Von Mises stress on the longitudinal line between the notches was also recorded. The yield stress was not reached at this point in any of the tested simulations.

As expected, for each design, as the strength of the alloy increased, the maximum Von Mises stress also increased. However, the material properties had a relatively small effect on the maximum Von Mises stress, as the difference between the maximum stress in the low and high strength alloys was 9 – 19 MPa. As noted previously, the stress concentrations appeared nearly indistinguishable between alloy strengths. Thus, the mechanical properties of the alloy did not have a large impact on the Von Mises stress.

In contrast, variations in the surface features led to significant differences in both the maximum Von Mises stress as well as the stress distributions on the surface of the device. With increasing suture holes diameter, the maximum Von Mises stress increased in a range from 17 – 89 MPa. This finding could be explained by the corresponding stress distributions, which showed more concentrated areas of high stress in the models as the suture hole diameter increased (indicated by areas of green, yellow, and red in the diagram), while other areas experienced little stress (blue). Alternatively, with smaller suture holes, more moderate Von Mises stresses were found to be distributed more evenly throughout the surface of the device.

As predicted, increasing the depth of the notches also had a considerable effect on both the maximum Von Mises stress at the notches as well as the stress concentrations. Increasing the notch depth led to increases in the maximum Von Mises stress at the notches of up to 44 MPa in otherwise equivalent models. In fact, in one model (2.5 mm diameter ring, low strength alloy), Von Mises stress at the suture holes exceeded the yield stress of the material. Similar to the findings on the suture hole diameter, these results could also be explained by the stress distribution diagrams, which revealed high stress concentrations at the deeper notches, while areas around the notch sustained minimal stress. In contrast, with the shallow notches, lower stress levels were distributed more evenly on the surface of the ring. In terms of the maximum Von Mises stress on the device at the suture holes, there was not a clear pattern between shallow versus deep notches, as increases from 5 – 60 MPa were found in the 1.5 mm and 2.5 mm diameter suture hole models, respectively, while decreases of 11 – 15 MPa were found in the 2 mm diameter model.

Table 4: Resulting Von Mises stress from the parametric finite element analysis of the Mg ring (* indicates a value that has exceeded the yield stress; # indicates a value that has exceeded the failure stress)

		Suture hole diameter					
	Alloy Strength	1.5 mm		2 mm		2.5 mm	
		Maximum at suture holes	Maximum at notches	Maximum at suture holes	Maximum at notches	Maximum at suture holes	Maximum at notches
Shallow notches	Low	144.9*	77.6	192.2*	98.6	240.8 [#]	125.2
	Medium	147.0	83.3	197.7	103.2	247.7	128.0
	High	149.3	86.4	203.5	109.9	255.0	136.3
Deep notches	Low	150.7*	118.4	181.6*	118.3	258.7 [#]	136.4*
	Medium	154.8	124.1	183.9	125.7	267.6	144.4
	High	159.1	130.3	188.2	133.3	277.1	156.3

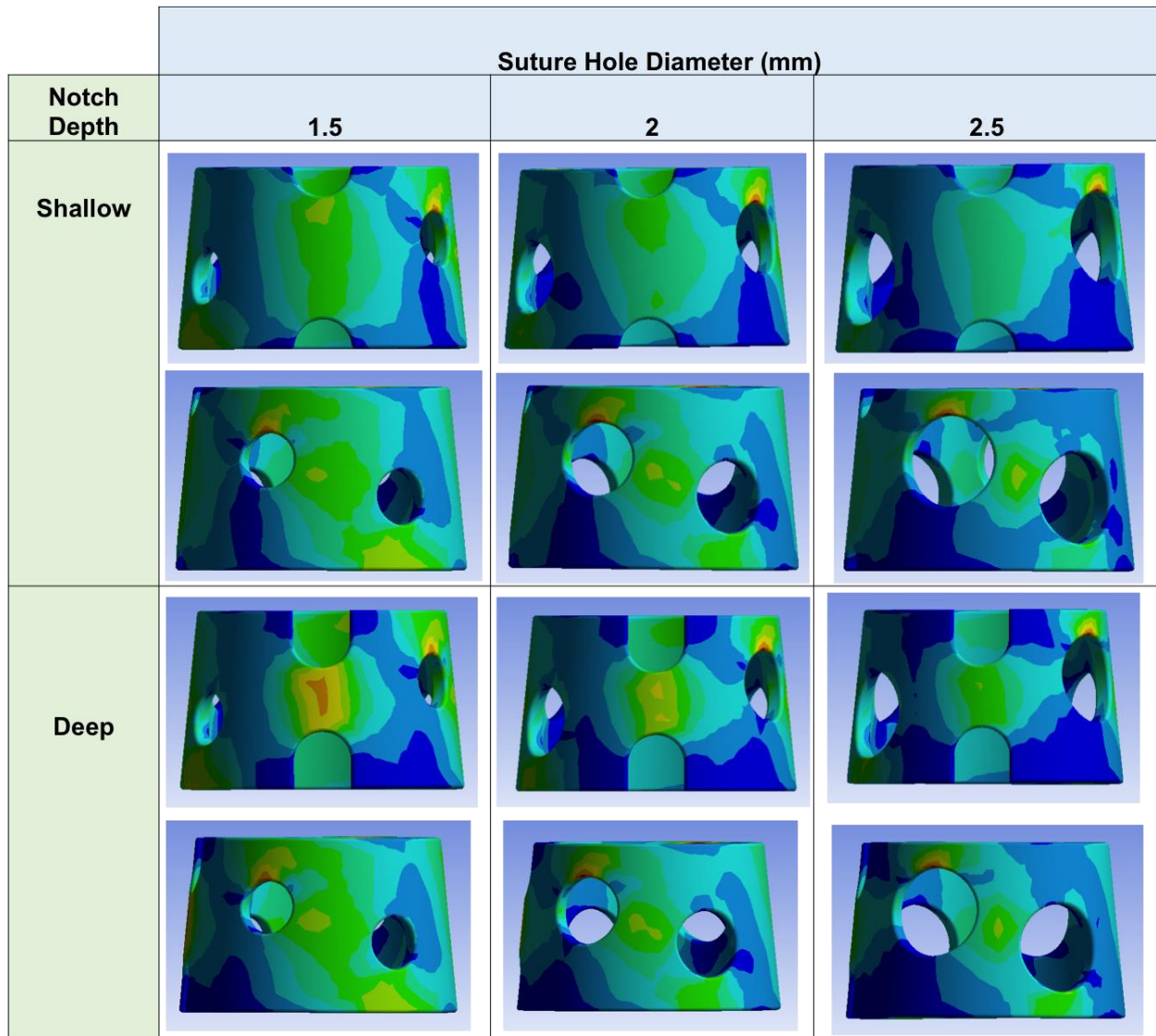


Figure 14: Results on the Von Mises stress distributions for the parametric finite element analysis of the Mg ring

In summary, results of the parametric finite element analysis suggested that a majority of Mg ring models and alloys would be suitable based on the minimum success criteria of not exceeding the failure stress of the material under the simulated loading conditions. The exception to this would be the models with 2.5 mm diameter suture holes using a low strength alloy. In all models, the low strength Mg alloy exceeded the yield load, indicating that plastic

deformation would occur. Overall, while the alloy strength did not greatly impact the maximum Von Mises stress in the ring, changes in the surface features, including the suture hole diameter and notch depth, led to substantial changes in the maximum Von Mises stress and stress distributions. Specifically, larger surface features (increased suture hole diameter and deeper notches) led to increases in both of these parameters.

The final selection of an Mg ring design suitable for further testing was made based on of the model results combined with surgical considerations. First, the ring models with deeper notches were eliminated due to the increased stress concentrations that were found between the notches. Empirically, it was confirmed that the notch depth did not affect the successful implantation of the Mg ring devices. Considering only the 3 designs with shallow notches, the design with 2.5 mm diameter suture holes was also eliminated, as the larger suture holes also led to increased maximum Von Mises stress and areas of high stress concentrations. With two designs remaining, production of physical prototypes of each revealed that implantation of the Mg ring was significantly less challenging using the ring design with 2 mm diameter sutures holes compared to 1.5 mm diameter holes. Thus, this design was selected as the most suitable design for further *in vitro* and *in vivo* applications.

For the material selection, although the maximum Von Mises stress was similar between low and high strength Mg alloys, their behavior *in vivo* would clearly differ, with higher strength alloys sustaining significantly higher loading prior to yielding or failure. However, some plastic deformation of the Mg ring *in vivo* could actually be beneficial, as it could allow the Mg ring to deform to the patient-specific geometry of the femoral intercondylar notch. This deformation could even prevent damage to the articular cartilage or other structures in the knee. But with the complex *in vivo* loading conditions, combined with the changing properties of the ring as it

degraded, the present finite element model would be unable to select the “best” Mg material. *In vivo* studies at a variety of time points would be required to accurately characterize and assess the performance of different Mg materials.

Nevertheless, the finite element developed in Specific Aim 1.2 was successful in allowing for the selection of a preferred Mg ring design for further testing, as well as providing insight into the stress levels and distributions it may be subject to *in vivo*. The model also indicated that alloys over a wide range of mechanical properties could be suitable for the Mg ring. These results gave us confidence in our selection of a ring design for further *in vitro* and *in vivo* testing in Specific Aims 2 and 3.

4.0 *IN VITRO* ROBOTIC/UFS EVALUATION OF MG RING REPAIR OF THE ACL

4.1 EXPERIMENTAL DESIGN

To evaluate the potential application of the Mg ring device for ACL repair, experiments were performed in Specific Aim 2 to address the following research question: could the use of this device to repair the ACL (“Mg ring repair”) restore joint function and the in-situ forces in the ACL to normal levels immediately after implantation using our established goat model ^{3, 170} ? To answer this question, a robotic/UFS testing system ¹³⁶ was employed to quantitatively evaluate the function of cadaveric goat stifle joints following Mg ring repair when external loads were applied mimicking those used in clinical examinations. Additionally, the in-situ forces in the medial meniscus were also measured, as studies have found significant increases in loading of the medial meniscus in the ACL-deficient knee ^{12, 169} and injuries to the medial meniscus are common following ACL injury ⁵⁰.

Fresh-frozen stifle joints from Boer goats were used. A total of 8 joints was determined to be the required sample size by an a priori power analysis using previous data to determine differences of 2 mm in stifle joint kinematics and 10 N in in-situ forces in the ACL. Intact stifle joints were thawed 24 hours prior to testing and prepared for testing as previously described ^{3, 142}. Briefly, the femur and tibia were cut 10-20 cm from the joint line, dissected free of soft tissue

around the joint, and potted in cylindrical molds using a fiberglass reinforced body filler (Everglass, Evercoat, Cincinnati, OH).

4.2 ROBOTIC TESTING PROCEDURE

The robotic/UFS testing system used in Specific Aim 2 was developed in our research center more than 20 years ago to improve upon previous methodologies to study joint function, including the linkage system^{95, 99}. The UFS system (Model 4015, JR3, Inc., Woodland, CA) can measure 3-dimensional forces and moments in a Cartesian coordinate system with a repeatability of 3.5 N for force and 0.35 N-m for torque, while the robotic manipulator (Puma Model 762, Unimate, Inc., Pittsburgh, PA) has a position and orientation repeatability of 0.2 mm and 0.2°, respectively. This system can be operated in force control mode to measure the 6-DOF joint kinematics under externally applied loads. It can also be used in position control mode to repeat previously-recorded kinematics such that the in-situ forces in joint structures can be determined^{3, 65, 136, 177, 230}.

The potted femur and tibia were bolted to the robotic/UFS testing system and secured within custom clamps, with the femur fixed in a rigid pedestal base and the tibia attached to the end effector of the robot (Figure 15). An anatomical coordinate system describing the position of the joint relative to the UFS was defined using the position of the femoral insertions of the MCL and LCL relative to the end effector of the robot¹³⁷. The subsequent testing procedure is summarized in Table 5. First, the passive path of flexion-extension was found from full extension to 90° of flexion, to be used as a reference position throughout testing to move between joint flexion angles. This was found by moving the joint in 1° increments and finding

the position where forces and moments were minimized for each angle. Next, the robotic/UFS testing system was operated in force-control mode to determine the stifle joint kinematics in response to externally applied loads simulating those used clinically to test for ACL function: (1) a 67-N anterior tibial load, and (2) a 67-N anterior tibial load with 100 N axial compression^{65, 94, 129}. Each loading condition was applied at 3 preselected angles of joint flexion (30°, 60°, and 90°), while the robot recorded the resulting 5-DOF kinematics.

Table 5: Experimental protocol and data obtained using the robotic/UFS testing system under a 67-N anterior tibial load without (I-III.A) and with (I-III.B) 100 N axial compression

Protocol	Data Obtained
I. Intact Joint	
Path of passive flexion-extension	
External loading conditions	
A. 67-N anterior tibial load	Intact kinematics (I.A)
B. 67-N anterior tibial load + 100 N axial compression	Intact kinematics (I.B)
Transect ACL	
II. ACL-deficient joint	
Repeat kinematics I.A., I.B.	In-situ forces in the ACL
Apply loads I.A, I.B	ACL-deficient kinematics (II.A, II.B)
III. Mg ring repair of the ACL	
Perform Mg ring repair	
Apply loads I.A, I.B.	Mg ring repair kinematics (III.A, III.B)
Release Mg ring	
Repeat kinematics III.A, III.B	In-situ forces in Mg ring-repaired ACL
IV. Medial meniscus-deficient joint	
Repeat kinematics I, II, III	In-situ forces in the medial meniscus

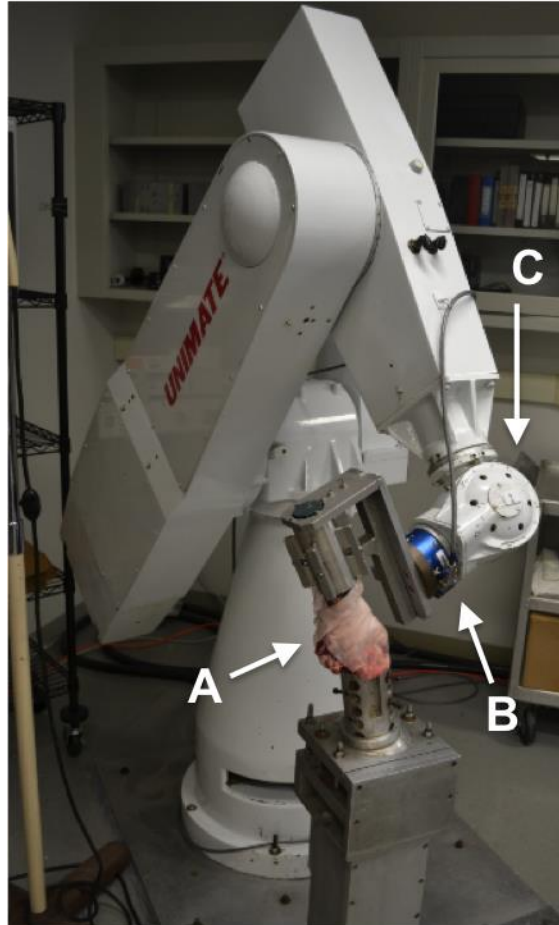


Figure 15: Photograph of the testing set-up for Specific Aim 2, depicting the cadaveric goat stifle joint (A), universal force-moment sensor (B), and robotic manipulator (C)

Next, the ACL was transected through its midsubstance using a medial parapatellar incision. The previously-recorded kinematics of the joint with an intact ACL were then repeated, while the UFS recorded new forces and moments. The in-situ forces in the intact ACL could then be determined in response to each of the loading conditions using the principle of superposition. The ACL-deficient kinematics were also recorded using loading conditions (1) and (2).

Then, Mg ring repair of the ACL was performed as described in Section 3.2. Once complete, the kinematics of the repaired joint were obtained using loading conditions (1) and (2). Finally, the ring was then removed and the previously-recorded kinematics were repeated to obtain the in-situ forces in the Mg ring-repaired ACL.

To measure the in-situ forces in the medial meniscus under each condition, it was carefully removed from the joint. The kinematics of the joint with the intact ACL, ACL-deficient joint, and repaired joint were repeated to determine its in-situ forces in each state using the principle of superposition.

For statistical analysis, a repeated measures analysis of variance (ANOVA) was performed at each knee flexion angle using SPSS Statistical Software (Version 21, IBM, Armonk, NY), with knee state used as the experimental factor. Bonferroni post-hoc tests were done for pairwise comparisons, with statistical significance set at $P \leq 0.05$.

4.3 RESULTS

The Mg ring could successfully connect the two ends of the transected ACL and provide mechanical augmentation to stabilize the goat stifle joint. Data on anterior tibial translation (ATT) in response to an applied 67-N anterior tibial load are summarized in Table 6A. For the joint with an intact ACL, the ATT was between 1.8 and 2.7 mm. These values were similar at 30° and 60°, but became lower at 90°. Following ACL transection, the ATT increased to more than 12 mm, representing a significant increase of 5 to 7-fold ($P < 0.05$). However, following

Mg ring repair, it was reduced to 4.3 to 5.8 mm, representing only 33-37% of those for the ACL-deficient state ($P < 0.05$), but remained 2 – 3 mm higher than that of the intact joint ($P < 0.05$).

The in-situ force data are detailed in Table 7A. Under the 67-N anterior tibial load, the in-situ force in the intact ACL was between 51 - 61 N, which was 73 – 90% of the applied load. Following Mg ring repair of the ACL, it was 55 - 63 N and was within ± 5 N of that in the intact ACL for all three joint flexion angles tested ($P > 0.05$). The corresponding in-situ force in the medial meniscus was found to be negligibly small when the ACL was intact, but it increased significantly to 29 – 40 N ($P < 0.05$) following ACL transection. With Mg ring repair, it was reduced to levels that were not statistically different from those in the joint with an intact ACL ($P > 0.05$)¹⁶⁹.

When a 100 N axial compressive load was added to the 67-N anterior tibial load, the ATT of the joint with an intact ACL was consistently 1 – 3 mm higher than those under the 67-N anterior tibial load alone (Table 6B). Following ACL transection, the ATT increased 4 to 6-fold ($P < 0.05$). After Mg ring repair, it was reduced by about 50% of those for the ACL-deficient state ($P < 0.05$), but remained 4 – 6 mm higher than that of the intact joint ($P < 0.05$).

Due to the additional compressive load, the in-situ force in the intact ACL was 18 - 31 N higher than under the anterior tibial load alone (Table 7B). Following Mg ring repair, it was restored to within ± 8 N of the intact ACL for all joint flexion angles tested. The in-situ force in the medial meniscus with an intact ACL was unchanged with the additional compressive load at 30° and 60°, but it increased by about 3-fold at 90° of knee flexion. After transection of the ACL, it increased significantly to 57 – 88 N ($P < 0.05$). Following Mg ring repair, it was again reduced by 74 – 85% compared to the ACL-deficient joint and was not statistically different from that in the joint with an intact ACL at 30° ($P > 0.05$).

Table 6: Anterior tibial translation (mean \pm SD) of the goat stifle joints tested at 30°, 60°, and 90° of flexion in response to: (A) a 67-N anterior tibial load and (B) a 67-N anterior tibial load + 100 N axial compression

	Flexion Angle		
	30°	60°	90°
A. 67-N Anterior Tibial Load			
Intact	2.5 \pm 0.6	2.7 \pm 0.9	1.8 \pm 1.0
ACL-deficient	15.2 \pm 2.3* [#]	15.8 \pm 1.7* [#]	12.4 \pm 1.6* [#]
Mg ring repair	5.0 \pm 1.0*	5.8 \pm 1.0*	4.3 \pm 1.3*
B. 67-N Anterior Tibial Load + 100 N axial compression			
Intact	3.8 \pm 0.8	4.6 \pm 0.7	3.3 \pm 1.0
ACL-deficient	17.4 \pm 2.7* [#]	17.8 \pm 2.7* [#]	13.6 \pm 2.9* [#]
Mg ring repair	8.0 \pm 1.4*	9.5 \pm 1.6*	7.0 \pm 1.6*

* significantly different compared to the intact knee ($P < 0.05$)

significantly different compared to Mg ring repair ($P < 0.05$)

Table 7: In-situ forces in N (mean \pm SD) in the: (I) ACL and (II) medial meniscus of the goat stifle joints at 30°, 60°, and 90° of flexion in response to (A) a 67-N anterior tibial load and (B) a 67-N anterior tibial load with 100 N axial compression

Flexion Angle	I. ACL			II. Medial Meniscus		
	30°	60°	90°	30°	60°	90°
A. 67-N anterior tibial load						
Intact joint	61 \pm 8	59 \pm 4	51 \pm 9	5 \pm 3	4 \pm 2	6 \pm 4
ACL-deficient joint	-	-	-	37 \pm 16* [#]	46 \pm 16* [#]	35 \pm 15* [#]
Mg ring repaired joint	62 \pm 7	63 \pm 7	55 \pm 7	7 \pm 4	8 \pm 8	16 \pm 9
B. 67-N anterior tibial load + 100 N axial compression						
Intact joint	82 \pm 13	91 \pm 19	78 \pm 33	9 \pm 6	8 \pm 6	22 \pm 12
ACL-deficient joint	-	-	-	57 \pm 29* [#]	88 \pm 40* [#]	85 \pm 39* [#]
Mg ring repaired joint	74 \pm 15	92 \pm 22	79 \pm 33	14 \pm 9	26 \pm 13*	50 \pm 21*

* significantly different compared to the intact knee ($P < 0.05$)

significantly different compared to Mg ring repair ($P < 0.05$)

To further determine the efficacy of Mg ring repair in restoring stifle joint stability and ACL function, the data obtained were compared to those collected from an earlier time-zero study from our research center whereby only sutures were applied to repair a transected ACL (“suture repair”) ⁶⁵. For suture repair, sutures were passed through the ACL stumps and through opposite bone tunnels, with a function similar to the fixation sutures used for Mg ring repair. However, the type (Ethibond #1 versus Ethibond #2) and amount of suture material (2 strands versus 4 strands) differed from suture repair to Mg ring repair. Also, unlike Mg ring repair, the sutures for suture repair were tied over the bone tunnels on both sides, rather than utilizing the double-spiked plate and fixation post for tibial fixation. We wished to compare Mg ring repair to suture repair because suture repair was also successfully used *in vivo* for ACL healing alongside an ECM bioscaffold ⁶⁶; thus, this comparison would determine the differences in mechanical augmentation between these methods that could lead to discrepancies in the *in vivo* healing responses. To make the statistical comparison, the data on the knee kinematics and in-situ forces in the repaired ACL and medial meniscus were normalized by values in the intact joint in order to reduce interspecimen variation, such that a value of 1.0 would indicate restoration to normal levels. Then, independent t-tests were used to compare the data, with significance set at $P \leq 0.05$.

Under the 67-N anterior tibial load, the normalized ATT after Mg ring repair ranged from 2.1 – 2.9 at the tested flexion angles, while for suture repair it was more than twice that and ranged from 5.3 – 6.2 ($P < 0.05$; Figure 16A). The corresponding normalized in-situ force in the ACL following Mg ring repair was similar to that in that intact joint and was between 1.0 – 1.1, which was significantly higher than 0.6 – 0.8 following suture repair ($P < 0.05$; Figure 17-I.A). This lower in-situ force in the ACL was concomitant with a significantly higher in-situ force in

the medial meniscus following suture repair compared to Mg ring repair (4.7 – 13.3 and 1.8 – 4.4, respectively; $P < 0.05$; Figure 17-II.A).

With the addition of 100 N axial compression, the differences between Mg ring repair and suture repair were more pronounced. Again, the normalized ATT after suture repair was more than two times higher than after Mg ring repair at the tested flexion angles (4.6 – 5.5 and 2.1 – 2.2, respectively; $P < 0.05$; Figure 16B). However, the in-situ force in the ACL following suture repair was reduced by more than 50% to just 0.1 – 0.3. This resulted in increases in in-situ force in the medial meniscus of up to 35 times that in the joint with the intact ACL. In contrast, after Mg ring repair, the in-situ force in the ACL was maintained at 0.9 – 1.0 ($P < 0.05$; Figure 17-I.B), and the normalized in-situ force in the medial meniscus was 2.0 – 4.5 ($P < 0.05$; Figure 17-II.B).

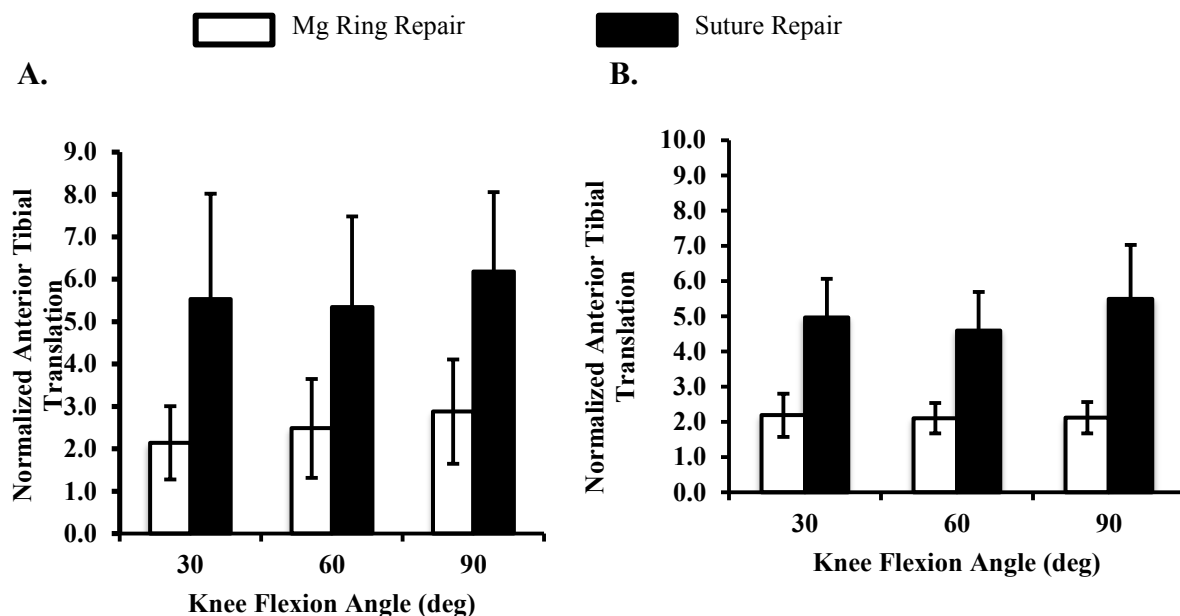


Figure 16: Normalized anterior tibial translation of the Mg ring-repaired and suture-repaired goat stifle joints at 30°, 60°, and 90° of flexion under (A) a 67-N anterior tibial load and (B) a 67-N anterior tibial load with 100 N axial compression

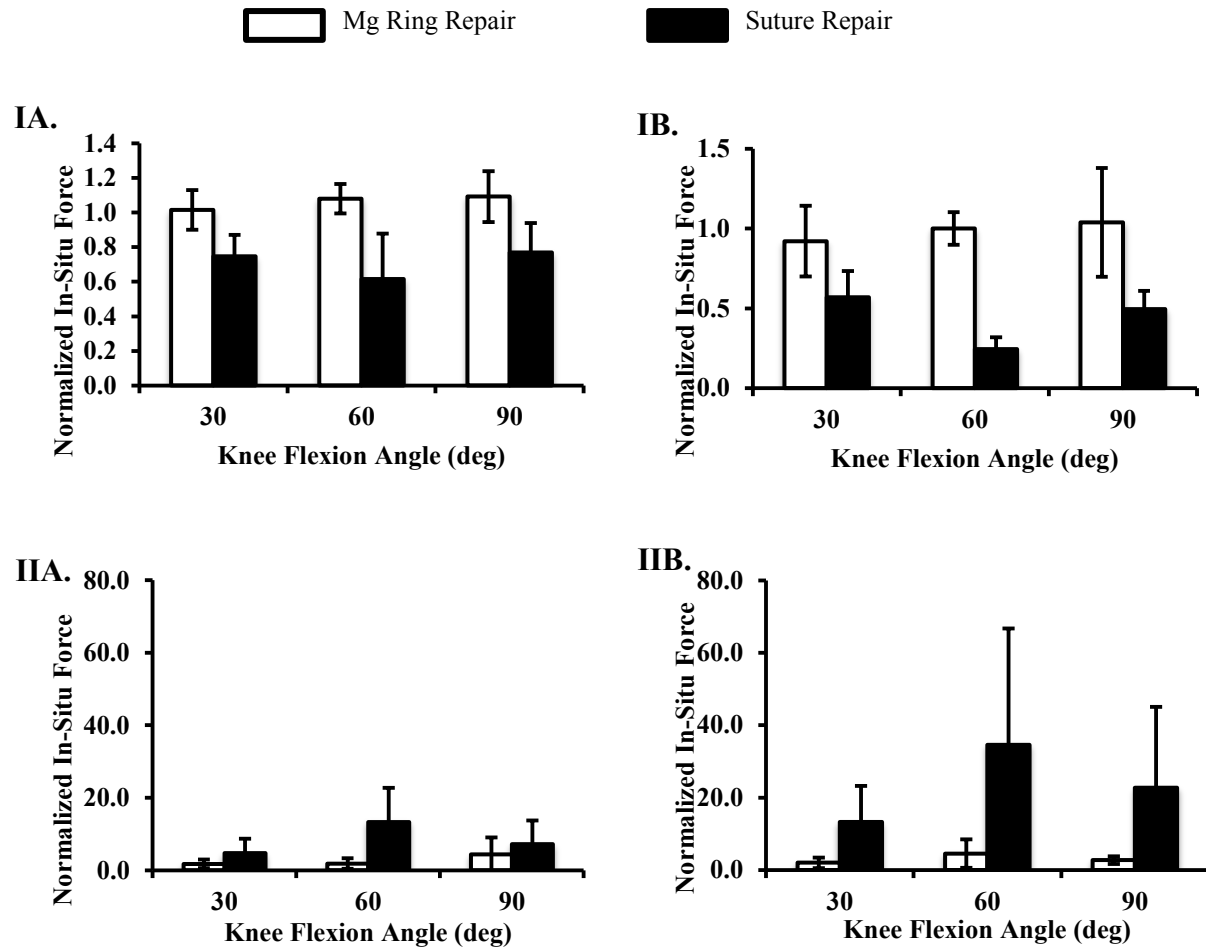


Figure 17: Normalized in-situ forces in (I) the ACL and (II) the medial meniscus in the Mg ring-repaired and suture-repaired goat stifle joints at 30°, 60°, and 90° of flexion under (A) a 67-N anterior tibial load and (B) a 67-N anterior tibial load with 100 N axial compression

5.0 COMBINED BIOLOGICAL AND MECHANICAL AUGMENTATION FOR ACL HEALING

5.1 *IN VITRO* CELL CULTURE STUDIES

5.1.1 Background

For a bioresorbable medical device, the effects of the degrading implant and its corrosion products on the surrounding tissues and cells are an important consideration, as they could elicit a harmful, neutral, or positive response in the body. The most important requirement for the Mg ring would be the absence of cytotoxic effects as it degraded, as the device itself must not be detrimental to ACL healing. Since the biocompatibility of Mg has been well-established, such effects were not anticipated to occur *in vivo*. However, recent studies in other orthopaedic as well as cardiovascular applications have indicated that Mg may actually have a positive effect on cell proliferation and function^{131, 171, 214, 220, 233}; thus, the Mg ring may elicit either a neutral or positive response on ACL healing.

In its *in vivo* application, the Mg ring was intended to be used solely as mechanical augmentation in combination with biological augmentation using an ECM bioscaffold to modulate the healing response. The underlying assumption was that any enhancement of the healing response would be due to the ECM treatment. However, if Mg had a therapeutic effect

on ACL fibroblasts, it may also contribute to healing. Without knowledge of the extent of these effects, we would not be able to discern whether the *in vivo* healing response was modulated by ECM alone, or the combination of ECM and Mg. For this reason, prior to performing the *in vivo* study, we wished to use *in vitro* method to address the research question of whether Mg materials elicited a positive response on the growth or function of goat ACL fibroblasts.

There are many *in vitro* methods that have been used to assess cytocompatibility and biocompatibility of Mg materials, including the live/dead assay, MTT cell viability assay, cell proliferation assays, and other experiments designed to assess cell function. The International Standard Organization (ISO) has also issued a standard for the biological evaluation of medical devices that discusses the preparation of fluid “extracts” that can be used in such experiments to determine biological reactivity. This standard was utilized in Specific Aim 3.1 to assess the cytocompatibility of 5 Mg materials, namely single crystal Mg, AZ31, ZJ40, ZJ41, and Mg-Ca-Zr (Figure 18).

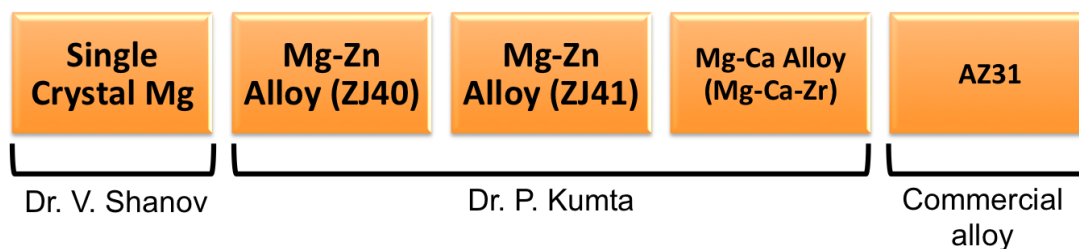


Figure 18: Mg materials selected for *in vitro* testing in Specific Aim 3.1

The Mg materials used in this Aim were chosen specifically for their clinical relevance and previous pre-clinical use as a biomaterial for orthopaedic applications. The first material selected was single crystal Mg, provided by our collaborators in Dr. Vesselin Shanov’s laboratory at the University of Cincinnati. We hoped to use this novel material for a future in

vivo application due to its advantageous properties. Specifically, with its lack of grain boundaries, single crystal Mg possessed a high ductility that could be beneficial for the Mg ring by allowing it to deform without fracture. With this lack of grain boundaries and the high purity of single crystal Mg, it would likely sustain slower and more even corrosion than other forms of pure Mg, thus preventing early fracture of the Mg ring device. In addition, with no alloying elements, its clinical relevance would be high. Next, three novel Mg alloys were selected, provided by our collaborators in Dr. Prashant Kumta's laboratory at the University of Pittsburgh. ZJ40 and ZJ41 were Mg-Zn-Sr-Zr alloys that were used as a represent of the multitude of Mg-Zn alloys currently being studied for biomedical applications. With its known biocompatibility and improvements to mechanical and corrosion properties, Mg-Zn alloys show much promise for these applications^{98, 250}. P13 was a novel Mg-Ca-Zr alloy that was chosen as a representation of Mg-Ca alloys, which have also been a popular choice for biomedical applications due to the known biocompatibility of Ca and its positive effects on device corrosion⁵⁹. The addition of Zr allows for grain refinement of these alloys, as well as a concomitant improvement in corrosion properties⁹⁸. Finally, a commercial alloy (AZ31) was selected. This was an aluminum-zinc alloy that has been widely studied *in vitro* and *in vivo*, largely due to its adequate mechanical properties and slow corrosion rate¹²¹, as well as its ease of availability. Although the presence of Al would not be clinically attractive due to the linkage between Al and neuron damage, dementia, and Alzheimer's disease²⁴⁰, this alloy was selected as a benchmark by which to assess the novel Mg materials.

According to EN ISO 10993-5:1999, cytotoxicity is measured via cell death, inhibition of cell growth, cell proliferation, or colony-forming ability. 75% cell viability is considered to be non-cytotoxic. Thus, a tetrazolium salt-based assay (3-(4,5-dimethyl-2-thia-zolyl)-2,5-diphenyl-

2H-tetrazolium bromide, or MTT) was initially chosen to assess viability of goat ACL fibroblasts in response to extracts from the Mg materials. However, preliminary results in our laboratory as well as published literature showed that this assay is heavily influenced by Mg ion release and increases in pH that occur as a result of Mg corrosion. This leads to inflated optical density values that reflect a false positive^{63, 173}. Additionally, even if it were suitable for use with Mg extracts, the MTT assay functions by assessing metabolic activity in cells and would not be able to differentiate between a cytotoxic (causing cell death) or cytostatic (reduced metabolic activity) effect.

For these reasons, to determine the effects of Mg on cell growth, a cell proliferation assay (Click-It EdU, Life Technologies, Grand Island, NY) was performed at 3 days of culture. To also assess cell function, the total soluble collagen in the cell culture media was measured (Sircol, Biocolor Life Science Assays, Carrickfergus, UK). Soluble collagen was used due to the relatively short culture period, after which the majority of collagen produced would be expected to be released into the cell culture media.

5.1.2 Experimental Methods

5.1.2.1 Preparation of extracts from Mg materials

Rods of single crystal Mg, ZJ40, ZJ41, P13, and AZ31 were machined into cylindrical discs of 5 mm diameter x 5 mm height. The discs were stored in ethanol prior to use, after which they were air-dried and sterilized using ultraviolet radiation for 1 hour. The samples were then placed into modified Eagle's medium alpha (α MEM, Life Technologies, Grand Island, NY) supplemented with 2% FBS and 1% penicillin/streptomycin (P/S) at 37° C, with a weight-to-extraction medium ratio of 0.2 g ml⁻¹. This ratio was selected in accordance with ISO standard

10993:12¹⁹⁶. Extracts were incubated for 3 days, after which the Mg discs were removed from the cell culture media.

Serial dilutions were prepared for each extract using α MEM supplemented with 2% FBS and 1% P/S and to make 50%, 25%, 12.5%, and 6% extract solutions. 100% extract was not used due to findings from preliminary experiments as well as previous literature that indicated a harmful effect on cells, possibly due to osmotic shock⁴⁵. The pH of each extract concentration was read using pH test strips. Additionally, the osmolality of all extract dilutions from all materials was measured using an osmometer (Advanced Model 3320 Micro-Osmometer, Advanced Instruments, Inc., Norwood, MA). Duplicate measurements of osmolality were recorded and averaged for each sample.

5.1.2.2 Cell culture methods

A primary line of ACL fibroblasts was harvested from skeletally mature female goats during another study requiring removal of the ACL. The ACL tissue was minced and incubated in Dulbecco's modified Eagle media (DMEM) with 1% penicillin/streptomycin, 10% FBS, and 1 $\mu\text{g ml}^{-1}$ collagenase for 2 hours. The solution was then centrifuged at 2,000 RPM for 15 minutes, and the supernatant was discarded. The precipitated cell pellet was resuspended in DMEM with 10% FBS. Passage 3 (p3) cells were used for all experiments.

5.1.2.3 Cell proliferation assay

Goat ACL fibroblasts were cultured in α MEM with 10% FBS and 1% P/S at 37° C in a humidified atmosphere with 5% CO₂. At the third passage, they were seeded in 96-well cell culture plates, with 5 x 10³ cells/200 μl media in each well. Following incubation for 24 hours for cell attachment, the cell culture media was then replaced with 200 μl Mg extract and

incubated for 3 days. Due to variability in data observed in preliminary experiments, 5 samples were used per Mg extract dilution. α MEM with 2% FBS (0% extract) served as a control.

The Click-It EdU microplate assay (Life Technologies, Grand Island, NY) was then performed per manufacturer's instructions to measure cell proliferation. This assay utilizes a nucleoside analog of thymidine (5-ethynyl-2'-deoxyuridine) that is incorporated into newly-synthesized DNA with a fluorescent label (Amplex UltraRed dye). This undergoes a "click" reaction with Oregon Green 488 azide. First, a 10 μ M solution of EdU was prepared and 10 μ l was added to each well. The samples were placed on a rotary shaker for 2 min to ensure adequate mixing, and were then incubated overnight (~16 hours). The media was then removed and 50 μ l of a fixative solution was added to each well and incubated for 5 min. The remainder of the assay steps were performed in a dark environment to prevent loss of the fluorescent signal due to photo-bleaching. 50 μ l of a reaction cocktail containing Oregon Green 488 azide was added to each well and incubated for 25 min. Sample wells were then washed with a blocking buffer, and 50 μ l of an anti-Oregon Green HRP conjugate was added to each and incubated for 30 min. Another wash was performed using Amplex UltraRed buffer, and 100 μ l of Amplex UltraRed was added to each well and incubated for 15 min. Finally, 10 μ l of a stop reagent was added to each well and fluorescence was read using a microplate reader (Infinite M200, Tecan, Morrisville, NC) set at 495/519 nm for excitation and emission, respectively.

For data analysis, measurements of fluorescence representing cell proliferation (relative fluorescence units, or RFU) were averaged between each set of 5 samples, and proliferation was expressed as a percentage of the control group (α MEM with 2% FBS, 1% P/S). A 2-way ANOVA was used for statistical comparisons using SPSS Statistics (Version 21, IBM, Armonk,

NY), with extract percentage and Mg material as experimental factors. Significance was set a $P \leq 0.05$, and Bonferroni post-hoc tests were performed for pairwise comparisons.

5.1.2.4 Collagen production assay

Goat ACL fibroblasts were cultured in α MEM with 10% FBS and 1% P/S at 37° C in a humidified atmosphere with 5% CO₂. At the third passage, they were seeded in a 6-well cell culture plates, with 4×10^5 cells/2 ml media in each well. After incubation for 24 hours for cell attachment, the media was replaced with 2 ml Mg extract and incubated for 3 days. α MEM with 2% FBS (0% extract) served as a control.

The Sircol collagen assay (Biocolor Life Science Assays, Carrickfergus, UK) was then performed as per manufacturer's instructions. This is a colorimetric assay that is designed to quantify collagen using a dye-binding mechanism of side chains in Sirius Red dye to those in collagen molecules. First, three 100 μ l samples were collected from the cell culture media of each extract dilution. Reference standards of the same volume were also prepared using a stock solution of 500 μ g ml⁻¹ soluble bovine skin collagen in 0.5 M acetic acid. 1 ml of the dye reagent (Sirius Red in picric acid) was added to each sample and standard, and they were placed on a mechanical shaker for 30 min. Samples were then placed in a microcentrifuge for 10 min at 12,000 rpm, and the excess dye was removed. An acid-salt wash was used to remove excess dye from the collagen pellet, and pellets were resuspended in 250 μ l of 0.5 M sodium hydroxide. Finally, 200 μ l of each sample was added to a 96-well plate, and the absorbance was read using a microplate reader (Infinite M200, Tecan, Morrisville, NC) set at 555 nm.

For data analysis, a standard reference curve was first generated by fitting a linear curve to the absorbance values from the prepared standards. The linear equation generated was then

used to calculate the collagen content of each 100 μ l sample. Each value was then normalized by the average value in the 0% extract group to represent a percentage of the control.

A 2-way ANOVA was used for statistical comparisons using SPSS Statistics (Version 21, IBM, Armonk, NY), with extract percentage and Mg material as experimental factors. Significance was set a $P \leq 0.05$, and Bonferroni post-hoc tests were performed for pairwise comparisons.

5.1.3 Results

Following incubation in α MEM for 3 days, all Mg disc samples showed visible signs of corrosion, and there were small amounts of particulate Mg present in the cell culture media. The extracts derived from AZ31, ZJ40, and ZJ41 had become clear in color, whereas the extracts prepared from P13 and single crystal Mg maintained the original color of the cell culture media. The resulting extracts showed small increases in pH of up to 1 pH unit in the highest dilution of extract (Table 8). By 3 days of culture, the pH had decreased by as much as 0.5 pH unit.

Table 8: Initial (left) and final (right) pH values of Mg extracts

	Extract Concentration (%)									
	0		6		12.5		25		50	
AZ31	8	7.5	8	8	8.5	8	8.5	8	8.5	8.5
Single crystal	8	7.5	8.5	7.5	8.5	8	8.5	8	8.5	8.5
ZJ40	8	7.5	8.5	8	9	8	9	8	9	8.5
ZJ41	8	7.5	8.5	8	8.5	8	8.5	8	9	8.5
P13	8	8	8.5	8	8.5	8	8.5	8.5	8.5	8.5

The osmolality of the extract dilutions is shown in Figure 19. The osmolality of the cell culture media alone ranged from 300 – 307 mOsm kg⁻¹, and for all materials there was a linear relationship between the Mg extract concentration and osmolality. At 50% extract, ZJ40 had the highest osmolality (484 mOsm kg⁻¹), followed by AZ31 (427 mOsm kg⁻¹). Single crystal, ZJ41, and Mg-Ca-Zr all had similar osmolality (357 mOsm kg⁻¹).

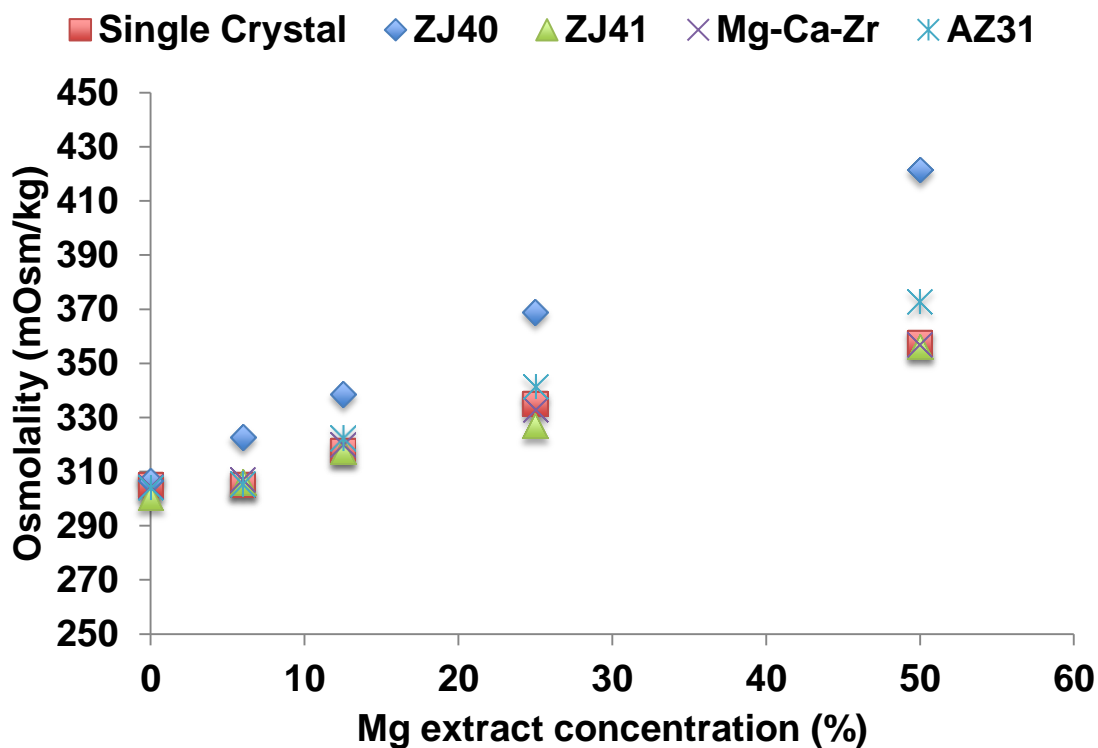


Figure 19: Osmolality (mOsm/kg) of Mg extract dilutions

When viewed under light microscopy, cells in the control and treated groups appeared to be healthy, with a characteristic spindle-shaped morphology. No signs of apoptosis were observed in any of the groups. In general, there were not visible differences between cells

cultured with different extract concentrations. However, in extracts from ZJ40 and ZJ41, the cells appeared larger and less densely packed when cultured with 50% extract.

The resulting cell proliferation of ACL fibroblasts when cultured with single crystal extracts is shown in Figure 20. With the addition of 6%, 12.5%, 25%, and 50% extract, the cell proliferation ranged from 89 – 137% at the tested extract concentrations and was not statistically different from that of the 0% control group ($P > 0.05$). The same pattern was observed for the other materials (Figure 21). In fact, results of the 2-way ANOVA indicated that there were no statistically significant main effects of either Mg material ($P = 0.175$) or extract concentration ($P = 0.284$) on cell proliferation.

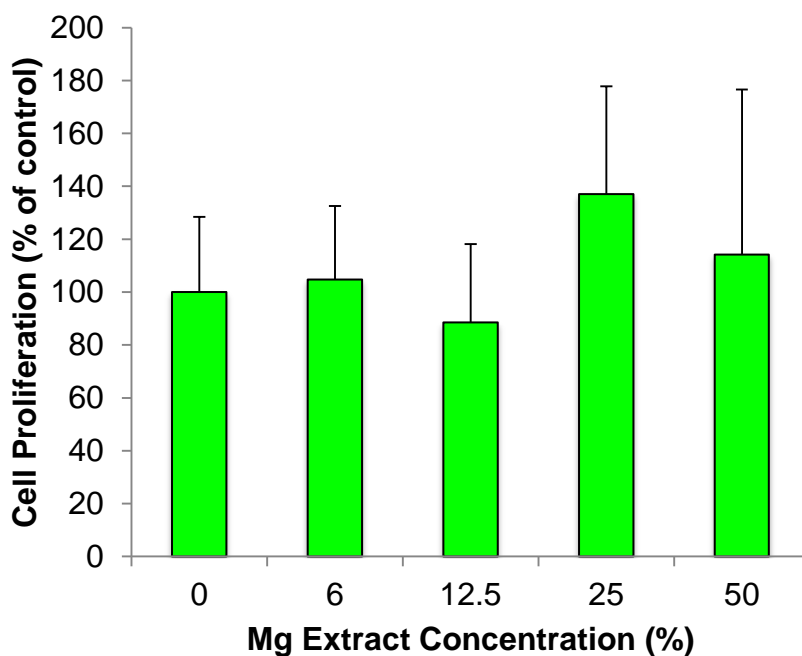


Figure 20: Resulting proliferation (% of control) of goat ACL fibroblasts after 3 days of culture with extracts prepared from single crystal Mg (mean \pm SD)

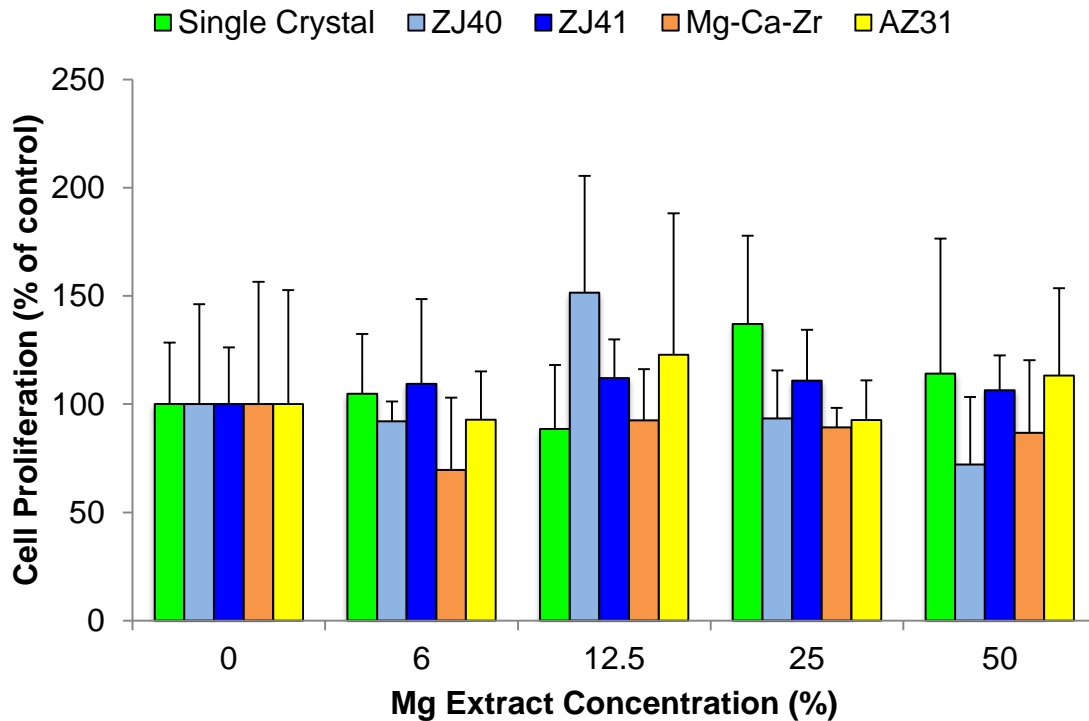


Figure 21: Resulting proliferation (% of control) of goat ACL fibroblasts after 3 days of culture with extracts prepared from Mg materials (mean \pm SD)

The resulting collagen production of ACL fibroblasts when cultured with single crystal Mg extracts is shown in Figure 22. From 0 – 50% extract, there was a steady decrease in total collagen produced by 3 days of culture. Upon the addition of 6%, 12.5%, 25%, and 50% extract, collagen production decreased by 19%, 10%, 21%, and 7%, respectively, representing 81%, 73%, 58%, and 54% of the collagen produced by the control. In fact, at 12.5%, 25%, and 50% extract, the collagen produced was significantly reduced compared to the control group, and by 50% extract, the average collagen produced was close to half of that of the control ($P < 0.05$).

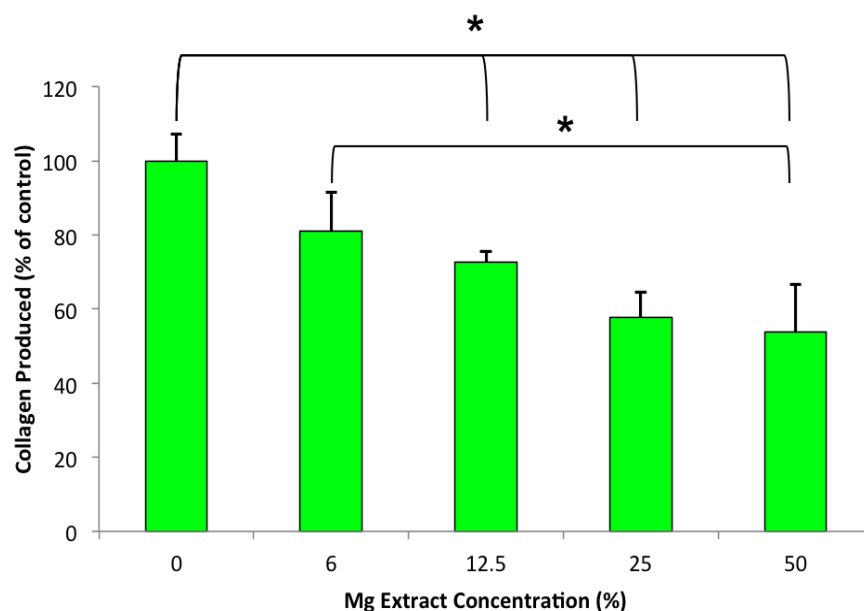


Figure 22: Soluble collagen produced (% of controls) by goat ACL fibroblasts after 3 days of culture with extracts prepared from single crystal Mg (mean \pm SD) (* indicates a statistically significant difference)

When the other Mg materials were assessed, consistent patterns were observed (Figure 23). Both the ZJ40 and ZJ41 groups displayed a similar gradual decrease in collagen production with increasing extract concentration, although the ZJ41 group consistently produced 10% or more collagen than the ZJ40 group. The Mg-Ca-Zr alloy group was the only one to show an increase in collagen with a higher extract concentration, with an increase of almost one-fifth from 6% to 12.5% extract (77% to 90% collagen). However, this increase was not statistically significant ($P > 0.05$), and subsequent higher extract concentrations resulted in the same downward trend. Interestingly, the AZ31 group was 40% or more lower than all of the other Mg materials at 6% extract, with 47% collagen produced compared to the control group ($P < 0.05$). However, this group showed a more gradual decrease at higher concentration, such that by 50% extract it was not significantly different from the other Mg materials ($P > 0.05$). Overall, at the

50% extract concentration, all of the Mg material groups produced 36 – 56% of the collagen of the control group.

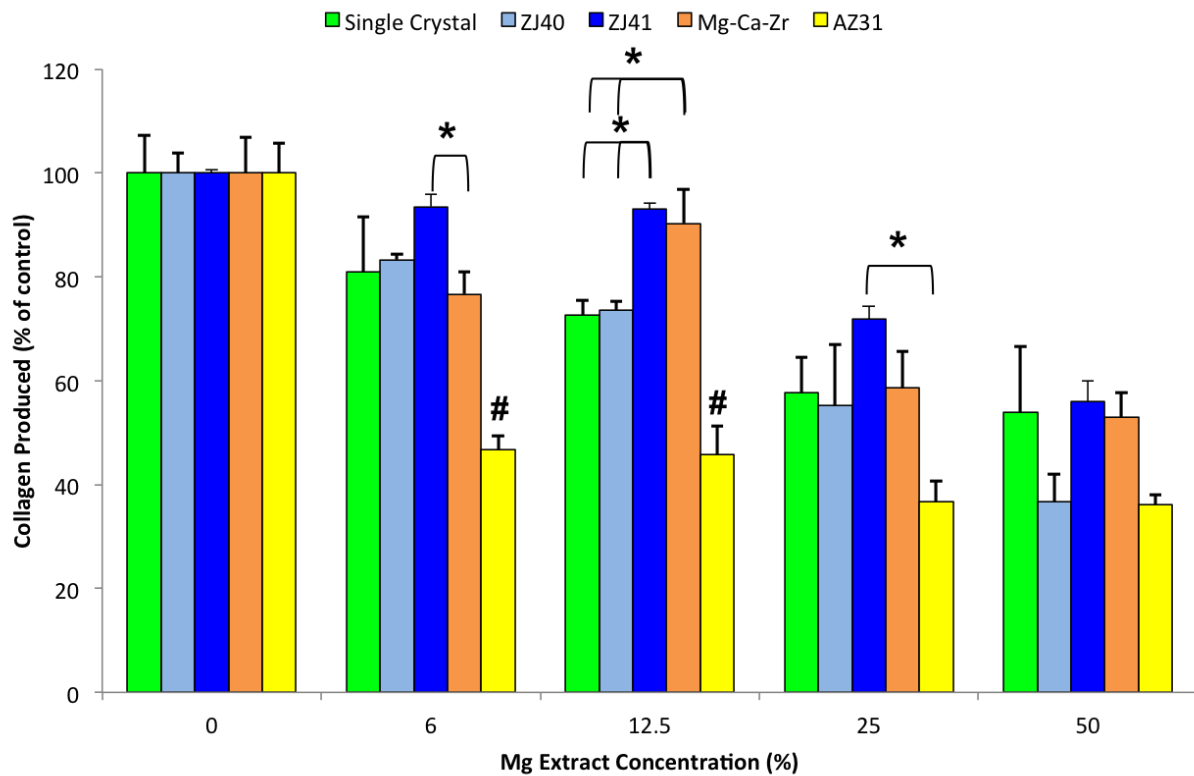


Figure 23: Soluble collagen produced (% of control) by goat ACL fibroblasts after 3 days of culture with extracts prepared from Mg materials (mean \pm SD) (* indicates a statistically significant difference, # indicates statistical difference from all other materials)

5.2 IN VIVO ACL HEALING STUDY

5.2.1 Experimental Methods

5.2.1.1 Animal model

Skeletally-mature (4 – 6 years of age), female Spanish goats were used for Specific Aim 3.2. This animal model has a large size and robust activity level that makes it well-suited for studies of the knee. Additionally, the goat has been successfully used in our research center and others for studies of ACL reconstruction and healing^{3, 60, 66, 141, 158, 170}.

5.2.1.2 Preparation of Mg ring devices

For *in vivo* experiments, single crystal Mg was used to produce the Mg ring devices. These crystals of pure (99.95%) Mg were produced at the University of Cincinnati (courtesy of Dr. V. Shanov) using the Bridgman technique. Briefly, polycrystalline Mg slugs (Alfa Aesar, Ward Hill, MA) were melted at 780 – 800° C inside a graphite crucible housed in a sealed quartz cylindrical housing with a seed crystal on one end. The crucible was translated at a speed of 30 mm/hour towards a cooler region of the furnace, where crystal growth at the seed crystal began once the solidification temperature of Mg was reached. During the growth process, an inert argon environment at an ambient pressure of 720 Torr was maintained. X-ray diffraction was used to characterize the crystals to verify that a monocrystalline structure had been produced.



Figure 24: A single crystal of Mg produced using the Bridgman technique (courtesy of Dr. V. Shanov)

The finished cylindrical crystals (> 8 mm diameter, > 30 mm length) were machined into the Mg ring geometry at the University of Pittsburgh's Bioengineering Machine Shop using the methods described in Section 3.2. Finally, to protect against corrosion, the crystals were coated with a ceramic oxidation coating in Dr. Yeoheung Yun's laboratory at North Carolina Agricultural and Technical Institute. Briefly, micro-arc oxidation treatment was applied by immersing the Mg rings attached to copper wires in electrolytic solution and applying pulse waveforms. The oxidation process resulted in a < 20 μm thick oxidation coating, which could be observed macroscopically as an opaque white layer (Figure 25). Following the application of the MAO coating, Mg ring devices were sterilized for surgery using ethylene oxide.



Figure 25: Single crystal Mg rings before (left) and after coating via micro-arc oxidation (right)

5.2.1.3 Preparation of ECM bioscaffolds

ECM sheets and pre-gel digests derived from the porcine urinary bladder matrix (UBM) were provided by our collaborators in Dr. Stephen Badylak's laboratory. Although previous work in our laboratory had utilized ECM from the porcine small intestine submucosa (SIS) for healing of the ACL as well as other ligaments and tendons^{66, 115, 132, 133}, published studies as well as preliminary data from our research center indicated that there was not a significant difference between SIS and UBM in terms of the growth factors, collagen, and glycosaminoglycan content, nor the surface morphology of hydrogels. Thus, due to its greater interest in clinical applications in orthopaedics, UBM was selected for the present study.

Well-established protocols were used to prepare the bioscaffolds from urinary bladders of market-weight pigs obtained from a local abattoir⁷³. Briefly, the bladders were first cut open and the urothelial, serosal, and muscular layers were scraped away. The remaining tissue (basement membrane and tunica propria) was treated with a 0.1% peracetic acid/ 4% ethanol solution and then lyophilized. 5 x 40 mm sheets were cut and sterilized with ethylene oxide.

To prepare the UBM hydrogels, additional lyophilized UBM was powdered using a Wiley Mill and filtered through a 40 mesh screen^{74, 81}. Then, the UBM powder was enzymatically digested under continuous stirring using 1 mg ml⁻¹ pepsin in 0.01 N HCl for 72 hours, and the resulting pre-gel digest (10 mg ECM ml⁻¹ dry weight) was frozen at -20° C. On the day of surgery, the pre-gel digest was thawed in 2.5 ml aliquots during the operation, and neutralized by adding one-tenth the volume of 0.1 N NaOH, one-ninth the volume of 10X PBS, and then diluting to a final concentration of 6 mg ml⁻¹ using 1X PBS. The hydrogel was then passed through a sterile filter and stored on ice until injection *in vivo*.

5.2.1.4 Surgical procedure

The surgical protocol used in this study was approved by the University of Pittsburgh's Institutional Animal Care and Use Committee, and procedures were performed with sterile techniques using general endotracheal anesthesia. In all animals, Mg ring repair was performed on the right stifle joint, while the left served as a sham-operated control.

A longitudinal incision was first made on the midline of the stifle joint from 1-2 cm above the patella to just below the tibial insertion of the patellar tendon. An arthrotomy was then performed medially to the patellar tendon, such that the patellar tendon could be retracted laterally and the ACL exposed. With clear visualization of the ACL, four bone tunnels were drilled in the femur and tibia using a 1.5 mm guide wire. On the tibial side, tunnels were made medial and lateral to the ACL's entheses, while on the femoral side, two parallel tunnels were made anterior to the entheses. Mg ring repair was then performed as described in Section 3.2. Before fixation sutures were secured in place outside of the bone tunnels, a 5 x 40 mm UBM sheet sutured to a similarly-sized fibrin sponge (Surgifoam, Ethicon, Inc., Bridgewater, NJ) was wrapped around the Mg ring. After fixation of the ring, additional UBM hydrogel^{66, 74, 159} (~4

ml) was injected directly into the injury site using an 18-gauge needle ⁶⁶. A local analgesic (Bupivacaine, 1 mg kg⁻¹) was injected subcutaneously for local pain management, and wounds were closed using sutures.

5.2.1.5 Post-operative care

Following surgery, animals were allowed free cage activity. For pain management, Banamine was administered twice daily subcutaneously (1.1 mg kg⁻¹) for 5 days post-surgery, and Metacam was administered every 3-5 days subsequently as deemed necessary by the site veterinarian. Animals were assessed daily for general health and the weight-bearing status of the treated joint. A scale was used for qualitative assessment of lameness (Table 9).

Table 9: Lameness scoring scale

Score	Weight-bearing status
0	Three-legged walking
1	Clear walking lameness/toe-touching
2	Mild walking lameness, clear during running
3	Minimal running lameness
4	Normal

At the end point of the study, animals were humanely euthanized. They were first sedated using an intramuscular injection of Ketamine/Xylazine (7 mg kg⁻¹ Ketamine, 0.1 mg kg⁻¹ Xylazine), followed by a lethal injection of sodium pentobarbital (1 ml (390 mg)/ 10 lbs). Both treated and sham-operated legs were harvested using a scalpel by disarticulation of the hip joint.

A time point of 6 weeks was selected for a pilot study to preliminarily assess the proof of concept of the novel approach for ACL healing early in the healing process before proceeding with a longer study. For the goats sacrificed at 6 weeks (N = 2), stifle joints were used for histology (N = 1) and analysis of degradation of the Mg ring using microcomputed tomography (micro-CT; N = 1). A time point of 12 weeks was selected as previous studies of the healing of ligaments and tendons in goats have demonstrated substantial healing by this time ^{2, 66, 158}. For the goats sacrificed at 12 weeks (N = 7), stifle joints were used for histology (N = 1) and biomechanical testing (N = 6).

5.2.1.6 Gross morphology

The gross morphology of the healing ACL was assessed following dissection of the FATC. The size, shape, color, alignment, and continuity of the healing tissue were recorded. The cross-sectional area and shape of the ACL were measured quantitatively using a laser micrometer system developed in our research center ^{149, 223}, which can take non-contact measurements of cross-sectional area (CSA) with an accuracy of $\pm 5\%$. Measurement of the CSA was only taken in the 12-week group due to the presence of the Mg ring in the 6-week group that could not be separated from the healing tissue. The value reported was an average of two measurements taken at different points near the midsubstance of the ACL.

The articulating surface of the patella and the femoral condyles were inspected for the presence of osteochondral lesions, and the fusion of the bone tunnels was assessed by the ability of the fixation sutures to slide freely through.

Degradation of the Mg ring was assessed using the qualitative scale shown in Table 10. If Mg fragments were observed in the joint space, their size and location were also recorded. Finally, the presence of the fibrin sponge and ECM sheet were also noted.

Table 10: Qualitative scale describing degradation of the Mg ring

Score	Condition of the Mg Ring
0	Mg ring appeared to have fully degraded
1	Few Mg fragments observed
2	Many large Mg fragments observed
3	Mg ring was mostly intact

5.2.1.7 Histological evaluation

In the stifle joints designated for histological evaluation, the FATCs were dissected and trimmed immediately after harvest. They were submerged in 10% neutral-buffered formalin (Sigma Aldrich, St. Louis, MO) for 48 hours and then stored in 70% ethanol prior to use.

Histology was performed at Alizee Pathology, LLC (Thurmont, MD). Due to the challenges presented by sectioning through the Mg ring to prepare the histological slide, methylmethacralate (MMA) was required for embedding of the healing FATC. As a control, the contralateral sham-operated FATC was also evaluated, and was embedded in an oversized paraffin block after decalcification. All samples were then sectioned once longitudinally and twice serially, and stained with hematoxylin and eosin (H&E). They were evaluated using light microscopy.

5.2.1.8 *In vivo* degradation of the Mg ring

To quantitatively assess the *in vivo* degradation of the Mg ring, micro-CT scans were used. This analysis was only performed at 6 weeks of healing (N = 1) as the degradation of the Mg ring by

12 weeks was very substantial and the device had degraded or fragments had migrated away from the ACL.

Immediately after sacrifice, the healing FATC was dissected and trimmed, then submerged in 10% neutral-buffered formalin for 48 hours and stored in 70% ethanol prior to use. It was dried in 100% ethanol and embedded in epoxy resin, and imaged using a Skyscan 1172 scanner (Skyscan-Bruker, Kontich, Belgium) using 10 μ m voxel size, 60 KVp energy, 400 ms exposure, and 6 exposures averaged per lateral view to reduce noise. An offset mode was required as the specimen was larger than the available field of view for the desired magnification. The total scan time was 12 hours.

Reconstruction of raw files into the 3D volume was done using Skyscan ReCon software (Skyscan-Bruker, Kontich, Belgium), and processing for quantitative analysis of the remaining volume of Mg was performed using Skyscan DataViewer and CTAn software. From 2D cross-sectional slices in the superior-inferior direction, regions of interest could be defined manually surrounding the degrading Mg ring (Figure 26). With each slice, a corresponding histogram was generated representing the voxel mineral densities within the region of interest. Within the histogram, peaks were identified representing the surrounding bone, intact Mg, and Mg degradation products. Thus, the region of interest was segmented using the inflection point between each of the peaks. By then summing the voxels from each micro-CT slice, the total volume of intact Mg as well as the Mg degradation products could be determined. These volumes were expressed as a percentage of the total initial volume of the Mg ring to represent the degradation of the Mg ring.

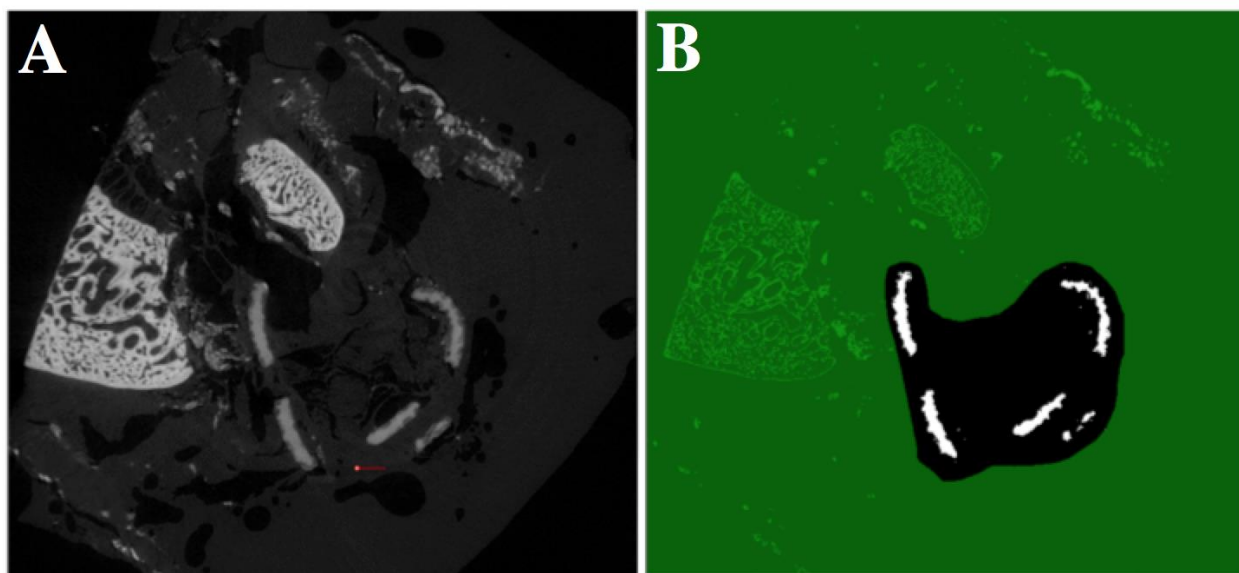


Figure 26: Cross-sectional slice of the degrading Mg ring from micro-CT scan (A), with manually-selected region of interest surrounding the Mg ring depicted in black and intact Mg depicted in white (B)

5.2.1.9 Analysis of synovial fluid

1 ml samples of synovial fluid were collected from treated and sham stifle joints immediately after sacrifice using an 18-gauge needle. This analysis was only performed in the 12-week group. A small amount (~100-200 μ l) of each sample was used to smear on a glass slide, and the JorVet Dip Quick Stain (Jorgensen Laboratories, Inc., Loveland, CO) was used to qualitatively assess cytology. After air-drying the prepared slide, it was dipped into methanol for fixation, followed by polychromatic stains (eosin and thiazine) to allow detection and visualization of nucleic acids, protein eosinophil granules, and mast cell and basophil granules. Once prepared, the slides were observed under a light microscope. The total protein content was measured using a refractometer.

5.2.1.10 Biomechanical testing

Specimen designated for biomechanical testing ($N = 6$) were immediately sealed in plastic bags and frozen at -20°C following euthanasia. 24 hours prior to testing, specimen were thawed and prepared for testing as described in Section 4.1. During specimen preparation as well as throughout biomechanical testing, a 0.9% saline solution was periodically spritzed on the sample to prevent dehydration.

The joints were attached to the robotic/UFS testing system as described in Section 4.2. In this Aim, a new, high-payload system was used for the measurement of joint stability and ACL function (Figure 27). The UFS system (Model Theta, ATI Industrial Automation, Apex, NC) has a capacity of 1,500 N and 240 N-m, as well as a repeatability of 0.5 N and 0.05 N-m for force and torque, respectively. The robotic manipulator (KUKA Model KR 210, Kuka Robotics Corp, Shelby Township, MI) has a position and orientation repeatability of less than 0.1 mm and 0.1° .

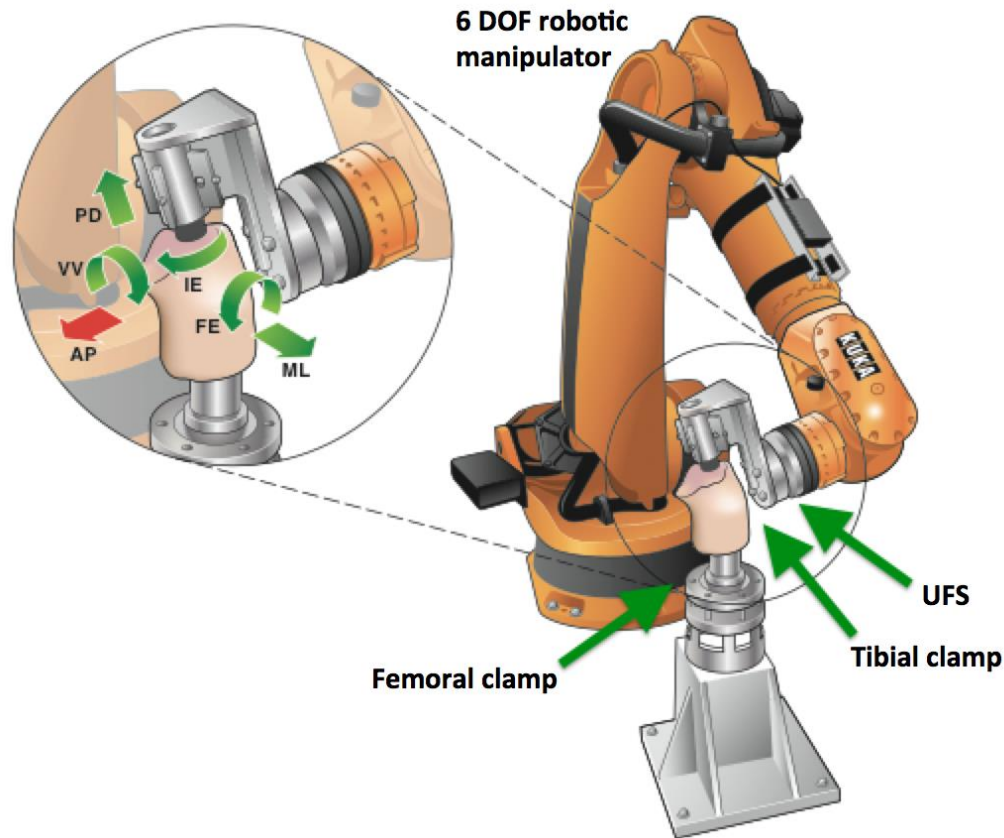


Figure 27: A schematic illustrating a joint being tested on the robotic/UFS testing system at preselected angles of joint flexion, providing 5-DOF joint kinematics (AP – anterior-posterior, FE – flexion-extension, IE – internal-external, ML – medial-lateral, PD – proximal-distal, VV – varus-valgus)

In Specific Aim 3.2, force control of the robotic/UFS testing system was employed to measure the resulting 5-DOF stifle joint kinematics in response to a single loading condition: a 67-N anterior-posterior tibial load, at 30°, 60°, and 90° of joint flexion. The anterior-posterior tibial translation (APTT) was measured and recorded as a measure of stifle joint stability. For this Aim, the measurement of the posterior tibial translation was included for two reasons. First, due to the reduced stability of the healing stifle joint, the robotic/UFS testing system may not have chosen the true neutral position, as multiple positions could be selected that would be below the desired force and moment threshold. Secondly, the stifle joint center of rotation may have

shifted forward or backward during the healing process. Measurement of APTT would be able to correct for these changes.

Once the kinematics under the 67-N anterior-posterior tibial load were recorded, they were repeated as each of the following knee structures was removed: MCL, soft tissue and LCL, medial meniscus, lateral meniscus, PCL, and bony contact. The corresponding in-situ force in each structure in the joint was calculated using the principle of superposition, and the final set of forces measured with only the FATC represented the in-situ force in the ACL.

After testing on the robotic/UFS testing system, uniaxial tensile testing was performed to determine the structural properties of the FATC. Each FATC was mounted to a materials testing machine (Model 4052, Instron, Canton, MA) using custom clamps such that the ACL was aligned anatomically in its natural direction of tensile loading (Figure 28). It was then preloaded to 3 N, and the gauge length was reset. It was then cyclically preconditioned between 0 – 1 mm of elongation, which was in the toe region of the load-elongation curve, for 10 cycles at a crosshead speed of 50 mm min^{-1} . Finally, the 3 N preload was reapplied, and the FATC was loaded to failure at a crosshead speed of 10 mm min^{-1} . From the resulting long-elongation curve, the structural properties of the FATC were determined, including the stiffness, ultimate load, and ultimate elongation.

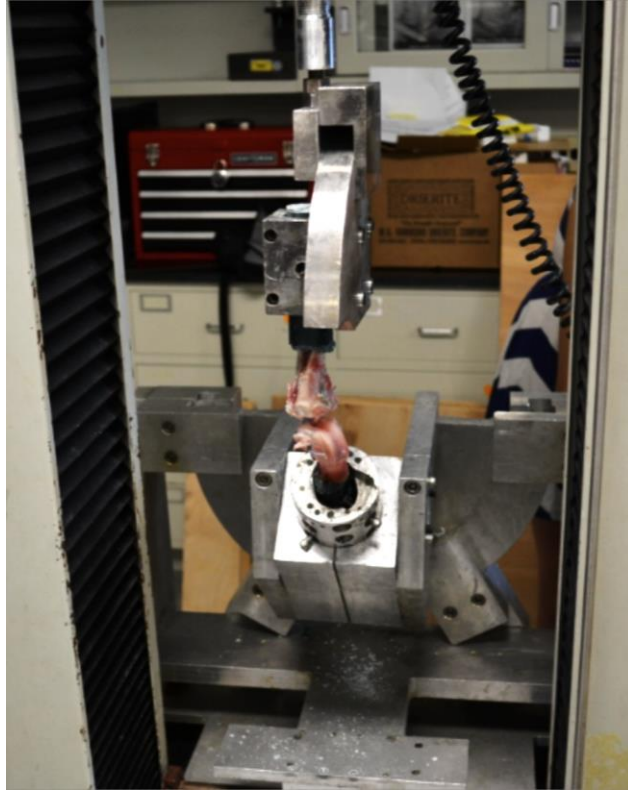


Figure 28: The FATC mounted on the materials testing machine for uniaxial tensile testing

5.2.1.11 Data analysis

All statistical analysis was performed using SPSS Statistics (Version 21, IBM, Armonk, NY), with statistical significance set at $P \leq 0.05$. Data representing the cross-sectional area, total protein content of the stifle joint synovial fluid, joint kinematics, in-situ forces, and tensile properties were compared using two-tailed paired t-tests. For the data on joint kinematics and in-situ forces, statistical analyses were performed separately for data at each joint flexion angle.

5.2.2 Results

All goats recovered well from surgery and were mobile and able to bear weight on the treated joints within 1-2 hours post-operatively. By day 17, most were able to walk with a small limp that was more pronounced during running (lameness score ≥ 2), and by day 45, all could run freely with little to no limp (lameness score ≥ 3).

During the 12-week study, three goats of an original group to 10 did not survive to the 12-week time point due to complications not related to the experiment. Following sacrifice at 12 weeks, one specimen was observed to have undergone a surgical error, and it was excluded from the study. Another specimen was damaged by the robotic/UFS testing system and was also excluded. Thus, the total sample sizes were $N = 2$ at 6 weeks of healing and $N = 5$ at 12 weeks of healing.

5.2.2.1 Gross morphology of the healing ACL

By 6 weeks, the stifle joint had minimal swelling. The healing ACL was composed of translucent neo-tissue growing within and around the degrading Mg ring, in addition to slightly reddish, opaque tissue where the preserved ends of the ACL remained (Figure 29). There was no hypertrophy of the healing ACL, and there was a small gap (< 1 mm) within the Mg ring between the two transected ends of the ACL. In both specimen, the Mg ring had fractured into 3 – 5 fragments, but these fragments appeared to have remained attached to the ACL by the healing tissue as well as the fixation sutures. The surface of the Mg ring was dull and dark gray in color. The ECM sheet and fibrin sponge were not visible in the joint space.



Figure 29: Gross morphology of the healing ACL at 6 weeks

By 12 weeks, the stifle joint was found to be stable upon manual examination and signs of swelling had subsided. Observation of the gross morphology of the healing ACL revealed a robustly healed neo-ligament that was mostly white and opaque in color (Figure 30). The tissue appeared to be well-aligned with longitudinal collagen bundles. The geometry of the healing ACL also resembled that of a normal ACL, except that it was slightly more oblong in shape. There was a small amount of hypertrophy, as the cross-sectional areas determined by the laser micrometer system increased from $28.9 \pm 4.0 \text{ mm}^2$ in the sham-operated ACL to $37.6 \pm 9.6 \text{ mm}^2$ in the healing ACL (Figure 31). However, this difference was not statistically significant ($P = 0.12$). Inspection of the femoral condyles and articulating surface of the patella revealed no signs of degenerative osteochondral lesions or defects.

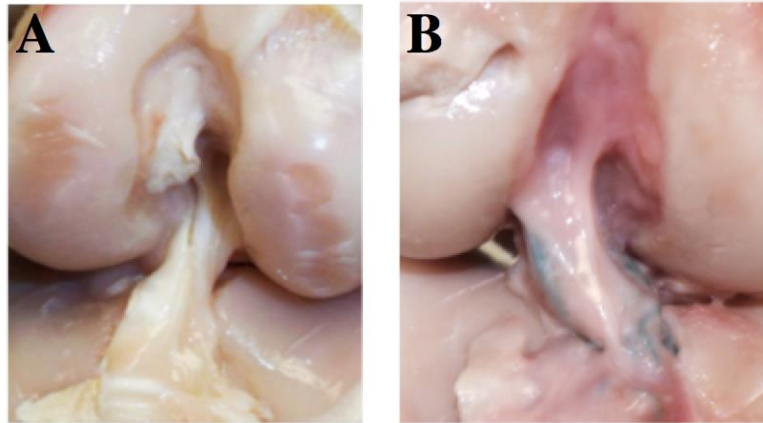


Figure 30: Gross morphology of the sham-operated ACL (A) and Mg ring-repaired ACL (B)

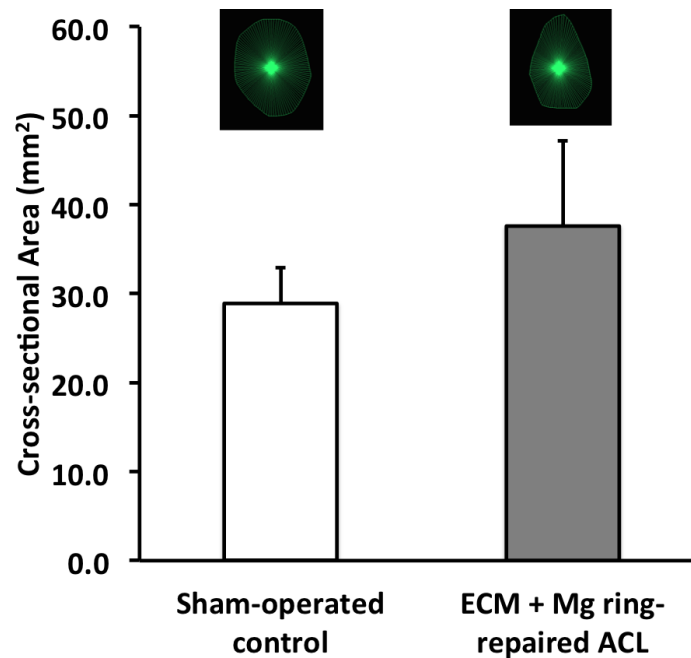


Figure 31: Cross-sectional area and shape of the sham-operated and healing ACL

The scores representing the condition of the Mg ring are shown in Table 11. In two animals, (ear tags #761 and #765) there was no visible trace of the Mg ring, which appeared to have fully degraded. In two other animals (ear tags #740 and #714), fragments (< 3 mm diameter) were found attached to the ACL, and some had migrated in the joint space. The

fragments attached to the ACL had become encased in a small fibrous capsule that was attached to the ligament. However, no cytotoxic or adverse reaction was observed. In one animal (ear tag #550), the Mg ring appeared to be mostly intact, though it had fractured into 3-5 large pieces that were embedded mostly in the healing ACL.

Table 11: Scores representing the degradation of the Mg ring at 12 weeks of healing

Goat Ear Tag #	Score	Presence of ring fragments
740	2	Cluster of tiny fragments on the anterior region of the ACL; one large fragment adjacent to the lateral meniscus
550	3	Mostly intact Mg ring embedded in the healing ACL; one fragment adjacent to the PCL
714	2	Fragments embedded in the medial anterior ACL midsubstance and medial meniscus
761	1	None
765	1	None

5.2.2.2 Histological evaluation

The histology of the sham-operated ACL was found to be characteristic of a normal ACL. It was composed of dense collagen bundles that were longitudinally aligned (Figure 32A), and was covered with a synovium that was 30-40 μ m thick (Figure 32B).

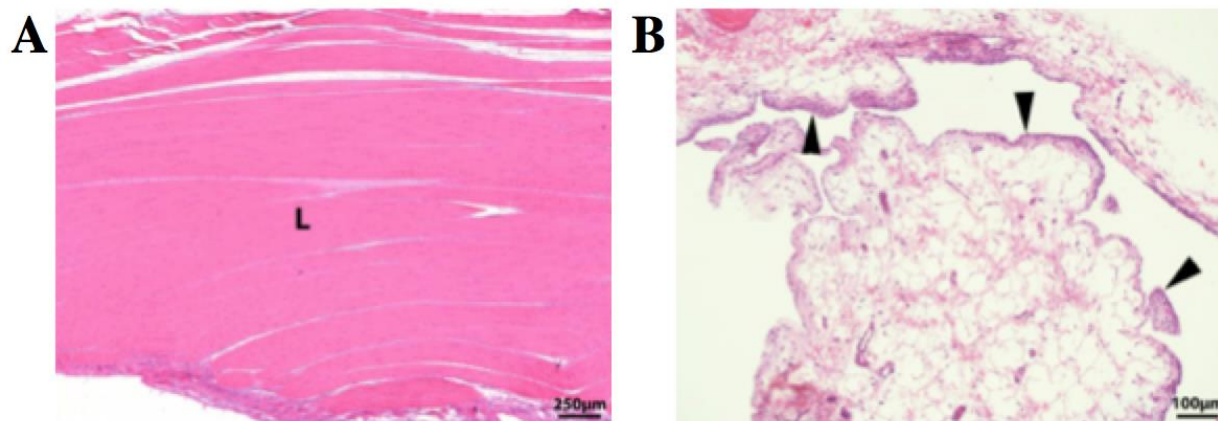


Figure 32: Histology of the sham-operated ACL, depicting longitudinally-aligned collagen bundles (A) and normal synovium (B) (L – ligament)

A longitudinal section of the healing FATC at 6 weeks of healing is shown in Figure 33. A 0.5 – 2.5 mm gap was observed between the transected ends of the ACL that was partially filled with granulation tissue at the proximal side of the Mg ring. Within this tissue were some macrophages, a few foreign body giant cells, and rare neutrophils. Inflammation observed in the granulation tissue was concentrated near fixation suture material, which was a minor and expected foreign body response.

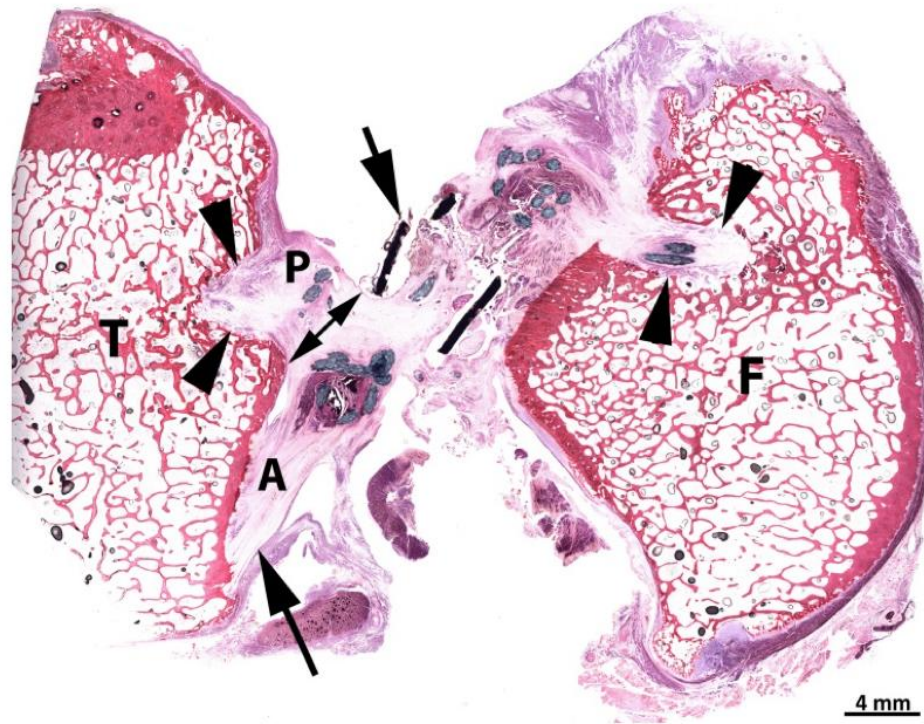


Figure 33: Histological section of the healing FATC at 6 weeks of healing using H&E staining (T= tibia, A= ACL, P= PCL, F= femur)

The healing ACL enclosed within the degrading Mg ring at the same healing time point is shown in Figure 34A. The Mg ring contained pits of corrosion that were lined with hyalinized collagen (Figure 34B), and at the interface of the ring with the ACL, there was also a minimal to mild inflammatory response. Nearby the fracture site of the Mg ring and in close proximity to the gap observed between the transected ends, there were small amounts of crystalloid-like fragments of the Mg ring that were likely degradation products (Figure 34C). These fragments also elicited a mild inflammatory response that was composed of macrophages and a small number of lymphocytes. Around the majority of the healing ACL, there was a morphologically normal synovium. This synovium was not observed around the tissue within the Mg ring, which was likely due to the adhesion of this tissue to the inside surface of the Mg ring (Figure 34D).

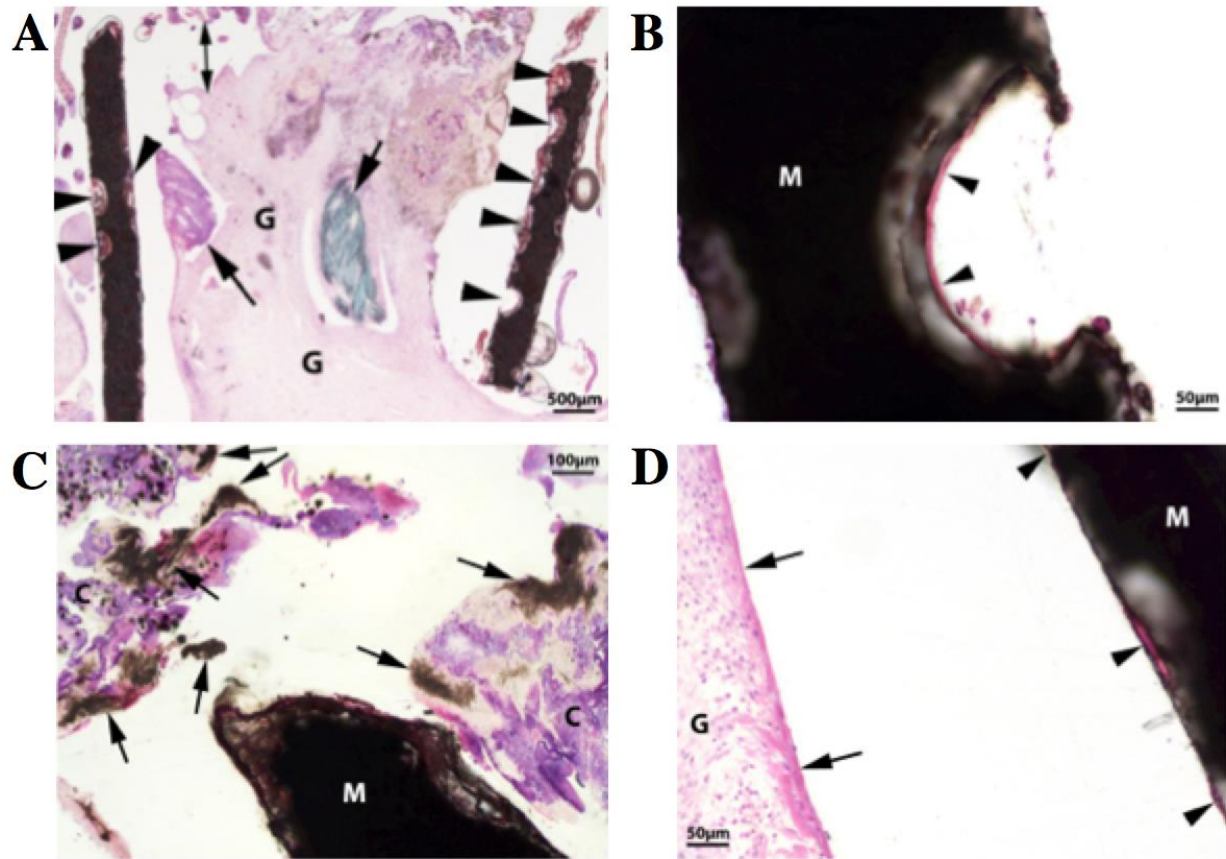


Figure 34: Histological image of the Mg ring–repaired ACL (A), pitting corrosion lined with hyalinized collagen (B), small degrading fragments of the Mg ring (C), and lack of normal synovium around ACL tissue adhered to inner surface of the Mg ring (D) (G= granulation tissue, M= Mg ring, C= collagen)

The histological appearance of the healing ACL at 12 weeks is shown in Figure 35. Whereas at 6 weeks the two ends of the transected ACL could be clearly distinguished, by 12 weeks of healing the healing ACL had become continuous, with some visible alignment of its collagen fibers. Small fragments of Mg were also observed to be embedded in the healing ACL, but these did not appear to be detrimental to the surrounding tissue

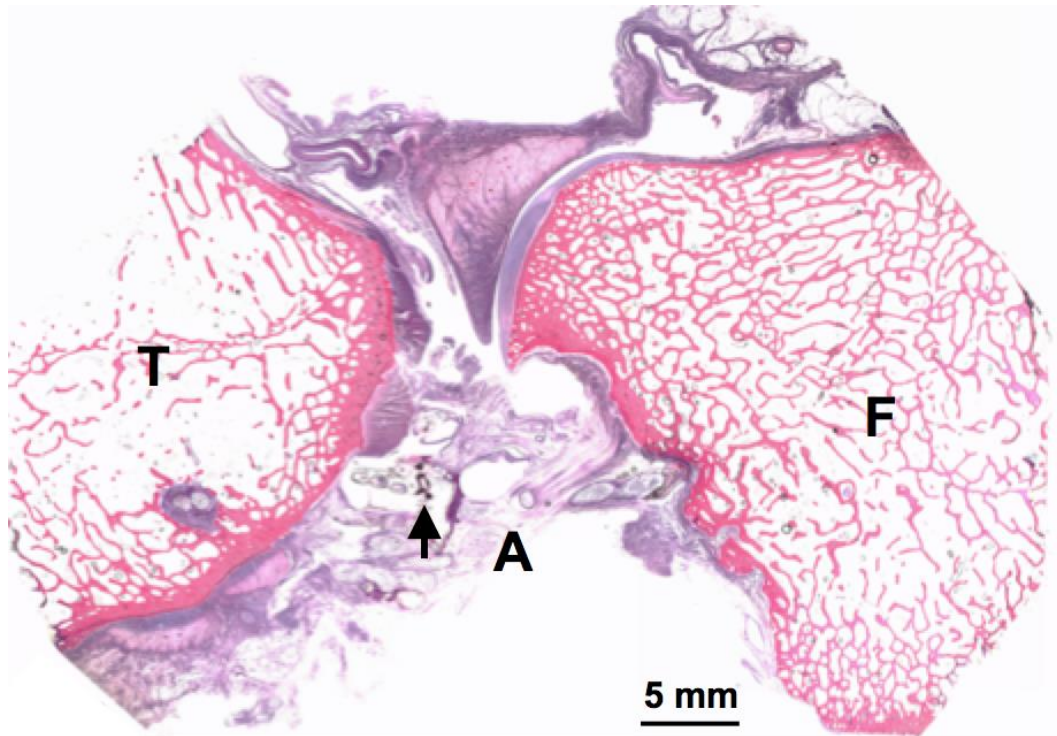


Figure 35: Histological section of the healing FATC at 12 weeks of healing using H&E staining (T= tibia, A= ACL, F= femur; arrow indicates Mg fragment)

5.2.2.3 Degradation of the Mg ring

A 3D reconstruction of the degrading Mg ring at 6 weeks of healing is shown in Figure 36, with the ring shown in orange and the trimmed femur and tibia depicted in green. This illustrated how the ring had fractured *in vivo*, yet retained the fragments near the ACL due to embedding in the healing tissue as well as attachment to fixation sutures. Examination of this reconstruction indicated fracture of the Mg ring device at predicted locations: between the notches as well as adjacent to suture holes.

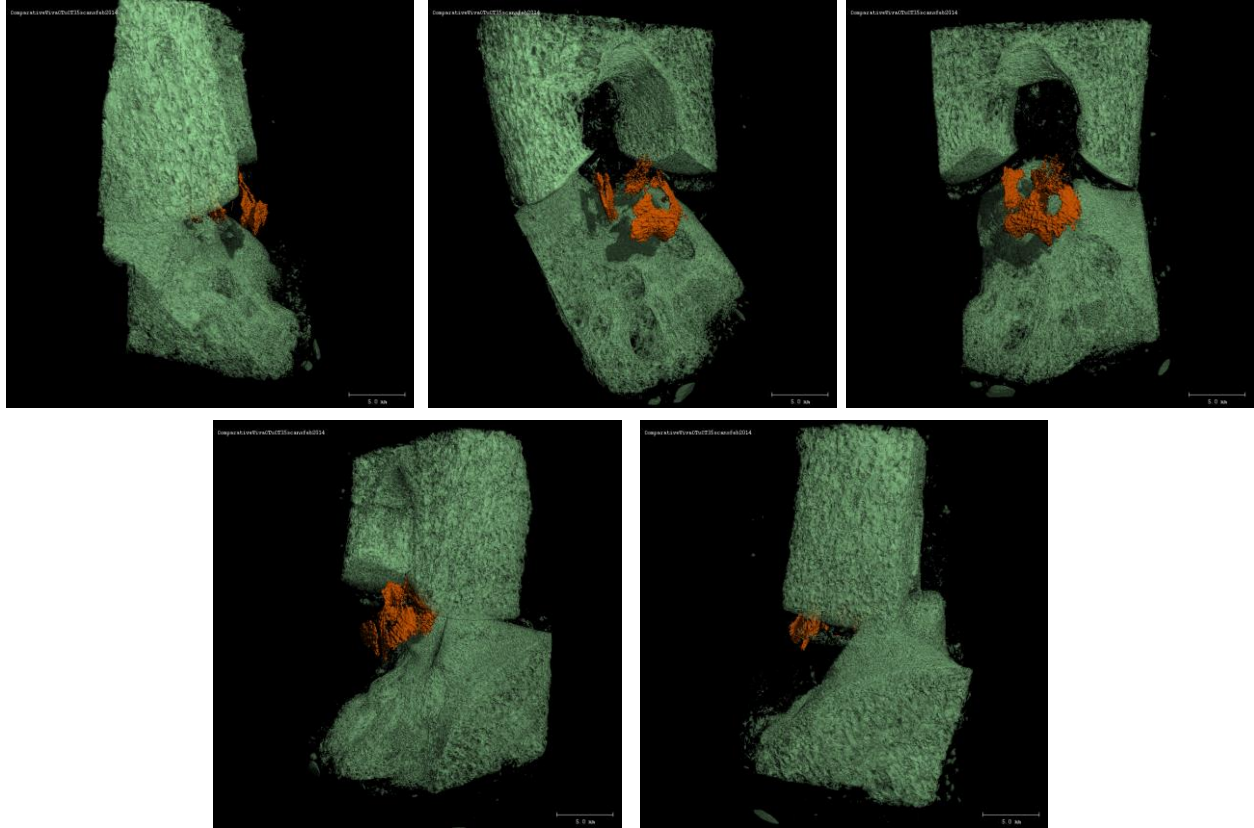


Figure 36: 3D rendering of the degrading Mg ring at 6 weeks of healing in the goat stifle joint with femoral and tibial bone blocks

By examining the 3D slices from the micro-CT scan, pitting corrosion was found to have occurred throughout the device. By then segmenting the densities of the intact and degrading Mg, the volume of intact Mg was found to be 21.0 mm^3 , which was 57% of the starting volume of Mg. The volume of degradation products was found to be 14.7 mm^2 . If it is assumed that there was no change in volume as intact Mg became degradation products, these values can be combined to be 35.7 mm^3 , which would indicate that 98% of the original Mg was still present in the ACL.

5.2.2.4 Cytology and total protein content of synovial fluid

The synovial fluid in the sham-operated joints was clear and slightly yellow in color and was very viscous. Due to sparse quantities, manipulation of the needle and the joint was required during sample collection such that sufficient fluid could be retrieved. In contrast, the synovial fluid in the healing stifle joint was slightly reddish in color and was less viscous. A larger quantity was also present, such that sample collection could be easily achieved without manipulating the needle or joint.

When the stained slide was viewed under light microscope, the cytology of the synovial fluid from the sham-operated and healing ACL was found to be similar. In both groups, there was low cellularity, with few synovial cells and red blood cells in a lacy matrix. In the treated group, there were a few more synovial cells, as well as a few lymphocytes and macrophages. There were no signs of infection or an abnormal inflammatory response.

The total protein content in the synovial fluid from the sham-operated joints was $2.6 \pm 0.2 \text{ g dl}^{-1}$, which was similar to the value of 2.4 g dl^{-1} estimated for normal joint synovial fluid in goats (one-third of the total blood serum protein content) (Figure 37) ¹⁰. The total protein content in the synovial fluid from the healing joints was $3.4 \pm 0.5 \text{ g dl}^{-1}$, and was significantly higher ($P = 0.02$). However, the values remained below the threshold of 4.5 g dl^{-1} above which significant inflammation has previously been reported ¹.

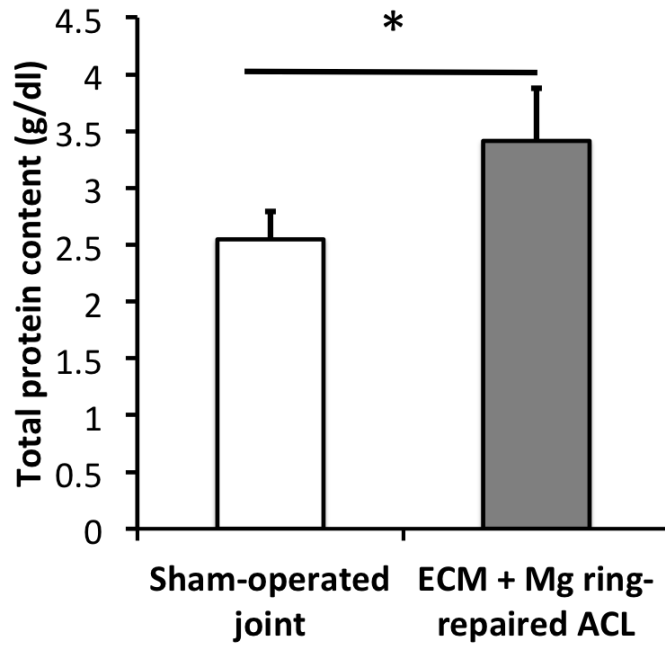


Figure 37: Total protein content in synovial fluid from sham-operated and healing goat stifle joints at 12 weeks of healing ($P < 0.05$)

5.2.2.5 Joint stability and in-situ forces

The curves representing the average APTT in the sham-operated and Mg ring-repaired joints are shown in Figure 38. As the patterns were similar at all tested joint flexion angles, results at 60° of joint flexion are shown for illustrative purposes. In the graph, elongation began at the point of maximum posterior tibial translation and continued to the point of maximum anterior tibial translation. With the PCL left intact in both groups, the posterior tibial translation in response to the 67-N posterior tibial load was similar between groups. The curve for the sham-operated group continued with a near-linear slope through the application of the 67-N anterior tibial load. However, near the neutral position (~20 N posterior tibial load), the Mg ring-repaired joint became less stable, and began to experience higher translation with small increases in loading.

This continued until 10-20 N of anterior tibial loading, after which the ACL and other joint structures were engaged to limit subsequent translation.

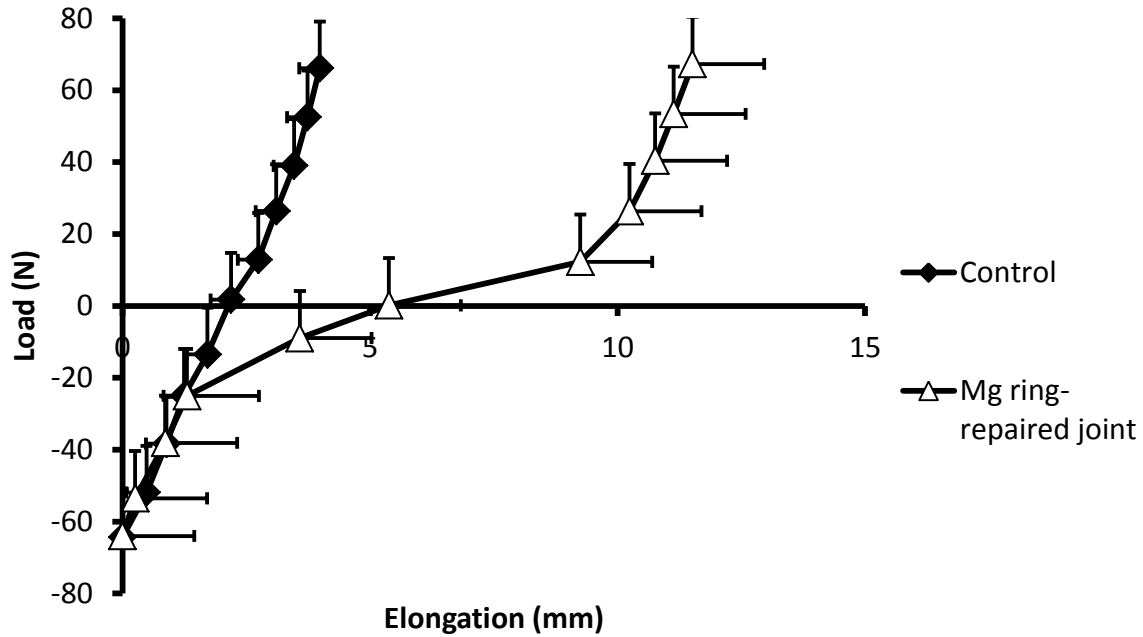


Figure 38: Average curves for the APTT in the sham-operated and Mg ring-repaired joints at 60° of stifle joint flexion under a 67-N anterior-posterior tibial load (mean \pm standard error)

The APTT in response to the 67-N anterior-posterior tibial load is shown in Table 12. In both the sham-operated and Mg ring-repaired joints, the APTT increased from 30° to 60° of stifle joint flexion, then decreased at 90°. The APTT in the sham-operated group ranged from 2 – 5 mm, and was similar to previously-reported values for a normal goat stifle joint^{3, 65, 66}. At all tested flexion angles, the APTT in the Mg ring-repaired joint was 2 – 3 times that in the sham-operated joint, and the differences were statistically significant at all tested flexion angles ($P \leq 0.05$).

The in-situ forces in the sham and Mg ring-repaired ACL in response to the 67-N anterior tibial load are also shown in Table 12. The in-situ force in the ACL in the sham-operated joint was close to the applied load and ranged from 53 – 64 N. The in-situ force in the Mg ring-repaired ACL was close to that of the sham-operated ACL at 30° of flexion ($P > 0.05$), and decreased by ~20 N at 60° of flexion, but the difference compared to that in the sham-operated ACL was not statistically significant ($P > 0.05$). At 90° of joint flexion, the in-situ force in the Mg ring-repaired ACL decreased again by ~20 N, and this was significantly lower than that in the sham-operated ACL ($P < 0.05$).

Table 12: Anterior-posterior tibial translation (A) and in-situ forces in the ACL (B) of the sham-operated and Mg ring-repaired goat stifle joints at 30°, 60°, and 90° of joint flexion (*indicates a statistically significant different compared to sham-operated controls; $P \leq 0.05$)

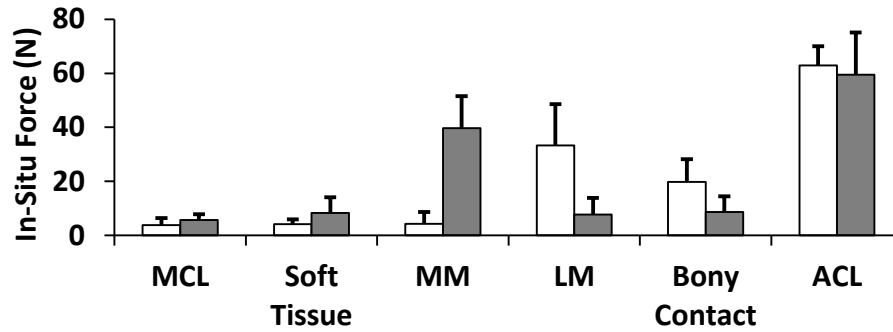
	Flexion Angle		
	30°	60°	90°
A. Anterior-posterior tibial translation			
Sham-operated group	3.8 ± 1.5	4.0 ± 1.5	3.4 ± 1.3
Mg ring-repaired group	9.8 ± 2.3*	11.5 ± 1.9*	9.4 ± 1.4*
B. In-Situ forces in the ACL			
Sham-operated group	63 ± 6	64 ± 6	53 ± 4
Mg ring-repaired group	59 ± 16	41 ± 29	19 ± 19*

To better understand the differences between the function of the sham-operated and healing stifle joints, it is useful to also compare the in-situ forces in other structures in the stifle joint. These forces are shown in Figure 39 for each tested joint flexion angle. The force

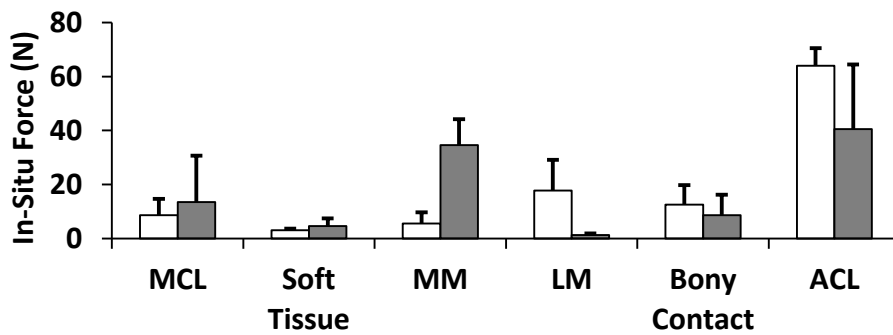
distribution amongst joint structures differed between the groups, as well as based on the flexion angle. At 30° of stifle joint flexion, the majority of the in-situ force under the 67-N anterior tibial load was in the ACL in both the sham-operated and healing groups. In the sham-operated joints, there were also smaller forces in the lateral meniscus (~40 N) and bony contact (~20 N), but in the healing joints these forces shifted to the medial meniscus (~40 N). At 60° of joint flexion, the majority of force in the sham-operated group was again carried by the ACL, and the forces carried by the lateral meniscus and bony contact decreased by half to ~20 N and 10 N, respectively. In contrast, in the healing joints, the in-situ force in the ACL was decreased, with forces also carried by the medial meniscus (~40 N) and MCL (~20 N). Finally, at 90° of flexion, the in-situ forces in the sham-operated joints were again carried mostly by the ACL, with smaller forces carried by the MCL, medial meniscus, and bony contact (~10 N each). Alternatively, in the healing joints, the ACL carried a much smaller force (~20 N), while other joint structures carried equal or higher forces, including the MCL (~20 N), soft tissue (~25 N) and medial meniscus (~30 N).

Sham-operated joint
 Mg ring-repaired joint

A.



B.



C.

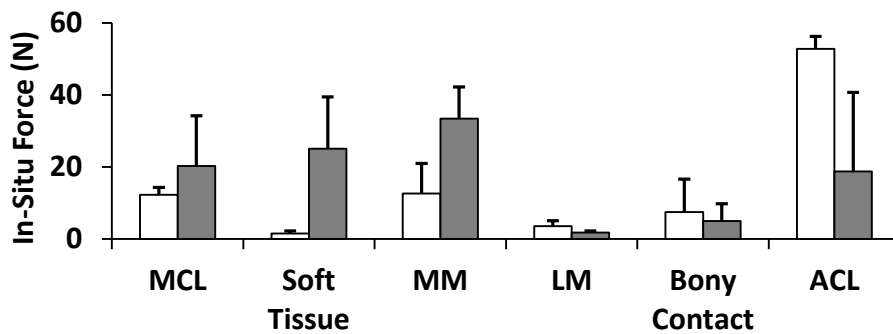


Figure 39: In-situ forces in the MCL, soft tissue, medial meniscus, lateral meniscus, bony contact, and ACL in the sham-operated and Mg ring-repaired goat stifle joints at 30° (A), 60° (B), and 90° (C) of joint flexion

5.2.2.6 Tensile properties

The load-elongation curves for the sham-operated and healing FATCs followed the expected trend for a ligament, beginning with a toe region of low stiffness for the first 1-1.5 mm of elongation, followed by a linear region of greater stiffness prior to failure. All of the healing ACLs failed in the midsubstance of the tissue.

The structural properties of the FATC are shown in Table 13. Two of the four specimen had distinctly higher structural properties, with stiffnesses of 110 and 101 N/mm, and ultimate loads of 553 and 601 N. In contrast, the other two specimen had lower properties, with stiffnesses of 53 and 44 N/mm and 185 and 143 N. For all specimen, the ultimate elongation was similar and was between 4.5 – 6.5 mm.

The average linear stiffness of the FATC with the healing ACL reached 60% of that of the sham-operated controls, but the difference was not statistically significant ($P > 0.05$). The average ultimate load reached 35% of the sham-operated control group, and this difference was statistically significant ($P < 0.05$). The ultimate elongation in the FATC with the healing ACL was approximately half that of the sham-operated control group, but the difference was not statistically significant ($P > 0.05$).

Table 13: Structural properties of the healing and sham-operated FATCs (*indicates a statistically significant different compared to sham-operated controls; $P \leq 0.05$)

	Healing	Sham-operated control
Stiffness (N/m)	77 ± 33	128 ± 25
Ultimate Load (N)	$371 \pm 240^*$	1070 ± 326
Ultimate Elongation (mm)	5.7 ± 0.8	10.7 ± 3.3

5.2.2.7 Comparison to ECM treatment alone

To further assess the advantages of ECM treatment with Mg ring repair, the cross-sectional area, joint kinematics, in-situ forces in the ACL, and tensile properties were compared to data previously collected in our laboratory using ECM alone for repair of a transected ACL at 12 weeks of healing ⁶⁶. For statistical comparison, data were first normalized by the respective value in the sham-operated controls (experimental/control, or e/c) to reduce interspecimen variability. Then, independent t-tests were used to compare groups, with significance set at $P \leq 0.05$.

All of the healing ACLs, regardless of treatment group, healed with continuous neo-tissue formation (Figure 40). The cross-sectional area of the ECM-treated ACL was $127 \pm 90\%$ of the sham-operated control, and was similar to those in the Mg ring-treated ACL ($130 \pm 26\%$; $P > 0.05$) (Figure 41). However, while the ECM + Mg ring-treated joints had a fairly consistent area, the ECM-treated joints showed more variability, with one joint each that was much larger or smaller than the sham-operated control.

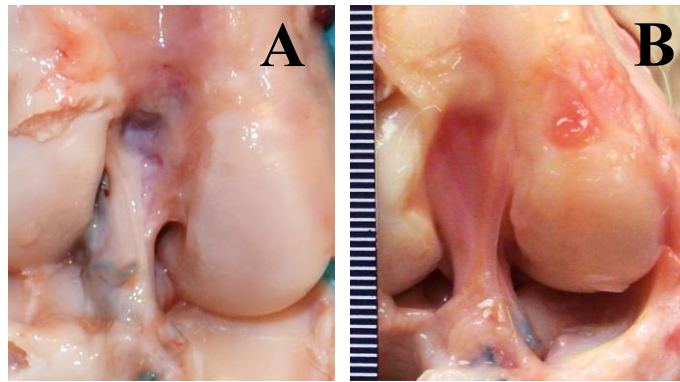


Figure 40: Gross morphology of the healing ACL with ECM treatment + Mg ring repair (A) and ECM treatment alone (B)

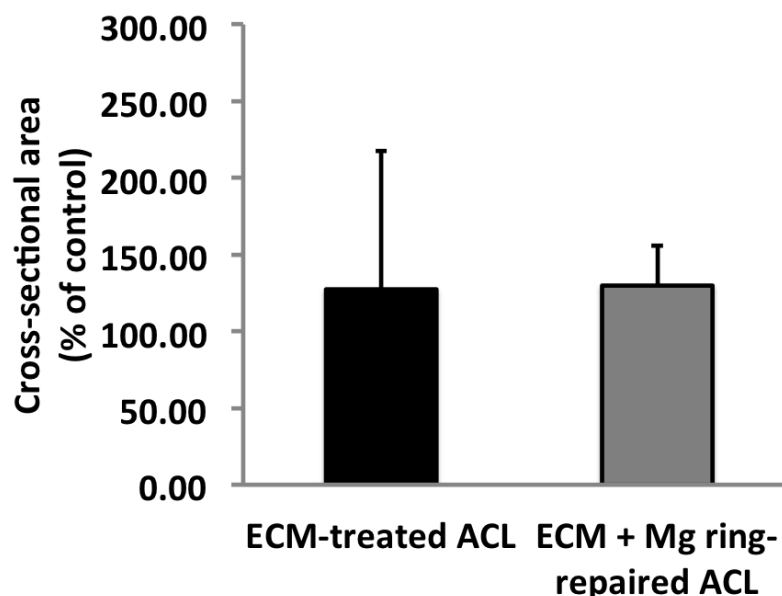
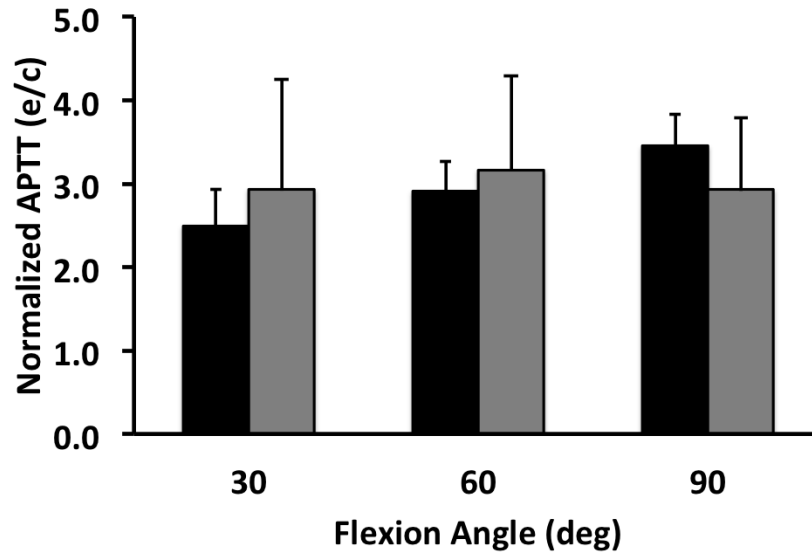


Figure 41: Cross-sectional area (% of control) of the ECM-treated ACL and ECM + Mg ring-repaired ACL

The normalized APTT and in-situ forces in the healing ACL are shown in Figure 42. Under the 67-N anterior tibial load, the normalized APTT with ECM treatment alone ranged from 2.5 – 3.5 at all tested flexion angles (Figure 42A). The normalized APTT for ECM treatment + Mg ring repair was similar and ranged from 2.9 – 3.2 ($P > 0.05$). The corresponding normalized in-situ force in the ACL with ECM treatment was 0.6 – 1.0 at the tested flexion angles. These values were again not statistically different compared to those with ECM treatment + Mg ring repair, which were 0.3 – 1.0 ($P > 0.05$; Figure 42B).



A.



B.

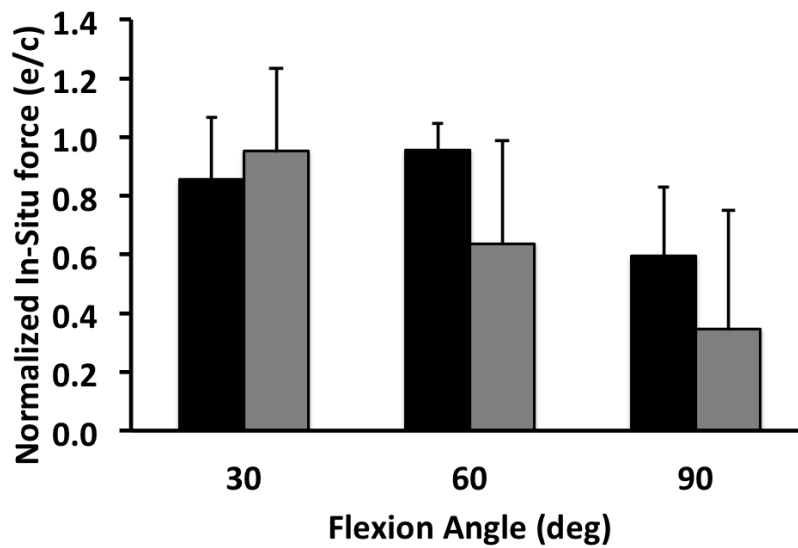


Figure 42: Normalized APTT (A) and in-situ forces in the ACL (B) in the healing goat stifle joints with ECM-treated or ECM + Mg ring-repaired ACLs

The structural properties of the healing FATCs in terms of normalized stiffness and ultimate load are shown in Figure 43. The normalized stiffness in the healing FATC after ECM treatment + Mg ring repair was 30% higher than that with ECM treatment alone ($62.7 \pm 34.5\%$ versus $48.1 \pm 18.8\%$, respectively), but this difference was not statistically significant (Figure 43A, $P > 0.05$). The normalized ultimate load in the healing FATC after ECM treatment + Mg ring repair was 2.5 times that with ECM treatment alone ($39.3 \pm 33.3\%$ versus $15.9 \pm 8.5\%$, respectively), but this difference was also not statistically significant (Figure 43B, $P > 0.05$).

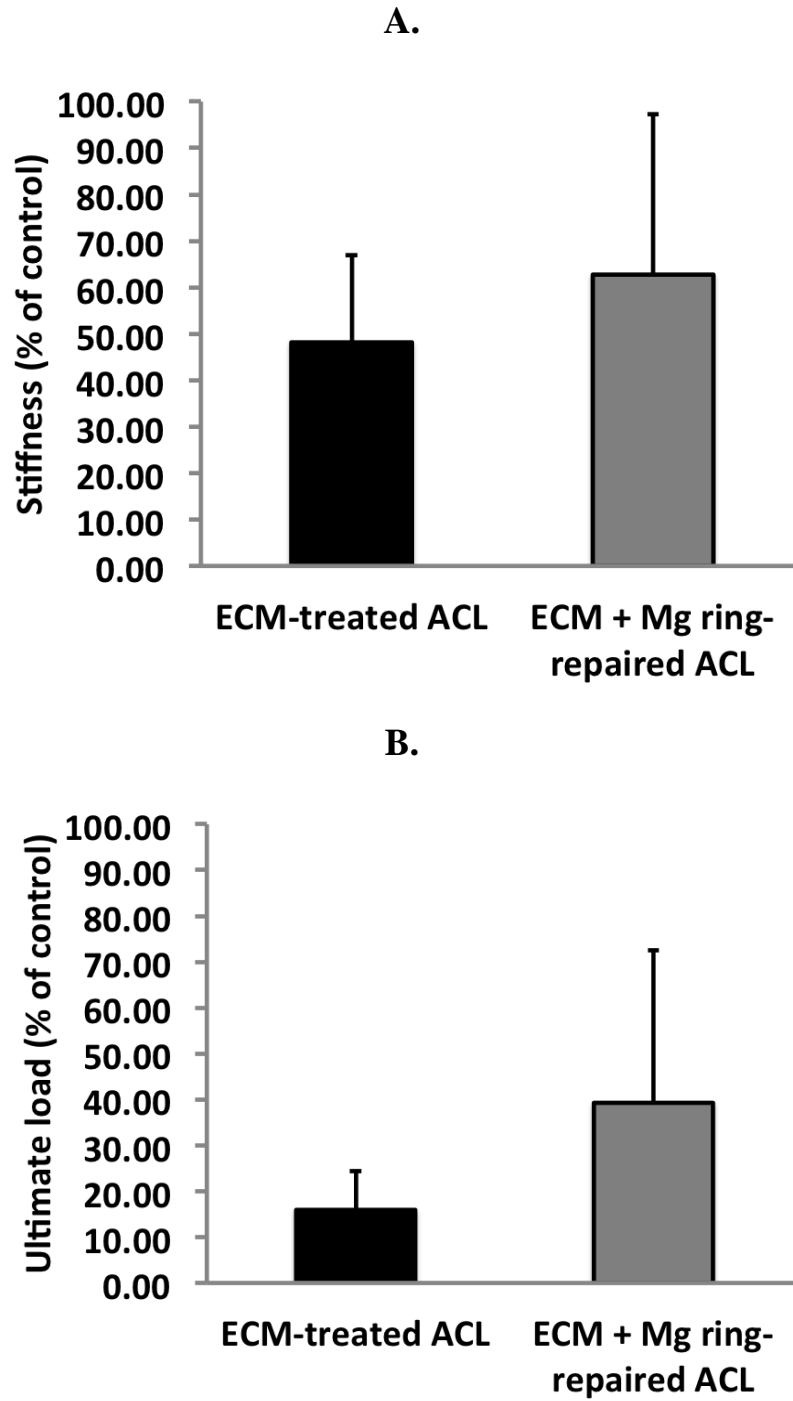


Figure 43: Normalized stiffness (A) and ultimate load (B) of the femur-ACL-tibia complex with the ECM-treated and ECM + Mg ring-repaired ACL

6.0 DISCUSSION AND FUTURE DIRECTIONS

In this dissertation, a novel methodology to improve the healing of a surgically transected ACL has been developed, using ECM bioscaffolds combined with a bioresorbable Mg ring device as biological and mechanical augmentation, respectively. To do this, the geometry of the Mg ring was first designed based on the ACL in a cadaveric goat model. A parametric finite element analysis was then used to select a Mg material and best design features such that the maximum Von Mises stress and stress concentrations on the device were reduced to be below failure stress levels. Using the final device design, a unique surgical implantation procedure was also developed. The ability of Mg ring repair to restore stifle joint stability and in-situ forces in the ACL and medial meniscus was then tested by means of a robotic/UFS testing system. Under externally-applied loads, Mg ring repair of the ACL could restore anterior tibial translation to within 2 – 6 mm of those for the joint with the intact ACL, as well as in-situ forces in the ACL to within ± 10 N of normal.

With these encouraging results, the potential of the Mg ring was assessed *in vitro* and *in vivo* by means of cell culture as well as use of the Mg ring in a live animal model. Culture of goat ACL fibroblasts with serial dilutions of extracts from 5 different Mg materials was used to assess the resulting cell proliferation and collagen production to determine whether Mg elicited a therapeutic on ACL fibroblasts. Mg extracts of up to 50% did not lead to increases in either the

cell proliferation nor collagen production; thus, Mg materials would not be expected to contribute to the healing response *in vivo*.

Finally, the Mg ring was tested *in vivo* alongside an ECM bioscaffold from the porcine urinary bladder matrix for repair of a surgically transected goat ACL, and was evaluated at 6 and 12 weeks of healing. By 6 weeks, healing tissue had begun to fill the gap between the two ends of the transected ACL, and the Mg ring had begun to degrade but remained attached to the healing ACL. By 12 weeks, the healing ACL was composed of robust, continuous tissue with aligned collagen fibers, and was similar in size and shape to that of the normal ACL. Biomechanically, the stifle joint stability and in-situ forces in the ACL were similar to those previously reported following ACL healing using ECM bioscaffolds as well as those following ACL reconstruction in the same animal model ^{3, 66, 157, 159}. On the other hand, the structural properties of the femur-ACL-tibia complex following Mg ring repair were improved over both of those treatments. These exciting findings suggest significant advances of Mg ring repair for treatment of a transected ACL.

6.1 DISCUSSION OF THE MG RING DESIGN

In Specific Aim 1, the primary goal was the development of a Mg ring design that was suitable for the studies proposed in Specific Aims 2 and 3. First, in Specific Aim 1.1, the Mg ring was designed based on the geometry of the goat ACL and then fabricated from a commercially-available Mg alloy. In collaboration with orthopaedic surgeons, an iterative design process with refinement through a series of prototypes was used such that a novel device design together with

an implantation technique was achieved to bridge the gap between the two ends of a surgically transected ACL in a cadaveric goat stifle joint.

Although Mg ring repair was based on previous strategies employed to repair an injured ACL^{64, 65}, the Mg ring design and suture repair technique was designed as a novel improvement upon these strategies to give the ACL a better chance to heal. The fixation sutures used for Mg ring repair restored approximately half of the stiffness of the native ACL immediately after surgery, while the repair sutures drew the two transected ends of the ACL back together. The passage of the fixation sutures out of the suture holes could protect the ACL from abrasion with neo-tissue at the injury site, and helped to align the ring. The ring itself also could serve as a barrier to protect the neo-tissue of the healing ACL from the synovial environment, as well as act as a reservoir to contain the ECM hydrogel. Thus, the novel Mg ring design and repair technique had many advantages over previous methodologies to help heal a transected ACL.

In Specific Aim 1.2, the goal was to use a finite element analysis under simulated loading conditions to assess the stresses and stress distributions on variations of the Mg ring design, such that a preferred design for subsequent testing could be selected. Through this analysis, we found that the mechanical properties of the Mg ring did not have a large effect on the maximum Von Mises stress or stress concentrations on its surface, but modification to its geometry, including deepening the notches and increasing the diameter of the suture holes led to large increases in stress. Based on the success criteria, the final ring design that was most suitable for repair of the ACL was selected.

In summary, the findings of Specific Aim 1 provided the basis for which a Mg ring design and suture technique were developed to bridge the gap between the two ends of a

transected goat stifle joint. The results of this Aim could then be applied directly to further *in vitro* and *in vivo* testing in Specific Aims 2 and 3.

6.2 IN VITRO ROBOTIC TESTING

In Specific Aim 2, the primary goal was to use the 6-DOF robotic/UFS testing system to test the stifle joint stability and ACL function after the transected ACL was repaired by the Mg ring device^{177, 230}. It was hypothesized that since suture (mechanical) augmentation was successful in restoring stifle joint stability and ACL function⁶⁵, the Mg ring repair of the ACL would also be able to restore anterior tibial translation (ATT) of the Mg ring-repaired ACL and in-situ force in the ACL to levels close to those in the intact stifle joint and ACL, respectively.

Indeed, we found that Mg ring repair could stabilize the cadaveric stifle joint by restoring its ATT to within 2 – 6 mm of those for stifle joint with an intact ACL following a 67-N anterior tibial load, with or without 100 N axial compression. The corresponding in-situ forces in the repaired ACL were also returned to those in the joint with the intact ACL. Thus, these findings confirmed our hypothesis and positively answered the research question. In addition, Mg ring repair of the ACL was also able to reduce excessive loading on the medial meniscus; thus, lowering the potential of its injury following ACL injury^{12, 50, 169}. The ATT and in-situ forces in the ACL and medial meniscus were also significantly improved compared to suture repair⁶⁵. In fact, they were close to those observed in previous studies using sutures for bone-to-bone fixation as well as those following ACL reconstruction^{65, 68, 142}.

The reasons for these significant improvements compared to suture repair can be attributed in part to the strength of the fixation sutures. Both suture repair and Mg ring repair drew the two ends of the transected ACL back together by attaching sutures to each end and passing them through tunnels drilled in the opposite bones. In suture repair, a single suture (Ethibond #1) was used for end side of the transected ACL, resulting in a total suture stiffness of 24 N/mm. However, in Mg ring repair, two stronger sutures (Ethibond #2) were used, resulting in a total suture stiffness of 52 N/mm. With more than double the suture stiffness, Mg ring repair ACL could more effectively restore stability to the stifle joint as well as load the repaired ACL.

The results on ATT in this Aim were consistently ~2 mm higher than those observed for a suture augmentation procedure in the same animal model ⁶⁵. It would not be possible to achieve the level of stability using an ACL repair technique compared to direct bone-to-bone fixation without risking cutting the remaining ACL stumps using high-stiffness sutures. However, the ATT was restored to within 6 mm of normal and the in-situ forces in the Mg ring-repaired ACL were returned to levels in the normal joint immediately after surgery. Thus, it was hoped that Mg ring repair could provide the needed mechanical augmentation for the transected ACL to heal and remodel with the help of the ECM bioscaffolds.

6.3 IMPACT OF THE *IN VITRO* AND *IN VIVO* EVALUATION OF THE MG RING FOR ACL HEALING

In Specific Aim 3, we first sought to evaluate the effect of Mg on goat ACL fibroblasts using *in vitro* cell culture studies (Specific Aim 3.1). Then, we wished to evaluate the efficacy of the Mg ring for ACL healing using *in vivo* experiments in a goat model (Specific Aim 3.2).

Studies on the effects of Mg extracts on goat ACL fibroblasts were performed to help to address the question whether Mg may enhance ACL healing *in vivo*. The results would help to elucidate what is modulating the healing response of a transected ACL: ECM alone or ECM in combination with the Mg ring. Goat ACL fibroblasts were cultured in the presence of extracts from 5 Mg materials ranging in concentration from 6 – 50%, and their proliferation and collagen production were measured. While the Mg extracts did not affect fibroblast proliferation ($P > 0.05$), significant decreases of up to 50% in collagen production were found between the highest extract concentration (50%) and the control group ($P < 0.05$), contrary to our hypothesis. The fact that Mg extracts did not increase cell proliferation was in agreement with the work of Fischer and associates, who found no statistical differences in the proliferation of human osteosarcoma cells at 3 days of culture with up to 50% extract ⁶³. Some studies using tetrazolium-based cytotoxicity assays have suggested that Mg extracts enhance cell viability at some concentrations, thus potentially eliciting a therapeutic effect ^{45, 98, 130}, but it has been noted that these assays heavily influenced by Mg ion release and increases in pH that occur as a result of Mg corrosion, which can generate a false positive result ⁶³. Thus, the positive effects on Mg on cellular activity remain mostly speculative.

The decreases observed in collagen synthesis may have been due to osmotic shock that was caused by the sudden increase in solute concentration when the Mg extracts were added ⁶². Indeed, measurement of the osmolality of the solution indicated that the osmolality increased with increasing extract concentration, with up to 40% higher osmolality found in the 50% extract compared to the control. Furthermore, increases in pH were observed compared to the control group in all extract solutions, which may also have contributed to the decreased production of

collagen. There are other factors that may have influenced collagen production that were not studied, such as the ion concentration of the Mg materials and their corrosion products ⁴¹.

One of the most notable questions for all *in vitro* cytotoxicity studies of Mg is the actual concentration of Mg at the site of a degrading implant, and how to simulate it using an Mg extract dilution. The answer to this question is multi-factorial and time-dependent, with location in the body and the degradation profile of the implant also playing a significant role. According to the current ISO standard typically utilized for these experiments, Mg extracts of up to 100% may be used for cell culture experiments, which clearly cause cytotoxicity and compromise of cell function due to osmotic shock. However, there is widespread belief that a ten-fold dilution may be a more appropriate representation of a physiological environment. For this reason, extract dilutions ranging from 6 – 50% were utilized in the present experiments.

The differences in the results on cell proliferation and collagen production were unexpected, and further study to fully characterize the effects of Mg extracts on ACL fibroblasts are warranted. It can be speculated that the use of primary cell lines may have resulted in a change in cell phenotype; alternatively, the changes observed in osmolality or pH may have affected the ability of the cells to produce collagen ¹²³. Further, there are distinct limitations to a static cell culture environment as a representation of a very complex *in vivo* environment. But as the primary goal of Specific Aim 3.1 was to assess the cytocompatibility of Mg materials on goat ACL fibroblasts and determine whether the presence of Mg would enhance the proliferation and collagen production of these cells, the present study did find that Mg did not elicit a positive response on either the cell proliferation or collagen production of goat ACL fibroblasts; thus, it is suggested that any enhancement of healing would most likely be a result of the application of the ECM bioscaffolds.

In Specific Aim 3.2, the *in vivo* model designed to assess the effectiveness of the Mg ring used alongside our earlier model of an ECM bioscaffold and hydrogel to heal a transected ACL was tested ⁶⁶. By 6 weeks, neo-tissue had begun to form between the transected ends of the ACL, and by 12 weeks post-operatively, substantial healing had taken place and the neo-tissue of the ACL was robust and close in size and shape to that of the normal ACL. Morphologically, it also showed significant improvement over those using ECM treatment alone ⁶⁶. This improvement was due to the additional mechanical augmentation provided by the Mg ring, which loaded the healing ACL and helped to stabilize the stifle joint and as a result, aided in the healing process.

The *in vivo* degradation and failure appeared to differ between specimen, and by 12 weeks, the Mg ring had resorbed partially, completely, or barely at all. In all cases, the ring had fractured into multiple pieces. Comparing the ACL healing response with the ring degradation, it can be observed that healing was generally better when the ring had fragmented or degraded away completely. This may be because larger pieces of the ring could shift in their orientation and block the formation of continuous tissue between the transected ends of the ACL. Indeed, the presence of small ring fragments adjacent to the ACL or elsewhere in the joint space did not appear to lead to complications in any of the goats. Thus, a ring that is faster to degrade and be released from the ACL may be preferable for healing.

The results on the anterior-posterior tibial translation (APTT) under the externally applied 67-N anterior-posterior load were elevated compared to the sham-operated controls, and increased compared to our time-zero findings in Specific Aim 2. However, these findings are consistent with both ECM treatment alone as well as studies of ACL reconstruction in a goat model ^{3, 49, 157}, after which elevated translations have been observed even one year after surgery.

The most exciting finding was that the structural properties of the healing FATC were improved compared to ECM treatment alone. The stiffness (e/c) of the FATC was 30% higher and ultimate load (e/c) 2.5 times higher. These findings confirmed our hypothesis that the combination of biological and mechanical augmentation had enhanced ACL healing. In addition, when compared to ACL reconstruction (at the same time point and in the same animal model), these results also compared favorably; i.e., the stiffness and the ultimate load were two times and 1.4 times higher, respectively ¹⁵⁷. All of these findings could have large clinical impact on the treatment of an injured ACL, and the details will be discussed further in Section 6.6.

It should be noted that there was variability observed in the biomechanical data, which was consistent with other findings from our research center in goats ⁶⁶ and can be expected with animal research ^{69, 150, 158}. Two of the specimen had the most robust healing response, and the stiffness of the FATC 101 N/mm and 110 N/mm and ultimate loads of 553 N and 600 N, respectively, while the other two had lower biomechanical properties that were close to those using ECM treatment alone ⁶⁶. We recognized that the level of healing may have been related to the fixation of the sutures outside the femoral and tibial bone tunnels. For the latter specimen, the sutures attaching the Endobutton appeared to be loosened and had migrated away from the original fixation site, and the fixation sutures could glide freely through the femoral bone tunnels (Figure 44). As the Endobutton loosened, the stifle joint stability would be lost, even if the ACL healed. Thus, the lack of joint stability would prevent sufficient loading of the healing ACL and would influence its healing capability.

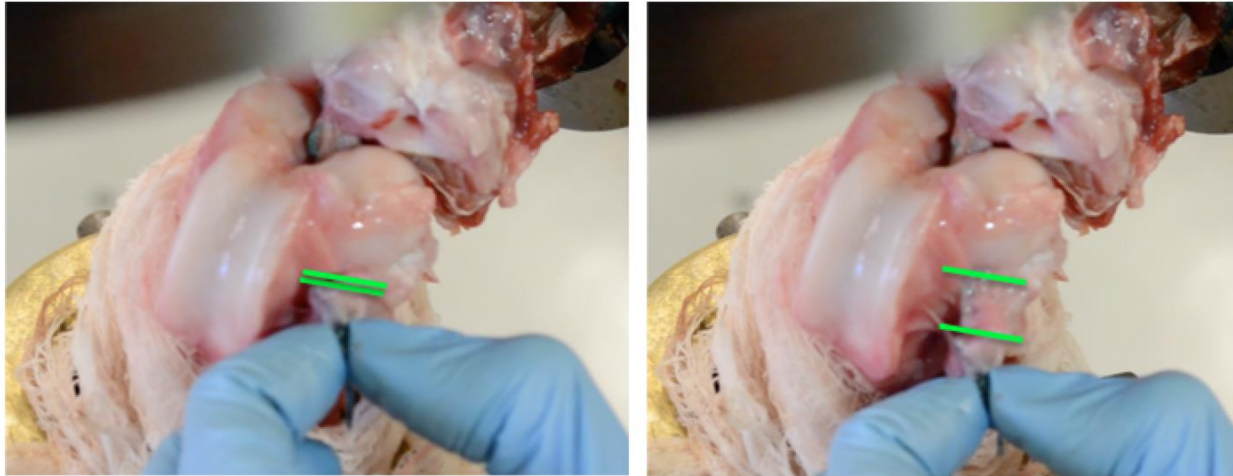


Figure 44: Photographs illustrating sliding of the femoral fixation sutures at 12 weeks of healing in 2 specimen, showing the gap between the Endobutton and femur before (left) and after applying tension (right)

On the tibial end, the fixation of the double-spiked plate and fixation post was remained tight by 12 weeks, given that this fixation method rigidly attaches the sutures to the bone. Thus, for future studies, the femoral fixation needs to be improved in order to gain more consistent results on improved ACL healing with superior biomechanical properties.

6.4 IMPACT AND IMPLICATION FOR TISSUE ENGINEERING AND REGENERATIVE MEDICINE

The findings of this dissertation clearly demonstrated the potential of using a combined approach of biological and mechanical augmentation for healing of an injured ACL. The Mg ring repair together with an ECM bioscaffold will lead to a stronger ACL over those using ECM treatment alone as well as ACL reconstruction. Following ACL reconstruction, there are clearly

unfavorable long-term results, including the early onset of osteoarthritis^{7, 27, 165}. The majority of ACL reconstruction patients are reasonably young, so this could have especially significant impact on their quality of life in the future. Thus, successful development of an ACL healing approach could shift the paradigm of clinical management. A healed ACL has a number of advantages and could represent a promising alternative to ACL reconstruction with better long-term results. Furthermore, new technologies could be extended and employed to aid in the healing and regeneration of other “hard to heal” ligaments and tendons, including those in the shoulder, elbow, and ankle.

The newly developed Mg ring device has also provided a valuable testbed for studying the use of a Mg device *in vivo*. As a relatively unexplored class of biomaterials, Mg and its alloys have not been fully characterized, and many questions remain regarding biocompatibility, degradation behavior, and effects on the healing response. Prior to approval for clinical use by the Food and Drug Administration, rigorous benchtop as well as pre-clinical testing of Mg devices will be required, and the work in this dissertation can be added to the growing body of literature characterizing the use of Mg-based devices for a variety of healing applications.

6.5 LIMITATIONS

There are a number of limitations to the work described in this dissertation. First, the advantages of Mg ring repair in a goat model may not be directly applicable to the human knee due to differences in its size, shape, range of motion, loading conditions, and so on. However, the goat model has been successfully used in a number of preclinical studies involving the ACL^{3, 66, 142,}

^{170, 204}, and is considered to be an acceptable animal model. With its large size and robust activity level, it is one of the most suitable animal models for pre-clinical studies of the knee.

In the design of the Mg ring in Specific Aim 1, the finite element analysis was a simulation of simplified and estimated loading conditions on the Mg ring that would be experienced *in vivo*. Further, the parametric analysis was done on a small number of selected designs and Mg alloys, and they would need to be experimentally validated. However, the model did provide a simple, standardized tool with which we could assess a number of design features so that the most promising for *in vitro* and *in vivo* applications in Specific Aims 2 and 3 could be chosen.

The loading conditions for the *in vitro* robotic testing in Specific Aim 2 were chosen to simulate those used in clinical examinations to test for ACL function, and represent average loads applied to the goat ACL during gait ⁹⁴, but do not represent complex loading conditions in a live animal. In the future, biplanar fluoroscopy technology could be used to record 6-DOF joint kinematics during activities of daily living, which could then be repeated on the robotic/UFS testing system to determine the corresponding joint kinematics and in-situ forces in the ACL. Testing using the robotic/UFS testing system also measured the passive response of the structures of the goat stifle joint and did not simulate the complex neural response of the ligaments and tendons. Although this is an inherent limitation of this technology, the data obtained from this system on non-contact measurement of the in-situ forces in the ACL and other joint structures was extremely valuable to understanding of the contribution and function of the Mg ring-repaired ACL.

Further, the ACL was transected through its midsubstance prior to Mg ring repair, which is not representative of ACL rupture clinically. However, our goal was to first demonstrate the

feasibility of ACL repair and regeneration using the Mg ring. Future work should include development of an injury model to generate a more realistic tear.

In Specific Aim 3.1, the *in vitro* techniques for proliferation and collagen production of goat ACL fibroblasts had several limitations. In terms of the collagen production, only soluble collagen was measured, as the majority of collagen was anticipated to be released into the cell culture media during the relatively short culture period. However, further work to quantify insoluble collagen may be warranted to more accurately capture the fibroblast collagen production. Overall, due to the use of static, *in vitro* cell culture, the data are also not directly representative of the *in vivo* conditions of those in Specific Aim 3.2, as they did not replicate the complex intraarticular environment, with synovial fluid, vascular and nutrient supply, mechanical loading, and other cell types also playing a role in modulating ACL healing. Furthermore, the cells used in the present experiments were normal ACL fibroblasts. For the future, a dynamic cell culture system as well as the use of healing ACL fibroblasts would be needed to better mimic the *in vivo* environment. However, the goal of this Aim was to utilize a simple cell culture system to elucidate whether Mg may contribute to the ACL healing process *in vivo*, and was sufficient to address our research question.

In the *in vivo* experiment of Specific Aim 3.2, due to the high costs of a large animal model, we were limited to a final sample size of only 2 goats at 6 weeks of healing and 5 goats at 12 weeks of healing. Results of a power analysis indicated that more than double the sample size would be required adequate statistical power ($\beta = 0.8$). Additionally, due to the costly nature of a large animal study, we were unable to include a control group. For this reason, for comparative purposes, data from previous work using ECM treatment alone were normalized by that of the sham-operated control to reduce interspecimen variation and used for comparison of

biomechanical properties. Post-operative rehabilitation of the animals was also not ideal, as bracing or controlled motion was not possible, and animals were generally running, jumping, and head-butting as shortly as a few hours after surgery. To limit physical activity as well as fighting, animals were thus housed individually in a smaller enclosure for 4 – 7 days post-surgery. Finally, a rigorous assessment of the biology of the healing response could not be made in terms of specific cells and cell phenotypes or gene expression due to the lack of available antibodies and PCR primers in goats. Development of new methods for such as assessment will be the subject of future work. In spite of these limitations, we successfully demonstrated the proof of concept of ACL healing using the Mg ring device in combination with an ECM bioscaffold, and future work will be done to increase the sample size for statistical power as well as add control groups.

6.6 FUTURE DIRECTIONS

In this dissertation, a novel strategy on combining biological and mechanical augmentation to heal a surgically transected ACL was successfully executed. Still, much work remains before this new approach could be ready for clinical application. The immediate next step for evaluation of the Mg ring-repaired ACL would be to perform a longer-term animal study to assess whether Mg ring repair could prevent disuse atrophy of the ACL's insertion sites, as well as further improve the biomechanical properties of the FATC. As a control, an ACL reconstruction group of goats should also be included for comparison. Such a study would allow for the assessment of stifle joint function, biomechanical properties of the FATC, cross-sectional area of the healing ACL or replacement graft, histomorphology of the healing ACL and joint

capsule, as well as the degenerative changes in the articular cartilage, so as to determine whether the Mg ring-repaired ACL may be advantageous over the current “gold standard” of treatment. This would need to be proven to overcome the clinical barrier impeding adoption of an alternative treatment option by orthopaedic surgeons. Following the successful proof of concept of ACL healing using the Mg ring at multiple time points, an injury model will be developed in goats that is representative of an ACL tear clinically, to be used in subsequent pre-clinical studies.

Of course, with the numerous strategies available for biological and mechanical augmentation of an injured ACL, further study of modified or alternative approaches are also warranted. A schematic diagram representing further development of such an approach is shown in Figure 45, depicting the feedback loop between biological and mechanical augmentation approaches with both *in vitro* and *in vivo* experiments to optimize the ACL healing strategy.

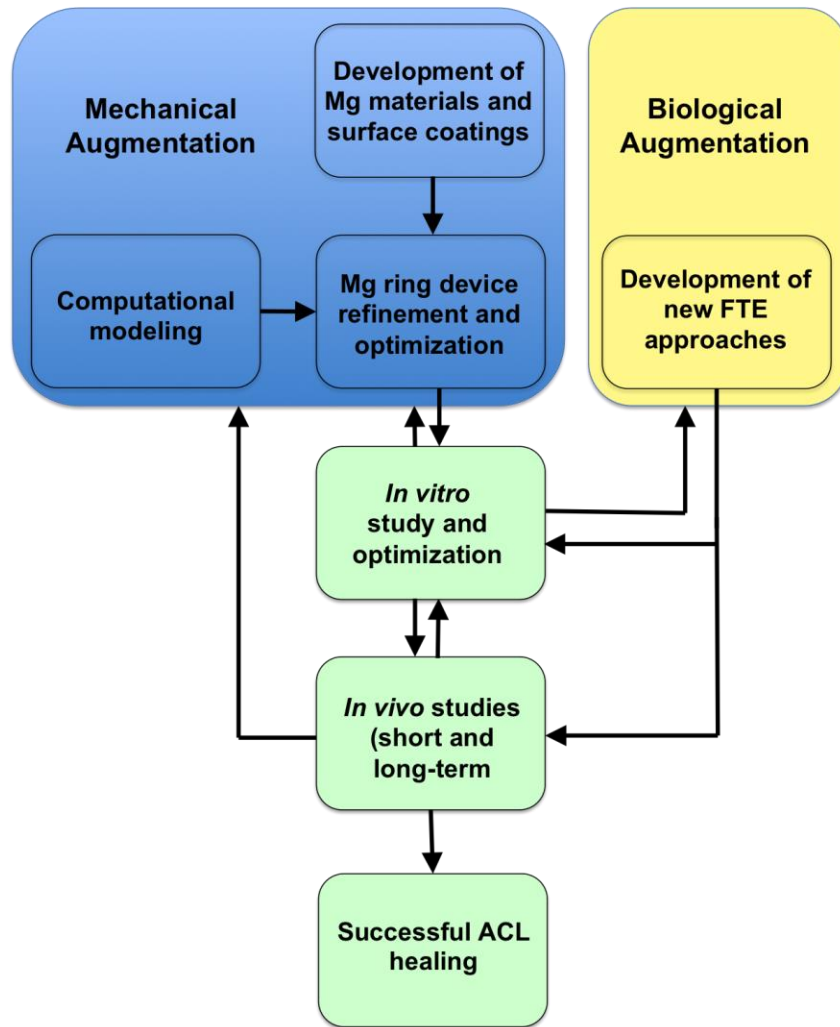


Figure 45: Schematic diagram for further development of a combined biological and mechanical augmentation strategy to heal an injured ACL

In terms of the biological augmentation, this work relied on an ECM sheet and hydrogel derived from the porcine urinary bladder matrix for ACL healing, and this and previous studies have shown that such an approach could lead to successful ACL healing. However, it might be more advantageous to consider using other new FTE approaches, including a multi-laminate ECM sheet to be a better scaffold for cells as well as to better enclose the Mg ring device such that particulate matter from the device degradation could be kept at the site and could not migrate

into the joint space. Additionally, a “pillow” composed of ECM powder enclosed within two ECM sheets could be designed to be inserted into the Mg ring device as an alternative to a hydrogel for more sustained release. The ring itself could even assist in biological augmentation using new technologies such as the application of laser micro-wells to be used for the delivery of bioactive molecules. Further development of methods to assess the healing response from a biological standpoint could also be developed to understand how ECM bioscaffolds modulates the healing response.

On mechanical augmentation, consideration should be given to new and improved fixation sutures, including resorbable sutures of different strengths. In the future, an expansion of the computational finite element analysis could also help to predict the behavior of the Mg ring and Mg ring-repaired ACL *in vivo*. Temporal effects of repeated loading as well as degradation of the ring could be incorporated into the model. These effects would also be important in addition to the mechanical properties of the device to predict when and how failure of the device would occur, and would be a useful tool in a more rigorous selection of an appropriate device design and Mg material. This would be of particular importance when scaling the Mg ring for human application, for which device behavior could not be validated by *in vivo* studies. In addition, incorporation of the ACL into the model would be a useful tool to demonstrate how loading of the Mg ring-repaired ACL is distributed between the ring and the ACL substance and insertion sites.

This finite element analysis should be done in concert with a more rigorous analysis of the Mg ring’s degradation *in vivo*. Some variability was observed in the current study, where in some animals, the ring had completely degraded while in others multiple fragments remained embedded in the ACL. With data on degradation rates, one can consider development of other

Mg materials and coatings or surface treatment to provide a consistent degradation profile that matches the rate of ACL healing.

With advances in the computational modeling and the development of Mg materials and surface coatings, the Mg ring device design can be refined and optimized. New and improved designs can be studied and evaluated *in vitro* and *in vivo* in combination with new FTE approaches for biological augmentation, in order to select the best combination for ACL healing.

Following pre-clinical work, the Mg ring technology can then be scaled up for human application. This would include modifications to the device itself as well as the development of a much simpler, arthroscopic procedure to insert the ring device and sutures on to the ruptured ACL. Devices of different sizes and shapes could be designed for variations in patient body size, or patient-specific ring geometries could be made using 3-D printing. If successful, the ring technology could also be extended as a novel alternative approach for the healing of other “hard to heal” injured ligaments and tendons. With the success of such approaches, we will move forward towards the long-term goal of the Musculoskeletal Research Center of improving the management of soft tissue injuries and reducing complications; thus, leading to better patient outcomes and long-term quality of life.

BIBLIOGRAPHY

1. *Clinical Methods: The History, Physical, and Laboratory Examinations*. 3rd ed: Butterworths; 1990.
2. Abramowitch SD, Papageorgiou CD, Debski RE, Clineff TD, Woo SL-Y. A biomechanical and histological evaluation of the structure and function of the healing medial collateral ligament in a goat model. *Knee Surg Sports Traumatol Arthrosc*. 2003;11(3):155-162.
3. Abramowitch SD, Papageorgiou CD, Withrow JD, Gilbert TW, Woo SL-Y. The effect of initial graft tension on the biomechanical properties of a healing ACL replacement graft: a study in goats. *J Orthop Res*. 2003;21(4):708-715.
4. Aglietti P, Buzzi R, Menchetti PPM, Giron F. Arthroscopically assisted semitendinosus and gracilis tendon graft in reconstruction for acute anterior cruciate ligament injuries in athletes. *American Journal of Sports Medicine*. 1996;24(6):726-731.
5. Agrawal V, Tottey S, Johnson SA, Freund JM, Siu BF, Badylak SF. Recruitment of Progenitor Cells by an Extracellular Matrix Cryptic Peptide in a Mouse Model of Digit Amputation. *Tissue Engineering Part A*. 2011;17(19-20):2435-2443.
6. Agung M, Ochi M, Yanada S, et al. Mobilization of bone marrow-derived mesenchymal stem cells into the injured tissues after intraarticular injection and their contribution to tissue regeneration. *Knee Surgery Sports Traumatology Arthroscopy*. 2006;14(12):1307-1314.
7. Ahn JH, Kim JG, Wang JH, Jung CH, Lim HC. Long-term results of anterior cruciate ligament reconstruction using bone-patellar tendon-bone: an analysis of the factors affecting the development of osteoarthritis. *Arthroscopy-the Journal of Arthroscopic and Related Surgery*. 2012;28(8):1114-1123.
8. Ajuied A, Wong F, Smith C, et al. Anterior Cruciate Ligament Injury and Radiologic Progression of Knee Osteoarthritis A Systematic Review and Meta-analysis. *American Journal of Sports Medicine*. 2014;42(9):2242-2252.

9. Akoto R, Hoeher J. Anterior cruciate ligament (ACL) reconstruction with quadriceps tendon autograft and press-fit fixation using an anteromedial portal technique. *BMC Musculoskelet Disord.* 2012;13:161.
10. Alberghina D, Casella S, Vazzana I, Ferrantelli V, Giannetto C, Piccione G. Analysis of serum proteins in clinically healthy goats (*Capra hircus*) using agarose gel electrophoresis. *Veterinary Clinical Pathology.* 2010;39(3):317-321.
11. Allen CR, Livesay GA, Wong EK, Woo SLY. Injury and reconstruction of the anterior cruciate ligament and knee osteoarthritis. *Osteoarthritis and Cartilage.* 1999;7(1):110-121.
12. Allen CR, Wong EK, Livesay GA, Sakane M, Fu FH, Woo SLY. Importance of the medial meniscus in the anterior cruciate ligament-deficient knee. *Journal of Orthopaedic Research.* 2000;18(1):109-115.
13. Amiel D, Billings E, Harwood FL. Collagenase Activity in Anterior Cruciate Ligament - Protective Role of the Synovial Sheath. *Journal of Applied Physiology.* 1990;69(3):902-906.
14. Amiel D, Ishizue KK, Harwood FL, Kitabayashi L, Akeson WH. Injury of the Anterior Cruciate Ligament - the Role of Collagenase in Ligament Degeneration. *Journal of Orthopaedic Research.* 1989;7(4):486-493.
15. Amiel D, Naginei CN, Choi SH, Lee J. Intrinsic-Properties of Acl and Mcl Cells and Their Responses to Growth-Factors. *Medicine and Science in Sports and Exercise.* 1995;27(6):844-851.
16. Anderson CF, Mosser DM. A novel phenotype for an activated macrophage: the type 2 activated macrophage. *Journal of Leukocyte Biology.* 2002;72(1):101-106.
17. Anderson DR, Weiss JA, Takai S, Ohland KJ, Woo SL. Healing of the medial collateral ligament following a triad injury: a biomechanical and histological study of the knee in rabbits. *J Orthop Res.* 1992;10(4):485-495.
18. Andersson C, Odensten M, Gillquist J. Knee function after surgical or nonsurgical treatment of acute rupture of the anterior cruciate ligament: a randomized study with a long-term follow-up period. *Clin Orthop Relat Res.* 1991(264):255-263.
19. Aydog ST, Korkusuz P, Doral MN, Tetik O, Demirel HA. Decrease in the numbers of mechanoreceptors in rabbit ACL: the effects of ageing. *Knee Surg Sports Traumatol Arthrosc.* 2006;14(4):325-329.
20. Badylak S, Kokini K, Tullius B, Simmons-Byrd A, Morff R. Morphologic study of small intestinal submucosa as a body wall repair device. *J Surg Res.* 2002;103(2):190-202.

21. Badylak SF. The extracellular matrix as a biologic scaffold material. *Biomaterials*. 2007;28(25):3587-3593.
22. Badylak SF, Freytes DO, Gilbert TW. Extracellular matrix as a biological scaffold material: Structure and function. *Acta Biomaterialia*. 2009;5(1):1-13.
23. Badylak SF, Kochupura PV, Cohen IS, et al. The use of extracellular matrix as an inductive scaffold for the partial replacement of functional myocardium. *Cell Transplantation*. 2006;15:S29-S40.
24. Badylak SF, Lantz GC, Coffey A, Geddes LA. Small intestinal submucosa as a large diameter vascular graft in the dog. *J Surg Res*. 1989;47(1):74-80.
25. Badylak SF, Tullius R, Kokini K, et al. The use of xenogeneic small intestinal submucosa as a biomaterial for Achilles tendon repair in a dog model. *J Biomed Mater Res*. 1995;29(8):977-985.
26. Badylak SF, Valentin JE, Ravindra AK, McCabe GP, Stewart-Akers AM. Macrophage Phenotype as a Determinant of Biologic Scaffold Remodeling. *Tissue Engineering Part A*. 2008;14(11):1835-1842.
27. Barenius B, Ponzer S, Shalabi A, Bujak R, Norlen L, Eriksson K. Increased risk of osteoarthritis after anterior cruciate ligament reconstruction: a 14-year follow-up study of a randomized controlled trial. *Am J Sports Med*. 2014;42(5):1049-1057.
28. Beard DJ, Kyberd PJ, Fergusson CM, Dodd CAF. Proprioception after Rupture of the Anterior Cruciate Ligament - an Objective Indication of the Need for Surgery. *Journal of Bone and Joint Surgery-British Volume*. 1993;75(2):311-315.
29. Beaty JH. Knee and leg: soft tissue trauma. In: EA A, ed. *OKU orthopaedic knowledge update*. 1st ed. Rosemont, IL: American Academy of Orthopaedic Surgeons; 1999:xix, 442.
30. Bedi A, Musahl V, Steuber V, et al. Transtibial Versus Anteromedial Portal Reaming in Anterior Cruciate Ligament Reconstruction: An Anatomic and Biomechanical Evaluation of Surgical Technique. *Arthroscopy-the Journal of Arthroscopic and Related Surgery*. 2011;27(3):380-390.
31. Beynnon BD, Johnson RJ, Abate JA, Fleming BC, Nichols CE. Treatment of anterior cruciate ligament injuries, part I. *American Journal of Sports Medicine*. 2005;33(10):1579-1602.
32. Blawert C, Dietzel W, Ghali E, Song GL. Anodizing treatments for magnesium alloys and their effect on corrosion resistance in various environments. *Advanced Engineering Materials*. 2006;8(6):511-533.

33. Bray RC, Leonard CA, Salo PT. Vascular physiology and long-term healing of partial ligament tears. *Journal of Orthopaedic Research*. 2002;20(5):984-989.
34. Bray RC, Leonard CA, Salo PT. Correlation of healing capacity with vascular response in the anterior cruciate and medial collateral ligaments of the rabbit. *Journal of Orthopaedic Research*. 2003;21(6):1118-1123.
35. Bray RC, Leonard CA, Salo PT. Correlation of healing capacity with vascular response in the anterior cruciate and medial collateral ligaments of the rabbit. *J Orthop Res*. 2003;21(6):1118-1123.
36. Buckley SL, Barrack RL, Alexander AH. The Natural-History of Conservatively Treated Partial Anterior Cruciate Ligament Tears. *American Journal of Sports Medicine*. 1989;17(2):221-225.
37. Buss DD, Min R, Skyhar M, Galinat B, Warren RF, Wickiewicz TL. Nonoperative treatment of acute anterior cruciate ligament injuries in a selected group of patients. *Am J Sports Med*. 1995;23(2):160-165.
38. Butler DL, Goldstein SA, Guilak F. Functional tissue engineering: The role of biomechanics. *Journal of Biomechanical Engineering-Transactions of the Asme*. 2000;122(6):570-575.
39. Butler DL, Noyes FR, Grood ES. Ligamentous Restraints to Anterior-Posterior Drawer in the Human Knee - Biomechanical Study. *Journal of Bone and Joint Surgery-American Volume*. 1980;62(2):259-270.
40. Cameron M, Buchgraber A, Passler H, et al. The natural history of the anterior cruciate ligament-deficient knee. Changes in synovial fluid cytokine and keratan sulfate concentrations. *Am J Sports Med*. 1997;25(6):751-754.
41. Cao JD, Martens P, Laws KJ, Boughton P, Ferry M. Quantitative in vitro assessment of Mg65Zn30Ca5 degradation and its effect on cell viability. *Journal of Biomedical Materials Research Part B-Applied Biomaterials*. 2013;101B(1):43-49.
42. Chen CH, Chuang TY, Wang KC, Chen WJ, Shih CH. Arthroscopic anterior cruciate ligament reconstruction with quadriceps tendon autograft: clinical outcome in 4-7 years. *Knee Surg Sports Traumatol Arthrosc*. 2006;14(11):1077-1085.
43. Chen YJ, Huang CH, Lee IC, Lee YT, Chen MH, Young TH. Effects of cyclic mechanical stretching on the mRNA expression of tendon/ligament-related and osteoblast-specific genes in human mesenchymal stem cells. *Connective Tissue Research*. 2008;49(1):7-14.

44. Chong AKS, Ang AD, Goh JCH, et al. Bone marrow-derived mesenchymal stem cells influence early tendon-healing in a rabbit Achilles tendon model. *Journal of Bone and Joint Surgery-American Volume*. 2007;89A(1):74-81.
45. Chou DT, Hong D, Saha P, et al. In vitro and in vivo corrosion, cytocompatibility and mechanical properties of biodegradable Mg-Y-Ca-Zr alloys as implant materials. *Acta Biomaterialia*. 2013;9(10):8518-8533.
46. Clancy WG, Jr., Ray JM, Zoltan DJ. Acute tears of the anterior cruciate ligament. Surgical versus conservative treatment. *J Bone Joint Surg Am*. 1988;70(10):1483-1488.
47. Colombet P, Allard M, Bousquet V, de Lavigne C, Flurin PH, Lachaud C. Anterior cruciate ligament reconstruction using four-strand semitendinosus and gracilis tendon grafts and metal interference screw fixation. *Arthroscopy-the Journal of Arthroscopic and Related Surgery*. 2002;18(3):232-237.
48. Corry IS, Webb JM, Clingeleffer AJ, Pinczewski LA. Arthroscopic reconstruction of the anterior cruciate ligament - A comparison of patellar tendon autograft and four-strand hamstring tendon autograft. *American Journal of Sports Medicine*. 1999;27(4):444-454.
49. Cummings JF, Grood ES. The progression of anterior translation after anterior cruciate ligament reconstruction in a caprine model. *J Orthop Res*. 2002;20(5):1003-1008.
50. Daniel DM, Stone ML, Dobson BE, Fithian DC, Rossman DJ, Kaufman KR. Fate of the ACL-injured patient. A prospective outcome study. *Am J Sports Med*. 1994;22(5):632-644.
51. DeAngelis JP, Fulkerson JP. Quadriceps tendon--a reliable alternative for reconstruction of the anterior cruciate ligament. *Clin Sports Med*. 2007;26(4):587-596.
52. DeJardin LM, Arnoczky SP, Ewers BJ, Haut RC, Clarke RB. Tissue-engineered rotator cuff tendon using porcine small intestine submucosa - Histologic and mechanical evaluation in dogs. *American Journal of Sports Medicine*. 2001;29(2):175-184.
53. Derwin KA, Badylak SF, Steinmann SP, Iannotti JP. Extracellular matrix scaffold devices for rotator cuff repair. *Journal of Shoulder and Elbow Surgery*. 2010;19(3):467-476.
54. Drury JL, Mooney DJ. Hydrogels for tissue engineering: scaffold design variables and applications. *Biomaterials*. 2003;24(24):4337-4351.
55. Duthon VB, Barea C, Abrassart S, Fasel JH, Fritschy D, Menetrey J. Anatomy of the anterior cruciate ligament. *Knee Surgery Sports Traumatology Arthroscopy*. 2006;14(3):204-213.

56. Engebretsen L, Benum P, Fasting O, Molster A, Strand T. A Prospective, Randomized Study of 3 Surgical Techniques for Treatment of Acute Ruptures of the Anterior Cruciate Ligament. *American Journal of Sports Medicine*. 1990;18(6):585-590.
57. Engle CP, Noguchi M, Ohland KJ, Shelley FJ, Woo SL. Healing of the rabbit medial collateral ligament following an O'Donoghue triad injury: effects of anterior cruciate ligament reconstruction. *J Orthop Res*. 1994;12(3):357-364.
58. Eppley BL, Woodell JE, Higgins J. Platelet quantification and growth factor analysis from platelet-rich plasma: Implications for wound healing. *Plastic and Reconstructive Surgery*. 2004;114(6):1502-1508.
59. Erdmann N, Angrisani N, Reifenrath J, et al. Biomechanical testing and degradation analysis of MgCa0.8 alloy screws: A comparative in vivo study in rabbits. *Acta Biomaterialia*. 2011;7(3):1421-1428.
60. Farraro KF, Kim KE, Woo SL, Flowers JR, McCullough MB. Revolutionizing orthopaedic biomaterials: The potential of biodegradable and bioresorbable magnesium-based materials for functional tissue engineering. *J Biomech*. 2013;49(9):1979-1986.
61. Feagin JA, Jr., Curl WW. Isolated tear of the anterior cruciate ligament: 5-year follow-up study. *Am J Sports Med*. 1976;4(3):95-100.
62. Fischer J, Profrock D, Hort N, Willumeit R, Feyerabend F. Improved cytotoxicity testing of magnesium materials. *Materials Science and Engineering B-Advanced Functional Solid-State Materials*. 2011;176(11):830-834.
63. Fischer J, Prosenc MH, Wolff M, Hort N, Willumeit R, Feyerabend F. Interference of magnesium corrosion with tetrazolium-based cytotoxicity assays. *Acta Biomaterialia*. 2010;6(5):1813-1823.
64. Fisher MB, Jung HJ, McMahon PJ, Woo SL-Y. Evaluation of Bone Tunnel Placement for Suture Augmentation of an Injured Anterior Cruciate Ligament: Effects on Joint Stability in a Goat Model. *Journal of Orthopaedic Research*. 2010;28(10):1373-1379.
65. Fisher MB, Jung HJ, McMahon PJ, Woo SL-Y. Suture augmentation following ACL injury to restore the function of the ACL, MCL, and medial meniscus in the goat stifle joint. *J Biomech*. 2011;44(8):1530-1535.
66. Fisher MB, Liang R, Jung HJ, et al. Potential of healing a transected anterior cruciate ligament with genetically modified extracellular matrix bioscaffolds in a goat model. *Knee Surg Sports Traumatol Arthrosc*. 2012;20(7):1357-1365.
67. Fishman JM, Lowdell MW, Urbani L, et al. Immunomodulatory effect of a decellularized skeletal muscle scaffold in a discordant xenotransplantation model. *Proceedings of the*

- National Academy of Sciences of the United States of America*. 2013;110(35):14360-14365.
68. Fleming BC, Carey JL, Spindler KP, Murray MM. Can Suture Repair of ACL Transection Restore Normal Anteroposterior Laxity of the Knee? An Ex Vivo Study. *Journal of Orthopaedic Research*. 2008;26(11):1500-1505.
 69. Fleming BC, Spindler KP, Palmer MP, Magarian EM, Murray MM. Collagen-Platelet Composites Improve the Biomechanical Properties of Healing Anterior Cruciate Ligament Grafts in a Porcine Model. *American Journal of Sports Medicine*. 2009;37(8):1554-1563.
 70. Frank C, Schachar N, Dittrich D. Natural history of healing in the repaired medial collateral ligament. *Journal of Orthopaedic Research*. 1983(1):179-188.
 71. Frank C, Woo SL, Amiel D, Harwood F, Gomez M, Akeson W. Medial collateral ligament healing. A multidisciplinary assessment in rabbits. *Am J Sports Med*. 1983;11(6):379-389.
 72. Frank CB, Jackson DW. Current concepts review - The science of reconstruction of the anterior cruciate ligament. *Journal of Bone and Joint Surgery-American Volume*. 1997;79A(10):1556-1576.
 73. Freytes DO, Badylak SF, Webster TJ, Geddes LA, Rundell AE. Biaxial strength of multilaminated extracellular matrix scaffolds. *Biomaterials*. 2004;25(12):2353-2361.
 74. Freytes DO, Martin J, Velankar SS, Lee AS, Badylak SF. Preparation and rheological characterization of a gel form of the porcine urinary bladder matrix. *Biomaterials*. 2008;29(11):1630-1637.
 75. Frobell RB, Roos EM, Roos HP, Ranstam J, Lohmander LS. A randomized trial of treatment for acute anterior cruciate ligament tears. *N Engl J Med*. 2010;363(4):331-342.
 76. Fukuda Y, Woo SL, Loh JC, et al. A quantitative analysis of valgus torque on the ACL: a human cadaveric study. *J Orthop Res*. 2003;21(6):1107-1112.
 77. Gaweda K, Tarczynska M, Krzyzanowski W. Treatment of Achilles Tendinopathy with Platelet-Rich Plasma. *International Journal of Sports Medicine*. 2010;31(8):577-583.
 78. Ge ZG, Yang F, Goh JCH, Ramakrishna S, Lee EH. Biomaterials and scaffolds for ligament tissue engineering. *Journal of Biomedical Materials Research Part A*. 2006;77A(3):639-652.
 79. George MS, Dunn WR, Spindler KP. Current concepts review: Revision anterior cruciate ligament reconstruction. *American Journal of Sports Medicine*. 2006;34(12):2026-2037.

80. Gilbert TW, Stewart-Akers AM, Simmons-Byrd A, Badylak SF. Degradation and remodeling of small intestinal submucosa in canine Achilles tendon repair. *Journal of Bone and Joint Surgery-American Volume*. 2007;89(3):621-630.
81. Gilbert TW, Stolz DB, Biancaniello F, Simmons-Byrd A, Badylak SF. Production and characterization of ECM powder: implications for tissue engineering applications. *Biomaterials*. 2005;26(12):1431-1435.
82. Giove TP, Miller SJ, Kent BE, Sanford TL, Garrick JG. Non-Operative Treatment of the Torn Anterior Cruciate Ligament. *Journal of Bone and Joint Surgery-American Volume*. 1983;65(2):184-192.
83. Girgis FG, Marshall JL, Monajem ARSA. Cruciate Ligaments of Knee-Joint - Anatomical, Functional and Experimental Analysis. *Clinical Orthopaedics and Related Research*. 1975(106):216-231.
84. Griffin LY, Albohm MJ, Arendt EA, et al. Understanding and preventing noncontact anterior cruciate ligament injuries - A review of the Hunt Valley II Meeting, January 2005. *American Journal of Sports Medicine*. 2006;34(9):1512-1532.
85. Gu XN, Li N, Zhou WR, et al. Corrosion resistance and surface biocompatibility of a microarc oxidation coating on a Mg-Ca alloy. *Acta Biomaterialia*. 2011;7(4):1880-1889.
86. Gu XN, Zheng W, Cheng Y, Zheng YF. A study on alkaline heat treated Mg-Ca alloy for the control of the biocorrosion rate. *Acta Biomaterialia*. 2009;5(7):2790-2799.
87. Gu XN, Zheng YF, Cheng Y, Zhong SP, Xi TF. In vitro corrosion and biocompatibility of binary magnesium alloys. *Biomaterials*. 2009;30(4):484-498.
88. Gulotta LV, Kovacevic D, Packer JD, Deng XH, Rodeo SA. Bone Marrow-Derived Mesenchymal Stem Cells Transduced With Scleraxis Improve Rotator Cuff Healing in a Rat Model. *American Journal of Sports Medicine*. 2011;39(6):1282-1289.
89. Hall MP, Ryzewicz M, Walsh PJ, Sherman OH. Risk of Iatrogenic Injury to the Peroneal Nerve During Posterolateral Femoral Tunnel Placement in Double-Bundle Anterior Cruciate Ligament Reconstruction. *American Journal of Sports Medicine*. 2009;37(1):109-113.
90. Haus J, Halata Z. Innervation of the anterior cruciate ligament. *Int Orthop*. 1990;14(3):293-296.
91. Hawkins RJ, Misamore GW, Merritt TR. Follow-up of the Acute Nonoperated Isolated Anterior Cruciate Ligament Tear. *American Journal of Sports Medicine*. 1986;14(3):205-210.

92. Hildebrand KA, Woo SL, Smith DW, et al. The effects of platelet-derived growth factor-BB on healing of the rabbit medial collateral ligament. An in vivo study. *Am J Sports Med.* 1998;26(4):549-554.
93. Hodde JP, Badylak SF, Brightman AO, Voytik-Harbin SL. Glycosaminoglycan content of small intestinal submucosa: a bioscaffold for tissue replacement. *Tissue Eng.* 1996;2(3):209-217.
94. Holden JP, Grood ES, Korvick DL, Cummings JF, Butler DL, Bylskiaustrow DI. In-Vivo Forces in the Anterior Cruciate Ligament - Direct Measurements during Walking and Trotting in a Quadruped. *J Biomech.* 1994;27(5):517-526.
95. Hollis JM, Takai S, Adams DJ, Horibe S, Woo SLY. The Effects of Knee Motion and External Loading on the Length of the Anterior Cruciate Ligament (Acl) - a Kinematic Study. *Journal of Biomechanical Engineering-Transactions of the Asme.* 1991;113(2):208-214.
96. Hong D, Saha P, Chou DT, et al. In vitro degradation and cytotoxicity response of Mg-4% Zn-0.5% Zr (ZK40) alloy as a potential biodegradable material. *Acta Biomaterialia.* 2013;9(10):8534-8547.
97. Hort N, Huang Y, Fechner D, et al. Magnesium alloys as implant materials - Principles of property design for Mg-RE alloys. *Acta Biomaterialia.* 2010;6(5):1714-1725.
98. Huan ZG, Leeftang MA, Zhou J, Fratila-Apachitei LE, Duszczuk J. In vitro degradation behavior and cytocompatibility of Mg-Zn-Zr alloys. *Journal of Materials Science-Materials in Medicine.* 2010;21(9):2623-2635.
99. Inoue M, McGurkburleson E, Hollis JM, Woo SLY. Treatment of the Medial Collateral Ligament Injury .1. The Importance of Anterior Cruciate Ligament on the Varus-Valgus Knee Laxity. *American Journal of Sports Medicine.* 1987;15(1):15-21.
100. Inoue M, Woo SL, Gomez MA, Amiel D, Ohland KJ, Kitabayashi LR. Effects of surgical treatment and immobilization on the healing of the medial collateral ligament: a long-term multidisciplinary study. *Connect Tissue Res.* 1990;25(1):13-26.
101. Irrgang JJ, Harner CD. Loss of Motion Following Knee Ligament Reconstruction. *Sports Medicine.* 1995;19(2):150-159.
102. Ishizaki T, Shigematsu I, Saito N. Anticorrosive magnesium phosphate coating on AZ31 magnesium alloy. *Surface & Coatings Technology.* 2009;203(16):2288-2291.
103. Jacobs JJ, Gilbert JL, Urban RM. Corrosion of metal orthopaedic implants. *Journal of Bone and Joint Surgery-American Volume.* 1998;80A(2):268-282.

104. Jacobs JJ, Skipor AK, Patteson LM, et al. Metal release in patients who have has a primary total hip arthroplasty - A prospective, controlled, longitudinal study. *Journal of Bone and Joint Surgery-American Volume*. 1998;80A(10):1447-1458.
105. Jarvela T, Paakkala T, Kannus P, Jarvinen M. The incidence of patellofemoral osteoarthritis and associated findings 7 years after anterior cruciate ligament reconstruction with a bone-patellar tendon-bone autograft. *American Journal of Sports Medicine*. 2001;29(1):18-24.
106. Johnston M, Morse A, Arrington J, Pliner M, Gasser S. Resorption and Remodeling of Hydroxyapatite-Poly-L-Lactic Acid Composite Anterior Cruciate Ligament Interference Screws. *Arthroscopy-the Journal of Arthroscopic and Related Surgery*. 2011;27(12):1671-1678.
107. Jomha NM, Pinczewski LA, Clingeleffer A, Otto DD. Arthroscopic reconstruction of the anterior cruciate ligament with patellar-tendon autograft and interference screw fixation - The results at seven years. *Journal of Bone and Joint Surgery-British Volume*. 1999;81B(5):775-779.
108. Jones KG. Reconstruction of the Anterior Cruciate Ligament - a Technique Using the Central 1/3 of the Patellar Ligament. *Journal of Bone and Joint Surgery-American Volume*. 1963;45(5):925-932.
109. Joshi M, Salunke P, Zhang G, Chaswal V, Dong ZY, Shanov V. Magnesium Single Crystal as a Biodegradable Implant Material. Paper presented at: Materials Science and Technology 2015; October 4-8, 2015, 2015; Columbus, OH.
110. Kanamori A, Sakane M, Zeminski J, Rudy TW, Woo SL. In-situ force in the medial and lateral structures of intact and ACL-deficient knees. *J Orthop Sci*. 2000;5(6):567-571.
111. Kanamori A, Woo SL, Ma CB, et al. The forces in the anterior cruciate ligament and knee kinematics during a simulated pivot shift test: A human cadaveric study using robotic technology. *Arthroscopy-the Journal of Arthroscopic and Related Surgery*. 2000;16(6):633-639.
112. Kanamori A, Zeminski J, Rudy TW, Li G, Fu FH, Woo SLY. The effect of axial tibial torque on the function of the anterior cruciate ligament: A biomechanical study of a simulated pivot shift test. *Arthroscopy-the Journal of Arthroscopic and Related Surgery*. 2002;18(4):394-398.
113. Kanaya A, Deie M, Adachi N, Nishimori M, Yanada S, Ochi M. Intra-articular injection of mesenchymal stromal cells in partially torn anterior cruciate ligaments in a rat model. *Arthroscopy-the Journal of Arthroscopic and Related Surgery*. 2007;23(6):610-617.

114. Kannus P, Jarvinen M. Conservatively Treated Tears of the Anterior Cruciate Ligament - Long-Term Results. *Journal of Bone and Joint Surgery-American Volume*. 1987;69A(7):1007-1012.
115. Karaoglu S, M BF, Woo SL, Fu YC, Liang R, Abramowitch SD. Use of a bioscaffold to improve healing of a patellar tendon defect after graft harvest for ACL reconstruction: A study in rabbits. *J Orthop Res*. 2008;26(2):255-263.
116. Kartus J, Magnusson L, Stener S, Brandsson S, Eriksson BI, Karlsson J. Complications following arthroscopic anterior cruciate ligament reconstruction. A 2-5-year follow-up of 604 patients with special emphasis on anterior knee pain. *Knee Surg Sports Traumatol Arthrosc*. 1999;7(1):2-8.
117. Kartus J, Movin T, Karlsson J. Donor-site morbidity and anterior knee problems after anterior cruciate ligament reconstruction using autografts. *Arthroscopy*. 2001;17(9):971-980.
118. Keane TJ, Badylak SF. The host response to allogeneic and xenogeneic biological scaffold materials. *Journal of Tissue Engineering and Regenerative Medicine*. 2015;9(5):504-511.
119. Kessler MA, Behrend H, Henz S, Stutz G, Rukavina A, Kuster MS. Function, osteoarthritis and activity after ACL-rupture: 11 years follow-up results of conservative versus reconstructive treatment. *Knee Surgery Sports Traumatology Arthroscopy*. 2008;16(5):442-448.
120. Kimura Y, Hokugo A, Takamoto T, Tabata Y, Kurosawa H. Regeneration of anterior cruciate ligament by biodegradable scaffold combined with local controlled release of basic fibroblast growth factor and collagen wrapping. *Tissue Engineering Part C-Methods*. 2008;14(1):47-57.
121. Kirkland NT, Lespagnol J, Birbilis N, Staiger MP. A survey of bio-corrosion rates of magnesium alloys. *Corrosion Science*. 2010;52(2):287-291.
122. Knapp PM, Lingeman JE, Siegel YI, Badylak SF, Demeter RJ. Biocompatibility of small-intestinal submucosa in urinary tract as augmentation cystoplasty graft and injectable suspension. *J Endourol*. 1994;8(2):125-130.
123. Kohn DH, Sarmadi M, Helman JI, Krebsbach PH. Effects of pH on human bone marrow stromal cells in vitro: Implications for tissue engineering of bone. *Journal of Biomedical Materials Research*. 2002;60(2):292-299.
124. Kon E, Filardo G, Delcogliano M, et al. Platelet-rich plasma: New clinical application A pilot study for treatment of jumper's knee. *Injury-International Journal of the Care of the Injured*. 2009;40(6):598-603.

125. Kostogiannis L, Ageberg E, Neuman P, Dahlberg L, Friden T, Roos H. Activity level and subjective knee function 15 years after anterior Cruciate ligament injury - A prospective, longitudinal study of non reconstructed patients. *American Journal of Sports Medicine*. 2007;35(7):1135-1143.
126. LaPrade CM, James EW, Engebretsen L, LaPrade RF. Anterior medial meniscal root avulsions due to malposition of the tibial tunnel during anterior cruciate ligament reconstruction: two case reports. *Knee Surgery Sports Traumatology Arthroscopy*. 2014;22(5):1119-1123.
127. Lee EH, Hui JHP. The potential of stem cells in orthopaedic surgery. *Journal of Bone and Joint Surgery-British Volume*. 2006;88B(7):841-851.
128. Letson AK, Dahners LE. The Effect of Combinations of Growth-Factors on Ligament Healing. *Clinical Orthopaedics and Related Research*. 1994(308):207-212.
129. Li GA, Rudy TW, Allen C, Sakane M, Woo SLY. Effect of combined axial compressive and anterior tibial loads on in situ forces in the anterior cruciate ligament: A porcine study. *Journal of Orthopaedic Research*. 1998;16(1):122-127.
130. Li N, Li YD, Wang YB, et al. Corrosion resistance and cytotoxicity of a MgF2 coating on biomedical Mg-1Ca alloy via vacuum evaporation deposition method. *Surface and Interface Analysis*. 2013;45(8):1217-1222.
131. Li ZJ, Gu XN, Lou SQ, Zheng YF. The development of binary Mg-Ca alloys for use as biodegradable materials within bone. *Biomaterials*. 2008;29(10):1329-1344.
132. Liang R, Woo SL, Nguyen TD, Liu PC, Almarza A. Effects of a bioscaffold on collagen fibrillogenesis in healing medial collateral ligament in rabbits. *J Orthop Res*. 2008;26(8):1098-1104.
133. Liang R, Woo SL, Takakura Y, Moon DK, Jia F, Abramowitch SD. Long-term effects of porcine small intestine submucosa on the healing of medial collateral ligament: a functional tissue engineering study. *J Orthop Res*. 2006;24(4):811-819.
134. Lim JK, Hui J, Li L, Thambyah A, Goh J, Lee EH. Enhancement of tendon graft osteointegration using mesenchymal stem cells in a rabbit model of anterior cruciate ligament reconstruction. *Arthroscopy-the Journal of Arthroscopic and Related Surgery*. 2004;20(9):899-910.
135. Liu M, Qiu D, Zhao MC, Song G, Atrens A. The effect of crystallographic orientation on the active corrosion of pure magnesium. *Scripta Materialia*. 2008;58(5):421-424.
136. Livesay GA, Fujie H, Kashiwaguchi S, Morrow DA, Fu FH, Woo SL-Y. Determination of the in-Situ Forces and Force Distribution within the Human Anterior Cruciate Ligament. *Annals of Biomedical Engineering*. 1995;23(4):467-474.

137. Livesay GA, Rudy TW, Woo SLY, et al. Evaluation of the effect of joint constraints on the in situ force distribution in the anterior cruciate ligament. *Journal of Orthopaedic Research*. 1997;15(2):278-284.
138. Loh JC, Fukuda Y, Tsuda E, Steadman RJ, Fu FH, Woo SL. Knee stability and graft function following anterior cruciate ligament reconstruction: Comparison between 11 o'clock and 10 o'clock femoral tunnel placement. 2002 Richard O'Connor Award paper. *Arthroscopy-the Journal of Arthroscopic and Related Surgery*. 2003;19(3):297-304.
139. Lohmander LS, Englund PM, Dahl LL, Roos EM. The long-term consequence of anterior cruciate ligament and meniscus injuries - Osteoarthritis. *American Journal of Sports Medicine*. 2007;35(10):1756-1769.
140. Lu HH, Thomopoulos S. Functional Attachment of Soft Tissues to Bone: Development, Healing, and Tissue Engineering. *Annual Review of Biomedical Engineering, Vol 15*. 2013;15:201-226.
141. Ma CB, Papageogiou CD, Debski RE, Woo SL. Interaction between the ACL graft and MCL in a combined ACL+MCL knee injury using a goat model. *Acta Orthop Scand*. 2000;71(4):387-393.
142. Ma CB, Papageogiou CD, Debski RE, Woo SLY. Interaction between the ACL graft and MCL in a combined ACL plus MCL knee injury using a goat model. *Acta Orthopaedica Scandinavica*. 2000;71(4):387-393.
143. Marder RA, Raskind JR, Carroll M. Prospective Evaluation of Arthroscopically Assisted Anterior Cruciate Ligament Reconstruction - Patellar Tendon Versus Semitendinosus and Gracilis Tendons. *American Journal of Sports Medicine*. 1991;19(5):478-484.
144. McBride ED. Magensium screw and nail fixation in fractures. *South. Med. J*. 1938(31):508-514.
145. Mcdaniel WJ, Dameron TB. Untreated Ruptures of the Anterior Cruciate Ligament - a Follow-up-Study. *Journal of Bone and Joint Surgery-American Volume*. 1980;62(5):696-705.
146. Mills CD, Kincaid K, Alt JM, Heilman MJ, Hill AM. M-1/M-2 macrophages and the Th1/Th2 paradigm. *Journal of Immunology*. 2000;164(12):6166-6173.
147. Mizuta H, Kubota K, Shiraishi M, Otsuka Y, Nagamoto N, Takagi K. The Conservative Treatment of Complete Tears of the Anterior Cruciate Ligament in Skeletally Immature Patients. *Journal of Bone and Joint Surgery-British Volume*. 1995;77B(6):890-894.
148. Molloy T, Wang Y, Murrell GAC. The roles of growth factors in tendon and ligament healing. *Sports Medicine*. 2003;33(5):381-394.

149. Moon DK, Abramowitch SD, Woo SL. The development and validation of a charge-coupled device laser reflectance system to measure the complex cross-sectional shape and area of soft tissues. *J Biomech.* 2006;39(16):3071-3075.
150. Murray MM, Magarian E, Zurakowski D, Fleming BC. Bone-to-Bone Fixation Enhances Functional Healing of the Porcine Anterior Cruciate Ligament Using a Collagen-Platelet Composite. *Arthroscopy-the Journal of Arthroscopic and Related Surgery.* 2010;26(9):S49-S57.
151. Murray MM, Spindler KP, Abreu E, et al. Collagen-platelet rich plasma hydrogel enhances primary repair of the porcine anterior cruciate ligament. *Journal of Orthopaedic Research.* 2007;25(1):81-91.
152. Musahl V, Abramowitch SD, Gilbert TW, et al. The use of porcine small intestinal submucosa to enhance the healing of the medial collateral ligament--a functional tissue engineering study in rabbits. *J Orthop Res.* 2004;22(1):214-220.
153. Nagineni CN, Amiel D, Green MH, Berchuck M, Akeson WH. Characterization of the Intrinsic-Properties of the Anterior Cruciate and Medial Collateral Ligament Cells - an Invitro-Cell Culture Study. *Journal of Orthopaedic Research.* 1992;10(4):465-475.
154. Najibi S, Banglmeier R, Matta JM, Tannast M. Material Properties of Common Suture Materials in Orthopaedic Surgery. *The Iowa Orthopaedic Journal.* 2010(30):84-88.
155. Navarro M, Michiardi A, Castano O, Planell JA. Biomaterials in orthopaedics. *Journal of the Royal Society Interface.* 2008;5(27):1137-1158.
156. Nelson F, Billingham RC, Pidoux I, et al. Early post-traumatic osteoarthritis-like changes in human articular cartilage following rupture of the anterior cruciate ligament. *Osteoarthritis Cartilage.* 2006;14(2):114-119.
157. Ng GY, Oakes BW, Deacon OW, McLean ID, Lampard D. Biomechanics of patellar tendon autograft for reconstruction of the anterior cruciate ligament in the goat: three-year study. *J Orthop Res.* 1995;13(4):602-608.
158. Nguyen DT, Geel J, Schulze M, et al. Healing of the goat anterior cruciate ligament after a new suture repair technique and bioscaffold treatment. *Tissue Eng Part A.* 2013;19(19-20):2292-2299.
159. Nguyen DT, Geel J, Schulze M, et al. Healing of the Goat Anterior Cruciate Ligament After a New Suture Repair Technique and Bioscaffold Treatment. *Tissue Engineering Part A.* 2013;19(19-20):2292-2299.

160. Niyibizi C, Kavalkovich K, Yamaji T, Woo SL. Type V collagen is increased during rabbit medial collateral ligament healing. *Knee Surg Sports Traumatol Arthrosc.* 2000;8(5):281-285.
161. Noyes FR, Butler DL, Grood ES, Zernicke RF, Hefzy MS. Biomechanical Analysis of Human Ligament Grafts Used in Knee-Ligament Repairs and Reconstructions. *Journal of Bone and Joint Surgery-American Volume.* 1984;66A(3):344-352.
162. Odensten M, Hamberg P, Nordin M, Lysholm J, Gillquist J. Surgical or Conservative Treatment of the Acutely Torn Anterior Cruciate Ligament - a Randomized Study with Short-Term Follow-up Observations. *Clinical Orthopaedics and Related Research.* 1985(198):87-93.
163. Odonoghu.Dh, Rockwood CA, Frank GR, Jack SC, Kenyon R. Repair of Anterior Cruciate Ligament in Dogs. *Journal of Bone and Joint Surgery-American Volume.* 1966;A 48(3):503-&.
164. Ohno K, Pomaybo AS, Schmidt CC, Levine RE, Ohland KJ, Woo SL. Healing of the medial collateral ligament after a combined medial collateral and anterior cruciate ligament injury and reconstruction of the anterior cruciate ligament: comparison of repair and nonrepair of medial collateral ligament tears in rabbits. *J Orthop Res.* 1995;13(3):442-449.
165. Oiestad BE, Holm I, Engebretsen L, Risberg MA. The association between radiographic knee osteoarthritis and knee symptoms, function and quality of life 10-15 years after anterior cruciate ligament reconstruction. *British Journal of Sports Medicine.* 2011;45(7):583-588.
166. Orrego M, Larrain C, Rosales J, et al. Effects of Platelet Concentrate and a Bone Plug on the Healing of Hamstring Tendons in a Bone Tunnel. *Arthroscopy-the Journal of Arthroscopic and Related Surgery.* 2008;24(12):1373-1380.
167. Ostrowski NJ, Lee B, Roy A, Ramanathan M, Kumta PN. Biodegradable poly(lactide-co-glycolide) coatings on magnesium alloys for orthopedic applications. *Journal of Materials Science-Materials in Medicine.* 2013;24(1):85-96.
168. Paoloni J, De Vos RJ, Hamilton B, Murrell GAC, Orchard J. Platelet-Rich Plasma Treatment for Ligament and Tendon Injuries. *Clinical Journal of Sport Medicine.* 2011;21(1):37-45.
169. Papageorgiou CD, Gil JE, Kanamori A, Fenwick JA, Woo SLY, Fu FH. The biomechanical interdependence between the anterior cruciate ligament replacement graft and the medial meniscus. *American Journal of Sports Medicine.* 2001;29(2):226-231.

170. Papageorgiou CD, Ma CB, Abramowitch SD, Clineff TD, Woo SLY. A multidisciplinary study of the healing of an intraarticular anterior cruciate ligament graft in a goat model. *American Journal of Sports Medicine*. 2001;29(5):620-626.
171. Pietak A, Mahoney P, Dias GJ, Staiger MP. Bone-like matrix formation on magnesium and magnesium alloys. *Journal of Materials Science-Materials in Medicine*. 2008;19(1):407-415.
172. Pinczewski LA, Lyman J, Salmon LJ, Russell VJ, Roe J, Linklater J. A 10-year comparison of anterior cruciate ligament reconstructions with hamstring tendon and patellar tendon autograft - A controlled, prospective trial. *American Journal of Sports Medicine*. 2007;35(4):564-574.
173. Plumb JA, Milroy R, Kaye SB. Effects of the Ph-Dependence of 3-(4,5-Dimethylthiazol-2-Yl)-2,5-Diphenyl-Tetrazolium Bromide-Formazan Absorption on Chemosensitivity Determined by a Novel Tetrazolium-Based Assay. *Cancer Research*. 1989;49(16):4435-4440.
174. Prevel CD, Eppley BL, Summerlin DJ, Jackson JR, McCarty M, Badylak SF. Small intestinal submucosa: utilization for repair of rodent abdominal wall defects. *Ann Plast Surg*. 1995;35(4):374-380.
175. Price JS, Till SH, Bickerstaff DR, Bayliss MT, Hollander AP. Degradation of cartilage type II collagen precedes the onset of osteoarthritis following anterior cruciate ligament rupture. *Arthritis Rheum*. 1999;42(11):2390-2398.
176. Randelli PS, Arrigoni P, Cabitza P, Volpi P, Maffulli N. Autologous platelet rich plasma for arthroscopic rotator cuff repair. A pilot study. *Disability and Rehabilitation*. 2008;30(20-22):1584-1589.
177. Rudy TW, Livesay GA, Woo SLY, Fu FH. A combined robotic/universal force sensor approach to determine in situ forces of knee ligaments. *J Biomech*. 1996;29(10):1357-1360.
178. Sachs RA, Daniel DM, Stone ML, Garfein RF. Patellofemoral problems after anterior cruciate ligament reconstruction. *Am J Sports Med*. 1989;17(6):760-765.
179. Sakane M, Fox RJ, Woo SLY, Livesay GA, Li G, Fu FH. In situ forces in the anterior cruciate ligament and its bundles in response to anterior tibial loads. *Journal of Orthopaedic Research*. 1997;15(2):285-293.
180. Sakane M, Livesay GA, Fox RJ, Rudy TW, Runco TJ, Woo SLY. Relative contribution of the ACL, MCL, and bony contact to the anterior stability of the knee. *Knee Surgery Sports Traumatology Arthroscopy*. 1999;7(2):93-97.

181. Salunke P, Shanov V, Witte F. High purity biodegradable magnesium coating for implant application. *Materials Science and Engineering B-Advanced Functional Solid-State Materials*. 2011;176(20):1711-1717.
182. Sandberg R, Balkfors B, Nilsson B, Westlin N. Operative Versus Nonoperative Treatment of Recent Injuries to the Ligaments of the Knee - a Prospective Randomized Study. *Journal of Bone and Joint Surgery-American Volume*. 1987;69A(8):1120-1126.
183. Scherping SC, Schmidt CC, Georgescu HI, Kwoh CK, Evans CH, Woo SLY. Effect of growth factors on the proliferation of ligament fibroblasts from skeletally mature rabbits. *Connective Tissue Research*. 1997;36(1):1-8.
184. Shelbourne KD, Rettig AC, Hardin G, Williams RI. Miniarthrotomy versus arthroscopic-assisted anterior cruciate ligament reconstruction with autogenous patellar tendon graft. *Arthroscopy-the Journal of Arthroscopic and Related Surgery*. 1993;9(1):72-75.
185. Sheth U, Simunovic N, Klein G, et al. Efficacy of Autologous Platelet-Rich Plasma Use for Orthopaedic Indications: A Meta-Analysis. *Journal of Bone and Joint Surgery-American Volume*. 2012;94A(4):298-307.
186. Shin KS, Bian MZ, Nam ND. Effects of Crystallographic Orientation on Corrosion Behavior of Magnesium Single Crystals. *Jom*. 2012;64(6):664-670.
187. Shin KS, Jung, H.C., Bian, M.Z., Nam, N.D., Kim, N.J. Characterization of biodegradable magnesium single crystals with various crystallographic orientations. *European Cells and Materials*. 2013;26(Suppl. 5):4.
188. Sicari BM, Dziki JL, Siu BF, Medberry CJ, Dearth CL, Badylak SF. The promotion of a constructive macrophage phenotype by solubilized extracellular matrix. *Biomaterials*. 2014;35(30):8605-8612.
189. Smith BA, Livesay GA, Woo SLY. Biology and Biomechanics of the Anterior Cruciate Ligament. *Clinics in Sports Medicine*. 1993;12(4):637-670.
190. Smith CA, Tennent TD, Pearson SE, Beach WR. Fracture of Bilok interference screws on insertion during anterior cruciate ligament reconstruction. *Arthroscopy-the Journal of Arthroscopic and Related Surgery*. 2003;19(9).
191. Song GL, Atrens A. Corrosion mechanisms of magnesium alloys. *Advanced Engineering Materials*. 1999;1(1):11-33.
192. Song GL, Atrens A, Wu XL, Zhang B. Corrosion behaviour of AZ21, AZ501 and AZ91 in sodium chloride. *Corrosion Science*. 1998;40(10):1769-1791.

193. Song GL, Xu ZQ. Crystal orientation and electrochemical corrosion of polycrystalline Mg. *Corrosion Science*. 2012;63:100-112.
194. Songur M, Celikkan H, Gokmese F, Simsek SA, Altun NS, Aksu ML. Electrochemical corrosion properties of metal alloys used in orthopaedic implants. *Journal of Applied Electrochemistry*. 2009;39(8):1259-1265.
195. Spindler KP, Murray MM, Detwiler KB, et al. The biomechanical response to doses of TGF-beta 2 in the healing rabbit medial collateral ligament. *Journal of Orthopaedic Research*. 2003;21(2):245-249.
196. Standardization IOF. ISO-10993-12: Biological Evaluation of Medical Devices, Part 12. *Sample preparation and reference materials*. Arlington, VA: ANSI/AAMI; 2007.
197. Stapleton TR. Complications in anterior cruciate ligament reconstructions with patellar tendon grafts. *Sports Medicine and Arthroscopy Review*. 1997;5(2):156-162.
198. Supplements NIOHOOD. Magnesium. Available at: <http://ods.od.nih.gov/factsheets/Magnesium-HealthProfessional/>. Accessed May 23, 2015.
199. Takai S, Woo SLY, Livesay GA, Adams DJ, Fu FH. Determination of the in-Situ Loads on the Human Anterior Cruciate Ligament. *Journal of Orthopaedic Research*. 1993;11(5):686-695.
200. Taylor DW, Petrera M, Hendry M, Theodoropoulos JS. A Systematic Review of the Use of Platelet-Rich Plasma in Sports Medicine as a New Treatment for Tendon and Ligament Injuries. *Clinical Journal of Sport Medicine*. 2011;21(4):344-352.
201. Theut PC, Fulkerson JP, Armour EF, Joseph M. Anterior cruciate ligament reconstruction utilizing central quadriceps free tendon. *Orthop Clin North Am*. 2003;34(1):31-39.
202. Thomann M, Krause C, Bormann D, von der Hoh N, Windhagen H, Meyer-Lindenberg A. Comparison of the resorbable magnesium alloys LAE442 und MgCa0.8 concerning their mechanical properties, their progress of degradation and the bone-implant-contact after 12 months implantation duration in a rabbit model. *Materialwissenschaft Und Werkstofftechnik*. 2009;40(1-2):82-87.
203. Tibone JE, Antich TJ. A biomechanical analysis of anterior cruciate ligament reconstruction with the patellar tendon. A two year followup. *Am J Sports Med*. 1988;16(4):332-335.
204. Tsuda E, Fukuda Y, Loh JC, Debski RE, Fu FH, Woo SL. The effect of soft-tissue graft fixation in anterior cruciate ligament reconstruction on graft-tunnel motion under anterior tibial loading. *Arthroscopy-the Journal of Arthroscopic and Related Surgery*. 2002;18(9):960-967.

205. Turner NJ, Yates AJ, Weber DJ, et al. Xenogeneic Extracellular Matrix as an Inductive Scaffold for Regeneration of a Functioning Musculotendinous Junction. *Tissue Engineering Part A*. 2010;16(11):3309-3317.
206. Valentin JE, Badylak JS, McCabe GP, Badylak SF. Extracellular matrix bioscaffolds for orthopaedic applications - A comparative histologic study. *Journal of Bone and Joint Surgery-American Volume*. 2006;88A(12):2673-2686.
207. von Porat A, Roos EM, Roos H. High prevalence of osteoarthritis 14 years after an anterior cruciate ligament tear in male soccer players: a study of radiographic and patient relevant outcomes. *Annals of the Rheumatic Diseases*. 2004;63(3):269-273.
208. Vormann J. Magnesium: nutrition and metabolism. *Molecular Aspects of Medicine*. 2003(24):27-37.
209. Voytik-Harbin SL, Brightman AO, Kraine MR, Waisner B, Badylak SF. Identification of extractable growth factors from small intestinal submucosa. *J Cell Biochem*. 1997;67(4):478-491.
210. Walton M, Cotton NJ. Long-term in vivo degradation of poly-L-lactide (PLLA) in bone. *Journal of Biomaterials Applications*. 2007;21(4):395-411.
211. Wang J, Witte F, Zheng Y, et al. Recommendation for modifying current cytotoxicity testing standards for biodegradable magnesium-based materials. *Acta Biomaterialia*. 2015;21:237-249.
212. Wang JY, Wicklund BH, Gustilo RB, Tsukayama DT. Titanium, chromium and cobalt ions modulate the release of bone-associated cytokines by human monocytes/macrophages in vitro. *Biomaterials*. 1996;17(23):2233-2240.
213. Warren RF. Primary Repair of the Anterior Cruciate Ligament. *Clinical Orthopaedics and Related Research*. 1983(172):65-70.
214. Wei J, Jia JF, Wu F, et al. Hierarchically microporous/macroporous scaffold of magnesium-calcium phosphate for bone tissue regeneration. *Biomaterials*. 2010;31(6):1260-1269.
215. Weiss JA, Woo SLY, Ohland KJ, Horibe S, Newton PO. Evaluation of a New Injury Model to Study Medial Collateral Ligament Healing - Primary Repair Versus Nonoperative Treatment. *Journal of Orthopaedic Research*. 1991;9(4):516-528.
216. Wiig ME, Amiel D, VandeBerg J, Kitabayashi L, Harwood FL, Arfors KE. The early effect of high molecular weight hyaluronan (hyaluronic acid) on anterior cruciate ligament healing: an experimental study in rabbits. *J Orthop Res*. 1990;8(3):425-434.

217. Witte F. The history of biodegradable magnesium implants: A review. *Acta Biomaterialia*. 2010;6(5):1680-1692.
218. Witte F, Fischer J, Nellesen J, et al. In vivo corrosion and corrosion protection of magnesium alloy LAE442. *Acta Biomaterialia*. 2010;6(5):1792-1799.
219. Witte F, Hort N, Vogt C, et al. Degradable biomaterials based on magnesium corrosion. *Current Opinion in Solid State & Materials Science*. 2008;12(5-6):63-72.
220. Witte F, Kaese V, Haferkamp H, et al. In vivo corrosion of four magnesium alloys and the associated bone response. *Biomaterials*. 2005;26(17):3557-3563.
221. Wolf M, Daly K, Brennan-Pierce E, et al. Extracellular Matrix Hydrogels Prepared from Porcine Dermis and UrinaryBladder: Structure, Mechanics and In Vivo Remodeling. *Glycobiology*. 2012;22(11):1585-1586.
222. Wolf MT, Daly KA, Brennan-Pierce EP, et al. A hydrogel derived from decellularized dermal extracellular matrix. *Biomaterials*. 2012;33(29):7028-7038.
223. Woo SL, Danto MI, Ohland KJ, Lee TQ, Newton PO. The use of a laser micrometer system to determine the cross-sectional shape and area of ligaments: a comparative study with two existing methods. *J Biomech Eng*. 1990;112(4):426-431.
224. Woo SL, Newton PO, MacKenna DA, Lyon RM. A comparative evaluation of the mechanical properties of the rabbit medial collateral and anterior cruciate ligaments. *J Biomech*. 1992;25(4):377-386.
225. Woo SL, Takakura Y, Liang R, Jia F, Moon DK. Treatment with bioscaffold enhances the the fibril morphology and the collagen composition of healing medial collateral ligament in rabbits. *Tissue Eng*. 2006;12(1):159-166.
226. Woo SL-Y, Debski RE, Withrow JD, Janaushek MA. Biomechanics of knee ligaments. *Am J Sports Med*. 1999;27(4):533-543.
227. Woo SLY, et al. The response of ligaments to injury: Healing of the collateral ligaments. In: Daniel D, Akeson, W, O'Connor, J., ed. *Knee Ligaments: Structure, Function, Injury, and Repair*: Raven Press; 1990:351-364.
228. Woo SLY, Hollis JM, Adams DJ, Lyon RM, Takai S. Tensile Properties of the Human Femur-Anterior Cruciate Ligament-Tibia Complex - the Effects of Specimen Age and Orientation. *American Journal of Sports Medicine*. 1991;19(3):217-225.
229. Woo SLY, Inoue M, Mcgurkburleson E, Gomez MA. Treatment of the Medial Collateral Ligament Injury .2. Structure and Function of Canine Knees in Response to Differing Treatment Regimens. *American Journal of Sports Medicine*. 1987;15(1):22-29.

230. Woo SLY, Kanamori A, Zeminski J, Yagi M, Papageorgiou C, Fu FH. The effectiveness of reconstruction of the anterior cruciate ligament with hamstrings and patellar tendon - A cadaveric study comparing anterior tibial and rotational loads. *Journal of Bone and Joint Surgery-American Volume*. 2002;84A(6):907-914.
231. Wood JD, Simmons-Byrd A, Spievack AR, Badylak SF. Use of a particulate extracellular matrix bioscaffold for treatment of acquired urinary incontinence in dogs. *Javma-Journal of the American Veterinary Medical Association*. 2005;226(7):1095-1097.
232. Xin Y, Hu T, Chu PK. In vitro studies of biomedical magnesium alloys in a simulated physiological environment: A review. *Acta Biomaterialia*. 2011;7(4):1452-1459.
233. Xu LP, Pan F, Yu GN, Yang L, Zhang EL, Yang K. In vitro and in vivo evaluation of the surface bioactivity of a calcium phosphate coated magnesium alloy. *Biomaterials*. 2009;30(8):1512-1523.
234. Xu LP, Zhang EL, Yin DS, Zeng SY, Yang K. In vitro corrosion behaviour of Mg alloys in a phosphate buffered solution for bone implant application. *Journal of Materials Science-Materials in Medicine*. 2008;19(3):1017-1025.
235. Yagi M, Wong EK, Kanamori A, Debski RE, Fu FH, Woo SLY. Biomechanical analysis of an Anatomic anterior cruciate ligament reconstruction. *American Journal of Sports Medicine*. 2002;30(5):660-666.
236. Yamamoto Y, Hsu WH, Woo SL, Van Scyoc AH, Takakura Y, Debski RE. Knee stability and graft function after anterior cruciate ligament reconstruction: a comparison of a lateral and an anatomical femoral tunnel placement. *Am J Sports Med*. 2004;32(8):1825-1832.
237. Yan TT, Tan LL, Xiong DS, Liu XJ, Zhang BC, Yang K. Fluoride treatment and in vitro corrosion behavior of an AZ31B magnesium alloy. *Materials Science & Engineering C-Materials for Biological Applications*. 2010;30(5):740-748.
238. Yasuda K, Kondo E, Ichiyama H, et al. Anatomic reconstruction of the anteromedial and posterolateral bundles of the anterior cruciate ligament using hamstring tendon grafts. *Arthroscopy-the Journal of Arthroscopic and Related Surgery*. 2004;20(10):1015-1025.
239. Yasuda K, Kondo E, Ichiyama H, Tanabe Y, Tohyama H. Clinical evaluation of anatomic double-bundle anterior cruciate ligament reconstruction procedure using hamstring tendon grafts: comparisons among 3 different procedures. *Arthroscopy-the Journal of Arthroscopic and Related Surgery*. 2006;22(3):240-251.
240. Yokel RA. The toxicology of aluminum in the brain: A review. *Neurotoxicology*. 2000;21(5):813-828.

241. Young RG, Butler DL, Weber W, Caplan AI, Gordon SL, Fink DJ. Use of mesenchymal stem cells in a collagen matrix for Achilles tendon repair. *Journal of Orthopaedic Research*. 1998;16(4):406-413.
242. Yun Y, Dong ZY, Yang DE, et al. Biodegradable Mg corrosion and osteoblast cell culture studies. *Materials Science & Engineering C-Materials for Biological Applications*. 2009;29(6):1814-1821.
243. Yun Y, Jang Y, Wang J, et al. Biodegradable magnesium implant: in vivo and in vitro convergence. Paper presented at: ASME 2014 International Mechanical Engineering Congress and Exposition; November 14-20, 2014, 2014; Montreal, Quebec, Canada.
244. Yunes M, Richmond JC, Engels EA, Pinczewski LA. Patellar versus hamstring tendons in anterior cruciate ligament reconstruction: A meta-analysis. *Arthroscopy*. 2001;17(3):248-257.
245. Zantop T, Gilbert TW, Yoder MC, Badylak SF. Extracellular matrix scaffolds are repopulated by bone marrow-derived cells in a mouse model of Achilles tendon reconstruction. *Journal of Orthopaedic Research*. 2006;24(6):1299-1309.
246. Zantop T, Wellmann M, Fu FH, Petersen W. Tunnel positioning of anteromedial and posterolateral bundles in anatomic anterior cruciate ligament reconstruction: anatomic and radiographic findings. *Am J Sports Med*. 2008;36(1):65-72.
247. Zhang EL, Xu LP, Yu GN, Pan F, Yang K. In vivo evaluation of biodegradable magnesium alloy bone implant in the first 6 months implantation. *Journal of Biomedical Materials Research Part A*. 2009;90A(3):882-893.
248. Zhang J, Yang L, Tang ZY, et al. Expression of MMPs and TIMPs Family in Human ACL and MCL Fibroblasts. *Connective Tissue Research*. 2009;50(1):7-13.
249. Zhang JY, Wang JHC. Production of PGE(2) Increases in Tendons Subjected to Repetitive Mechanical Loading and Induces Differentiation of Tendon Stem Cells into Non-Tenocytes. *Journal of Orthopaedic Research*. 2010;28(2):198-203.
250. Zhang SX, Zhang XN, Zhao CL, et al. Research on an Mg-Zn alloy as a degradable biomaterial. *Acta Biomaterialia*. 2010;6(2):626-640.
251. Zheng YF, Gu XN, Witte F. Biodegradable metals. *Materials Science & Engineering R-Reports*. 2014;77:1-34.
252. Zierold AA. Reaction of bone to various metals. *Arch. Surg*. 1924(9):365-412.